Intramolecular signal transduction of the sensor histidine kinase DcuS and the aerobic and anaerobic fumarate proteome in the regulation of the *Escherichia coli* C$_4$-dicarboxylate metabolism

Dissertation

Zur Erlangung des Grades
„Doktor der Naturwissenschaften"

am Fachbereich Biologie
der Johannes Gutenberg-Universität Mainz

vorgelegt von

Marius Stopp
geb. am 05.03.1992 in Wiesbaden

Mainz, März 2021

Dekan:

1. Gutachter: Prof. Dr. Gottfried Unden

2. Gutachter:

Tag der Mündlichen Prüfung: 25.08.2021

Content

1   Abstract

The aerobic and anaerobic utilization of C_4-dicarboxylates in *Escherichia coli* is regulated by the DcuSR two-component system. Depending on oxygen availability, the transcription of the genes of fumarate respiration or the aerobic transporter DctA are induced. The C_4-dicarboxylate transporters DctA and DcuB act as co-regulators of DcuS and convert DcuS to its responsive state in the DcuS-transporter sensor complex. C_4-dicarboxylates bound at the periplasmic domain of DcuS and trigger a signal cascade across the membrane, emanating from the sensory PAS_P domain through TM2, a short Linker and the cytoplasmic PAS_C domain that results in cytoplasmic autophosphorylation at the C-terminal kinase domain of DcuS. TM2 was already shown to transduce the signal across the membrane via a piston type shift, but the entire mechanism in DcuS transmembrane signaling is unknown.

The structure and dynamics of the domains in DcuS intramolecular signal transduction were investigated by oxidative cysteine cross-linking. This revealed a membrane spanning dimeric continuous helix that is mostly stable in both DcuS signaling states. The continuous helix comprises the C-terminal $\alpha6$ helix of PAS_P, TM2, the linker, and the N-terminal $\alpha1$ helix of PAS_C and thus connects periplasmic signal input with the cytoplasmic signal output domains. The structural dynamics of selected DcuS residues in the DcuS signal transfer were tested by time-resolved cysteine cross-linking. TM2 was shown to be a rigid homo-dimer confirming the piston-type shift as major transmembrane signaling mechanism by TM2. In contrast, the linker represents a dynamic region in signal transduction. PAS_C also seems to undergo a restructuring in $\alpha1$ and $\beta1$ upon DcuS activation. Furthermore, time-resolved cysteine crosslinking in the absence of the co-regulator DctA showed that DcuS adopts cross-linking reactivity resembling the fumarate activated state. It seems likely that DctA stabilizes homo-dimerization of the linker and $\alpha1$ of PAS_C by direct interaction via the DctA helix 8b and thus converts DcuS in its responsive state in the DcuS-DctA sensor complex.

In addition, the aerobic and anaerobic *E. coli* fumarate proteome was investigated in a 'shotgun proteomics' approach. The transcriptional regulation by DcuSR was displayed in the proteomic results. Upregulation of almost all TCA cycle enzymes, anaplerotic reactions, and gluconeogenesis under aerobic conditions was observed. This regulatory effect can be related to an EIIA-P/EIIA ratio-dependent indirect regulation by cAMP/CRP, but a previously unknown regulation by DcuSR is also possible in some cases. The most abundant category of proteins, which was upregulated by fumarate under anaerobic conditions, can be assigned to chemotaxis and motility.

1   Zusammenfassung

Die aerobe und anaerobe Verwertung von C_4-Dicarboxylaten in *Escherichia coli* wird durch das DcuSR Zweikomponentensystem reguliert. Abhängig von der Sauerstoffverfügbarkeit wird die Transkription der Gene der Fumaratatmung oder des aeroben Transporters DctA induziert. Die C_4-Dicarboxylat-Transporter DctA und DcuB fungieren dabei als Co-Regulatoren und überführen DcuS im DcuS-Transporter Sensorkomplex in seinen responsiven Zustand. An der sensorischen PAS_P-Domäne von DcuS periplasmatisch gebundene C_4-Dicarboxylate lösen eine Signalkaskade über die Membran hinweg aus über TM2, einen Linker und die cytoplasmatische PAS_C-Domäne, die zu einer cytoplasmatischen Autophosphorylierung der C-terminalen Kinase-Domäne von DcuS führt. Es wurde bereits gezeigt, dass TM2 das Signal durch einen „piston-type shift" über die Membran leitet. Der vollständige Signaltransduktions-Mechanismus der DcuS Transmembrandomäne ist jedoch unbekannt.

Die Struktur und Dynamik der DcuS Domänen in der Signaltransduktion wurden mit oxidativem Cystein Cross-linking untersucht. Dies zeigte, dass eine dimere, kontinuierliche Helix den periplasmatischen Signaleingang über die Membran mit den cytoplasmatischen Signalausgangs-Domänen verbindet. Die kontinuierliche Helix umfasst die C-terminale α6-Helix von PAS_P, TM2, den Linker und die N-terminale α1-Helix von PAS_C und ist in beiden DcuS-Signalzuständen größtenteils stabil. Die Dynamik ausgewählter DcuS-Reste im Signaltransfer wurde mittels zeitaufgelöstem Cystein Cross-linking untersucht. Es wurde gezeigt, dass TM2 ein steifes Homodimer ist, was den „piston-type shift" als Hauptmechnismus der Signaltransduktion durch TM2 bestätigt. Der Linker repräsentiert einen dynamischen Bereich und auch PAS_C scheint bei der DcuS-Aktivierung eine Umstrukturierung in α1 und β1 zu erfahren. In Abwesenheit von DctA nimmt DcuS eine Cross-link Reaktivität an, die dem Fumarat-aktivierten Zustand ähnelt. Es ist wahrscheinlich, dass DctA die Homodimerisierung des Linkers und α1 von PAS_C durch Interaktion über die DctA-Helix 8b stabilisiert.

Darüber hinaus wurde das aerobe und anaerobe *E. coli* Fumarat-Proteom mittels „shotgun proteomics" untersucht. Die transkriptionelle Regulation durch DcuSR spiegelt sich im Proteom wider. Außerdem waren fast alle Enzyme des Citrat-Zyklus, anaplerotischer Reaktionen und der Gluconeogenese unter aeroben Bedingungen hochreguliert. Dieser Effekt hängt eventuell mit einer indirekten Regulation durch cAMP/CRP zusammen, die vom EIIA-P /EIIA Verhältnis abhängt. In einigen Fällen ist auch eine bisher unbekannte Regulation durch DcuSR möglich. Die häufigste Kategorie von Proteinen, die unter anaeroben Bedingungen durch Fumarat hochreguliert wurden, hängt mit Chemotaxis und Motilität zusammen.

2 Introduction

2.1 *Escherichia coli*

Escherichia coli was first described by Theodor Escherich (1886) as *Bacterium coli commune* and is a gram-negative, facultative anaerobic γ-proteobacterium from the *Enterobacteriaceae* family. The natural habitat of the rod-shaped bacterium is the mucosa of vertebrates' large intestine but can also be found in the small intestine (Wadolkowski *et al.* 1988; El Aidy *et al.* 2013). In addition to the commensal *E. coli* strains there are several pathogenic variants that can cause serious intra- and extraintestinal diseases with a potentially fatal outcome (Kaper *et al.* 2004). The commonly used K-12 strain derivatives were obtained from a stool isolate of a convalescent diphtheria patient from 1922. Since then *E. coli* was used for initial studies on biosynthesis (Gray and Tatum, 1944), genetic recombination (Tatum and Lederberg, 1947), and gene regulation (Jacob *et al.* 1960). Furthermore, the relatively small 4.6 kb genome with its 4288 structural genes was one of the first to be completely sequenced (Blattner *et al.* 1997). *E. coli* has thus become one of the best-studied model organisms.

2.2 Regulation of aerobic and anaerobic respiration in *E. coli*

As a facultative anaerobic bacterium *E. coli* is able to conserve energy under both aerobic and anaerobic conditions by aerobic and anaerobic respiration as well as through fermentation. The use of electron donors and acceptors is achieved by coupling of different types of dehydrogenases with one of several reductases each via the quinones within the membrane (Unden *et al.* 2014). Therefore, the use of the various electron acceptors is subject to a strict hierarchical regulation in order to use the available resources as efficiently as possible and is largely determined by the redox potential E_0' of the electron acceptor. Molecular oxygen is preferred under aerobic conditions, because it has the highest redox potential ($E_0' = + 0,82$ V) resulting in the highest energy/ATP yield. According to the redox potential of the alternative electron acceptors nitrate (NO_3^-, $E_0' = + 0,43$ V), Dimethylsulfoxid (DMSO, $E_0' = + 0,16$ V), Trimethylamin-N-oxid (TMAO, $E_0' = + 0,13$ V), und Fumarat ($E_0' = + 0,03$ V), their energy yield decreases from NO_3^- to fumarate (Gunsalus, 1992). In the absence of external electron acceptors *E. coli* conserves energy through fermentation (Clark, 1989). The global sensor FNR (fumarate nitrate reductase regulator) and the two-component system (TCS) ArcBA (anoxic redox control) serve as regulatory systems switching from aerobic to anaerobic respiration and fermentation. Under anaerobiosis FNR serves as a direct oxygen sensor detecting oxygen via a $[4Fe4S]^{2+}$-cluster (Khoroshilova *et al.* 1995; Jordan *et al.* 1997). FNR activates transcription of the genes of the nitrate reductase (*narGHJI*) and fumarate reductase (*frdABCD*) (Guest 1992;

Becker *et al*. 1996). The TCS ArcAB is an indirect oxygen sensor that detects the redox status of the cell via the quinol pool and inhibits the transcription of the genes for aerobic respiration in the absence of oxygen (Iuchi and Lin, 1988; Malpica *et al*. 2004). The use of other alternative electron acceptors is regulated by substrate-specific regulatory systems, which mainly regulate the expression of the respective terminal reductase (Unden *et al*. 2016a). The TCSs NarXL and NarPQ activate the transcription of the genes for nitrate respiration *fdnGHI* (formate dehydrogenase-N) and *narGHJI* (nitrate reductase) and simultaneously repress the transcription of the genes of alternative anaerobic respiration and fermentation (Rabin and Stewart, 1993; Stewart, 2003). Moreover, the TCS TorSR regulates the utilization of the electron acceptor TMAO (Simon *et al*. 1994; Jourlin *et al*. 1996). C_4-dicarboxylates (C4DCs) can also be used in anaerobic respiration. The DcuSR TCS activates the transcription of the genes of fumarate respiration and of associated transporters (Zientz *et al*. 1998; Golby *et al*. 1999).

2.3   *E. coli* aerobic and anaerobic C₄-dicarboxylate metabolism

As a glucophilic bacterium *E. coli* prefers glucose or hexoses as energy and carbon source for growth under aerobic conditions. The uptake and utilization of glucose is regulated by the glucose phosphotransfer system (PTS) (Deutscher *et al*. 2007). If no glucose is available, the central metabolism is adjusted according to the availability of other carbon and energy sources. cAMP and the regulator cAMP receptor protein (CRP) play a crucial role in transcriptional regulation of catabolite repression. This includes adaptation of transport, the glycolysis-gluconeogenesis switch, tricarboxylic acid (TCA) cycle, as well as aerobic respiration (Perrenoud and Sauer, 2005; Nanchen *et al*. 2008; Shimada *et al*. 2011).

As an alternative to glucose *E. coli* can utilize C4DCs under both aerobic and anaerobic conditions (Unden *et al*. 2016a). Under aerobic conditions uptake of C4DCs like fumarate, L-malate, and succinate is catalyzed by the transporter DctA (C_4-dicarboxylate transporter A) at neutral pH (Kay and Kornberg, 1971). At pH $\leq$ 5 the C4DC transport is carried out by the transporter DauA (Dicarboxylic acid uptake protein A) (Karinou *et al*. 2013). These C4DCs are fed directly into the TCA cycle via the succinate dehydrogenase, aerobic fumarases, and the malate dehydrogenase and are completely oxidized to CO_2. The Uptake of the C_4-amino acid L-aspartate is catalyzed by DctA as well as by the constitutively expressed antiporter DcuA in antiport with other C4DCs (Golby *et al*. 1998). L-aspartate can be fed to the TCA cycle after deamination by the L-aspartase (AspA) to fumarate. The released NH_4^+ can be used in nitrogen assimilation. Explicitly the antiport by DcuA of L-aspartate in exchange for fumarate represents a nitrogen shuttle and provides aspartate as a high-quality nitrogen source for *E. coli* (Strecker

et al. 2018; Schubert *et al*. 2020). In order to maintain the TCA cycle it is necessary that 50 % of the catabolized C4DCs are channeled through the pyruvate by-pass by the malic enzymes (MEZ) to provide acetyl-CoA. In addition, C4DCs can enter the gluconeogenetic pathway through the PEP carboxykinase (PckA) as well as the MEZ and the PEP synthetase (PpsA) as part of the pyruvate bypass (Unden *et al*. 2016a). D-malate is also transported by DctA. This is followed by oxidative decarboxylation to pyruvate by the D-malate dehydrogenase (DmlA) (Lukas *et al*. 2010) (Fig. 1). As a consequence of C4DC utilization in the TCA cycle the reduction equivalents NADH and ubiquinol (QH_2) are generated. Their oxidation within the aerobic respiratory chain leads to the build-up of a proton gradient enabling the synthesis of ATP by the ATP synthase (Maloney *et al*. 1974).
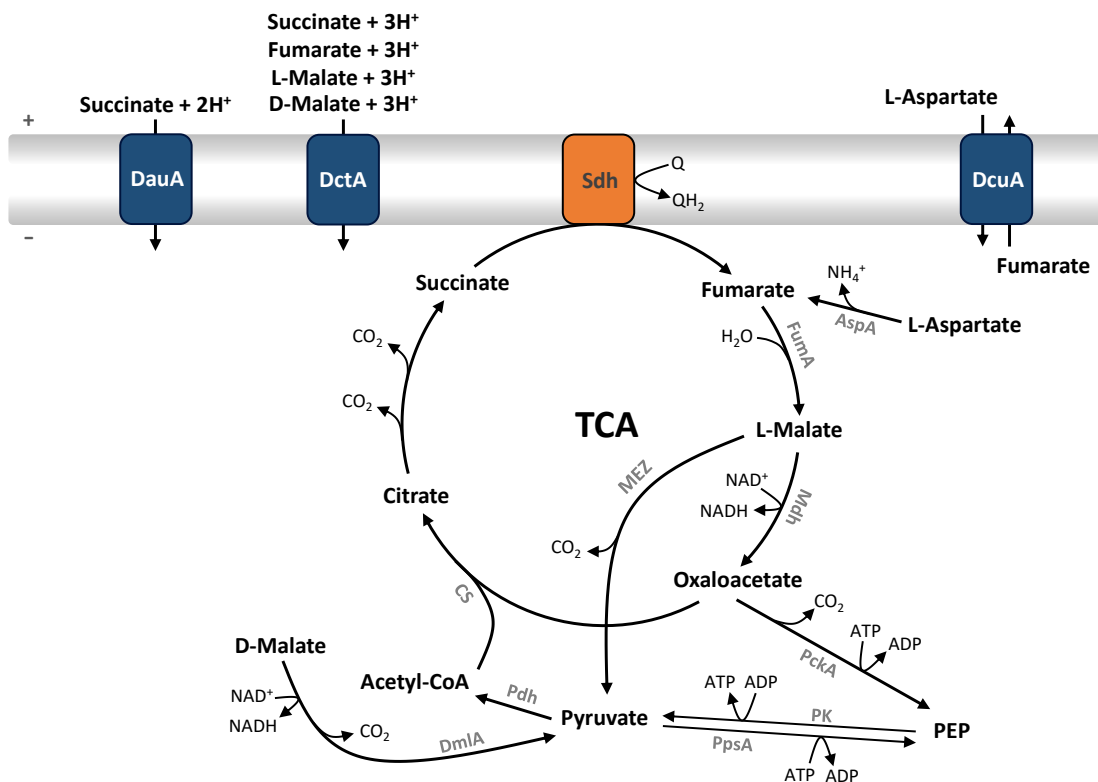
Figure 1. Overview of the aerobic C4DC metabolism of *E. coli*. For simplification only selected intermediates and pathways are shown. Abbreviations: (AspA) aspartase; (CS) citrate synthase; (DmlA) D-malate dehydrogenase; (FumA) fumarase A; (MEZ) NAD(P)H-dependent malic enzymes; (Mdh) malate dehydrogenase; (PckA) PEP carboxykinase; (PEP) phosphoenol pyruvate; (Pdh) pyruvate dehydrogenase; (PK) pyruvate kinase; (PpsA) PEP synthetase; (Sdh) succinate dehydrogenase; (Q) ubiquinone; (QH_2) ubiquinol. For details see main text of section 2.2.

In anaerobic growth fumarate respiration represents the predominant pathway in C4DC catabolism. Fumarate serves as terminal electron acceptor and is reduced to succinate by the fumarate reductase. However, growth requires additional substrates such as glucose or glycerol, which provide glycerine-3-phosphate or NADH, which serve in turn as electron donors for the

reduction of fumarate (Guest, 1979). Other C4DCs are converted to fumarate via the reductive branch of the TCA cycle. C4DCs that do not occur in the TCA cycle can also be converted to fumarate. L-aspartate is deaminated by AspA and L-tartrate is dehydrated to oxaloacetate by the L-tartrate dehydratase (TtdAB) (Kim *et al*. 2007). Further oxidation of succinate is not possible in anaerobiosis, since oxidation of QH_2 by the menaquinone-dependent (MQ) fumarate reductase is not possible (Wissenbach *et al*. 1990). Therefore, succinate is exported from the cell as the product of fumarate respiration. In return, uptake of C4DCs is catalyzed in an antiport with succinate, with DcuB acting as the main antiporter (Engel *et al*. 1992, 1994). DcuA and DcuC are further anaerobic C4DC transporters, whereby DcuC is primarily assigned to function as an efflux transporter for succinate generated by fermentation (Six *et al*. 1994; Zientz *et al*. 1999). The antiporter TtdT takes over the uptake of L-tartrate (Kim *et al*. 2007). Citrate uptake is catalyzed by the citrate/succinate antiporter CitT and is split into oxaloacetate and acetate by the citrate lyase (CL) in citrate fermentation (Pos *et al*. 1998).
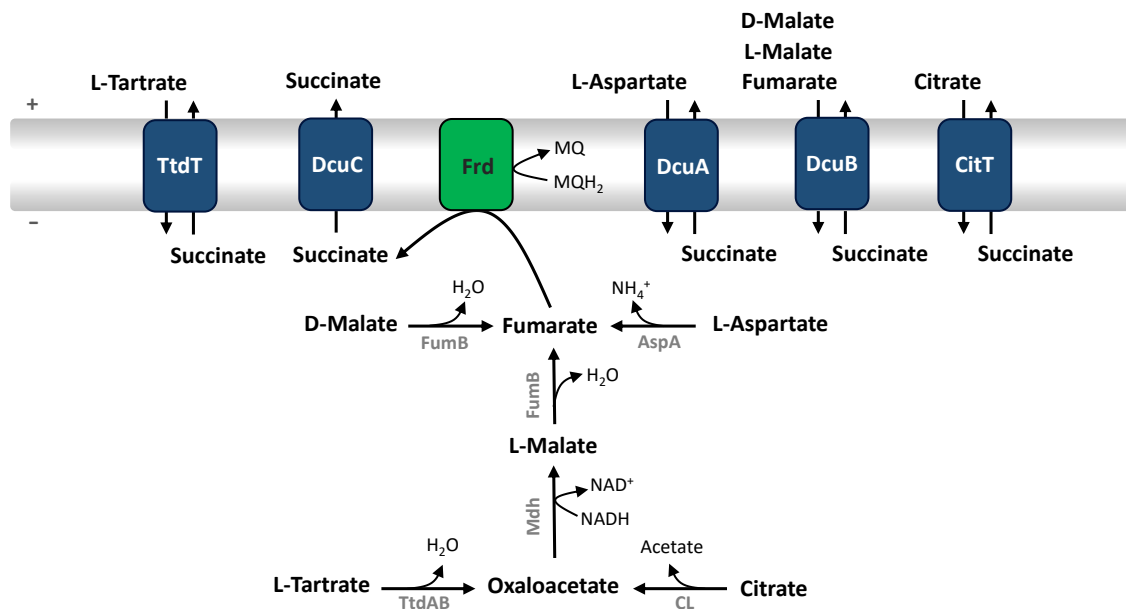
Figure 2. Overview of the anaerobic C4DC metabolism of *E. coli*. Abbreviations: (AspA) aspartase; (CL) citrate lyase; (Frd) fumarate reductase; (FumB) fumarase B; (Mdh) malate dehydrogenase; (MQ) menaquinone; (MQH_2) menaquinol; (TtdAB) L-tartrate dehydratase. For details see main text of section 2.2.

2.4 The DcuSR two-component system

The recognition of various environmental stimuli and the corresponding metabolic adaptation is crucial for bacterial survival. For this purpose bacteria often use TCS that are the second most frequent group of signal transduction proteins (Ulrich and Zhulin, 2010) and represent the most prevalent signal transduction pathway in bacteria (Zschiedrich *et al*. 2016). The evolutionary progenitor of the TCS is represented by the even more frequent one-component systems

(Wuichet *et al.* 2010). A TCS consists prototypically of a sensor histidine kinase and a cognate response regulator (Kofoid and Parkinson, 1988; Gross *et al.* 1989). The sensor histidine kinases perceive extracellular stimuli and are therefore usually membrane-bound proteins (Stock *et al.* 2000; Mascher *et al.* 2006). The division of a TCS into two separate components requires a signal of the sensor histidine kinase to be transmitted to the soluble response regulator. With appropriate stimulation a conserved histidine residue of the sensor histidine kinase is autophosphorylated and the phosphoryl group is transferred to a conserved aspartate residue of the response regulator (Stock *et al.* 2000).

2.4.1 Regulation of the C4DC metabolism

The DcuSR TCS consists of the sensor histidine kinase DcuS (Dicarboxylate uptake sensor) and the response regulator DcuR (Dicarboxylate uptake regulator) and represents a typical TCS. As most sensor histidine kinases DcuS is a membrane integral protein which is located at the cell poles. DcuR is homogeneously distributed in the cytoplasm, but co-localizes with DcuS at the cell poles, if both are co-expressed (Scheu *et al.* 2010, 2014). DcuS detects a broad range of C4DCs. These include D- and L-malate, fumarate, succinate, D- and L-tartrate, L-aspartate, and mesaconate but also the tricarboxylic acid citrate. L-malate and fumarate cause the strongest activation of the target genes (Krämer *et al.* 2007; Zeltner, 2017). The substrates are bound by the periplasmic Per-ARNT-Sim (PAS_P) domain (Kneuper *et al.* 2005). A signal generated in PAS_P is then transmitted to the kinase domain via the transmembrane (TM) domain, a short linker, and the cytoplasmic PAS_C domain. This triggers autophosphorylation of the conserved histidine residue His349. This phosphorylated histidine residue acts as a donor of the phosphoryl group, which is transferred to the conserved aspartate residue Asp56 of the response regulator DcuR (Janausch *et al.* 2002). Phosphorylated DcuR binds as a dimer via a helix-turn-helix motif to AT-rich regions upstream of the target genes (Abo-Amer *et al.* 2004; Janausch *et al.* 2004). This activates transcription of *dctA* under aerobic conditions, whereas under anaerobic conditions the transcription of *dcuB* and *fumB* as well as the genes of fumarate reductase (*frdABC*) is stimulated (Zientz *et al.* 1998; Golby *et al.* 1999) (Fig.3). In order to avoid the unregulated activation of the target genes, the DcuS kinase domain contains an ExxN phosphatase motif that possibly controls the dephosphorylation of DcuR (Gencheva, 2016). However, DcuR also seems to have an intrinsic phosphatase activity (Krämer *et al.* 2007).

The correct function of DcuS requires the presence of either the transporter DctA or DcuB under aerobic and anaerobic conditions, respectively. The transporters DctA and DcuB convert DcuS into the C4DC-sensitive state, since the absence of the transporters cause a constitutively

activation of DcuS (Kleefeld *et al*. 2009; Witan *et al*. 2012). Via a direct interaction with DcuS the transporters each form a sensor complex with DcuS, where they act as a co-regulator but not as a co-sensor (Kleefeld *et al*. 2009; Steinmetz *et al*. 2014; Wörner *et al*. 2016). However, small amounts of free DcuS are always present in the cell, ensuring that basal expression of the transporters (Wörner *et al*. 2018) (for details see section 2.4.3). Furthermore, DauA seems to influence the expression of DctA through an interaction with DctA (Karinou *et al*. 2017).
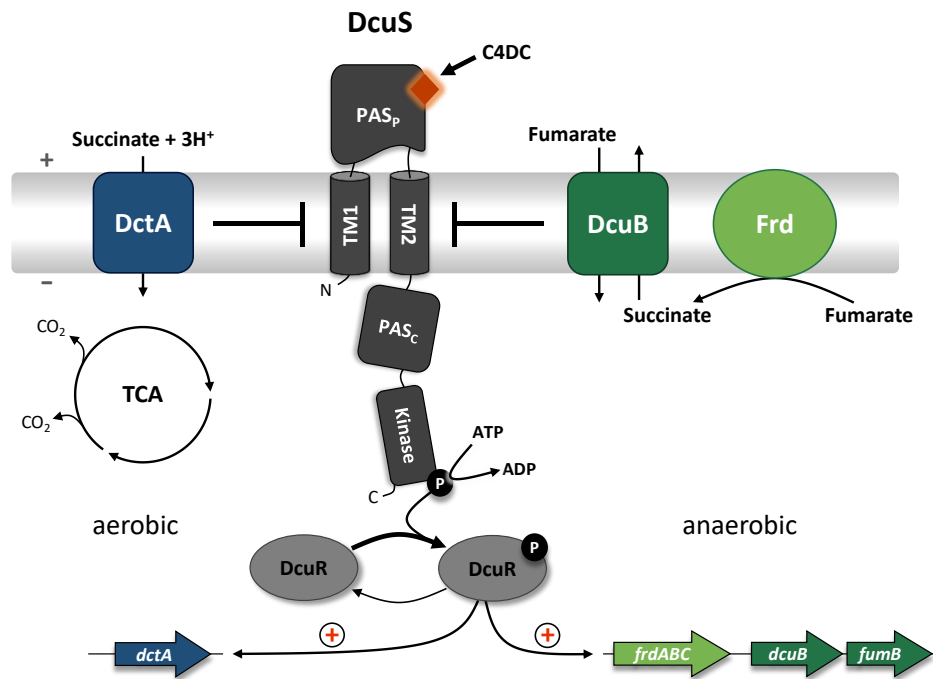
Figure 3. Regulation of the aerobic and anaerobic C4DC metabolism by DcuSR. DcuS detects periplasmic C4DC at the PAS$_P$ domain. This triggers autophosphorylation of the DcuS kinase domain. The phosphoryl group is then transferred to the response regulator DcuR. Under anaerobic conditions DcuR induces transcription of *frdABC*, *dcuB* and *fumB*. Under aerobic conditions DcuR induces the expression of *dctA*. The aerobic transporter DctA catalyzes the uptake of C4DCs such as succinate, which are metabolized in the TCA cycle. Fumarate serves anaerobically as an electron acceptor and is reduced to succinate by the fumarate reductase (Frd). Succinate is excreted from the cell by the anaerobic transporter DcuB in exchange for fumarate (or other C4DCs).

In addition to the regulation by DcuSR expression of *dctA* is repressed by ArcAB and stimulated by cAMP/CRP (Davies *et al*. 1999). The transcription of *dcuB* is also subject to catabolite repression by cAMP/CRP and nitrate repression by NarXL (Golby *et al*. 1998). Likewise, the expression of *dcuS* and *dcuR* itself is subject to the oxygen-dependent regulation by FNR and repression by NarXL in the presence of nitrate. In addition, there is a CRP binding site upstream of *dcuR* (within *dcuS*) (Oyamada *et al*. 2007). The expression of the other C4DC transporters is not regulated by DcuSR. *dcuA* is constitutively expressed together with *aspA* as co-transcript both under aerobic and under anaerobic conditions (Golby *et al*. 1998). *dcuC* is only expressed in anaerobiosis but is not repressed by glucose (Zientz *et al*. 1996).

2.4.2 DcuS structure and signal transduction

DcuS has a high sequence identity with several CitA proteins and is therefore a member of the CitA family of sensor histidine kinases (Bott *et al*. 1995; Janausch *et al*. 2002a). DcuS consists of 543 amino acids and has the typical domain architecture of the CitA family. DcuS comprises a periplasmic PAS (PASp) receptor domain flanked by two TM helices, a second cytosolic PAS (PASc) domain, and the kinase domain. In addition, as most sensor histidine kinases DcuS has a dimeric functional state and forms stable dimers and higher oligomers independent of effector availability (Stock *et al*. 2000; Scheu *et al*. 2010).

The sensory PAS_P domain located in the periplasm extends over positions 41 to 181 of DcuS and exhibits the typical PAS domain folding of a five-stranded β-sheet and six α-helices. PAS_P was crystallized as a monomer and therefore has no tendency to homo-dimerize in the isolated form (Cheung and Hendrickson, 2008). PAS_P preferentially binds C4DCs with an inter-carboxyl group spacing of 3.1 to 3.8 Å (Kneuper *et al*. 2005). L-malate appears to have the ideal conformation for the binding pocket of PAS_P (Cheung and Hendrickson, 2008; Zeltner, 2017).

In PAS_P of CitA from *Geobacillus thermodenitrificans* a binding pocket compaction causes an uplift or shift of the c-terminal α6 helix that triggers TM signaling (Salvi *et al*. 2017). The comparison of the crystal structures of L-malate bound PAS_P from DcuS (Cheung and Hendrickson, 2008) with the apo state PAS_P of CitA from *Klebsiella pneumoniae* (Sevvana *et al*. 2008) suggests a similar mechanism for DcuS of an α6 uplift that is directly reccieved by the transmembrane helix 2 (TM2) (Monzel and Unden, 2015).

The DcuS TM domain comprises the TM helices TM1 and TM2. In the inactive state of DcuS TM1 was assigned to the positions 20 to 40 and TM2 to positions 182 to 201 by accessibility studies (Monzel *et al*. 2015). TM1 changes its relative position in the membrane only minimally upon DcuS activation and the changes could not be assigned to any direction of movement. Therefore the primary function of TM1 was proposed to be anchoring in the membrane. (Monzel and Unden, 2015). Since TM2, in contrast to TM1, represents the direct physical connection between signal input in PAS_P and PAS_C in the cytoplasm, TM2 was suggested as a signal transducer in TM signaling (Sevvana *et al*. 2008). Changes in accessibility of TM2 in the membrane/water interface showed an axial piston-type shift of 4 - 6 Å of TM2 in the direction of the periplasm. α6 of PAS_P and TM2 form a joint α-helix that shifts as a parallel homo-dimer. However, the parallel shift was only shown for a small part of the N-terminus of TM2 (up to position 186) (Monzel and Unden, 2015). Furthermore, a SxxxGxxxG motif in TM2 appears to be important for DcuS function and homo-dimerization (Steinmetz, 2014).

TM2 and PAS_C are connected by a short linker of unknown function. However, some non-membrane-integral residues of the linker change the accessibility upon fumarate stimulated DcuS and (partial) deletions of the linker lead to inactivation of DcuS (Monzel, 2014; Monzel and Unden, 2015).

The cytoplasmic PAS_C domain can be assigned to DcuS positions 212 to 320 by solid state NMR data and the PAS_C homo-dimer crystal structure of CitA from *G. thermodenitrificans* (Etzkorn *et al*. 2008; Weisenburger *et al*. 2017). PAS_C has a high plasticity, which is proposed to be important for signal transduction (Etzkorn *et al*. 2008). Since the homo-dimerization of PAS_C is crucial for the C4DC sensitivity of DcuS, PAS_C was supposed to act as a silencer for the kinase. An incoming signal weakens the PAS_C homo-dimerization causing a reorganization, which transfers the signal to the kinase domain and activates the kinase activity (Monzel *et al*. 2013; Strecker, 2018).

The kinase domain consists of the N-terminal DcuS positions 321 to 543 The kinase domain includes the subdomains DHp (dimerization and histidine phosphotransfer) and CA catalytic and ATP-binding domain (CA). The two α-helices of the DHp subdomain form an anti-parallel four-helix bundle within a kinase dimer, which also contains the conserved histidine residue. Autophosphorylation by ATP is catalyzed by the CA subdomain (Marina *et al*. 2005; Bhate *et al*. 2015). The autophosphorylation can occur in either *cis* or *trans* in the kinase dimer and commonly depends on whether a left-handed (*cis*) or a right-handed (*trans*) helix bundle is present (Ashenberg *et al*. 2013). However, no detailed data on the structure and the mechanism of the kinase domain are available for DcuS.

2.4.3 The DcuS-transporter sensor complex: co-regulation by the C4DC transporters DctA and DcuB

The C4DC responsivity of DcuS and thus the regulation of target gene expression by DcuSR depends on the accessory function of the transporters DctA and DcuB. DctA and DcuB deficiency leads to C4DC-independent expression of the target genes due to constitutively active DcuS (Davies *et al*. 1999; Kleefeld *et al*. 2009; Witan *et al*. 2012b). It was possible to identify mutants for both DctA and DcuB which either have a defect in the transport or the regulatory function on DcuS. Consequently, the transporters do not have their own signal input site and DctA and DcuB do not represent co-sensors or metabolic flux sensors, but rather bifunctional co-regulators in the DcuS-DctA/DcuB sensor complex (Kleefeld *et al*. 2009; Steinmetz *et al*. 2014). Small amounts of free DcuS, which are always present in the cell and are not bound in the sensor complex, ensure the basal transcription of the transporters (Wörner

et al. 2018). For the transition to the sensor complex and the conversion of DcuS to an inactive but responsive state and vice versa a two-mode model was proposed. DcuB (DctA) acts as a molecular switch in order to ensure sufficient expression of the transporters even at low C4DC concentration (Unden *et al.* 2016b; Wörner *et al.* 2018). Due to the homology of DctA with GltP, which exists as a trimer (Raunser *et al.* 2006), it is assumed that the sensor complex with DcuS is formed with a transporter homo-trimer ($DcuS_2$-$DctA_3$) (Steinmetz *et al.* 2014; Wörner *et al.* 2018).

The co-regulatory function of the transporters is realized through a direct protein-protein interaction of DctA/DcuB with DcuS (Steinmetz *et al.* 2014; Wörner *et al.* 2016). The C-terminal amphipathic helix 8b of DctA, which is located in the cytoplasm, mediates the interaction with DcuS. It was shown that the LDxxxLxxxL motif of the helix 8b is essential both for the interaction with DcuS and for the co-regulatory function in the sensor complex (Witan *et al.* 2012). The PAS_C domain of DcuS is postulated to represent the counterpart for the interaction with DctA, but without considering the linker between TM2 and PAS_C separately (Monzel *et al.* 2013). A comparable interaction of the cytosolic helix 11b of DcuB which contains an AxxxAxxxA motif with DcuS has been proposed (Kleefeld *et al.* 2009; Witan, 2012). In addition, DcuS Cys accessibility studies indicate that TM2 position in the absence of DctA corresponds to the fumarate-activated state in presence of DctA (Monzel, 2014).

Based on these suggestions a model of signal transduction by DcuS in the sensor complex was proposed (Unden *et al.* 2016b) (Fig. 4). In the absence of DctA stabilization of the PAS_C dimer by the interaction with the helix 8B of DctA is lost. This leads to a relief of the PAS_C dimerization and abolishes its kinase silencing function, which in turn causes kinase activity (Fig. 4A). In presence of DctA and in the absence of external C4DC there is a stable interaction of DctA and DcuS, in which both the PAS_C dimer and the helix 8b act as silencers of the kinase and thus keep DcuS in the C4DC-responsive state (Fig. 4B). In the DcuS-DctA sensor complex C4DCs bound at the DcuS PAS_P domain trigger the piston-type uplift of TM2. This causes relieved PAS_C dimerization and activation of kinase activity (Fig. 4C). Uptake of C4DCs is catalyzed by DctA but has no effect on DcuS signal transduction. Nevertheless, molecular details of intramolecular DcuS signal transduction in the sensor complex are missing.
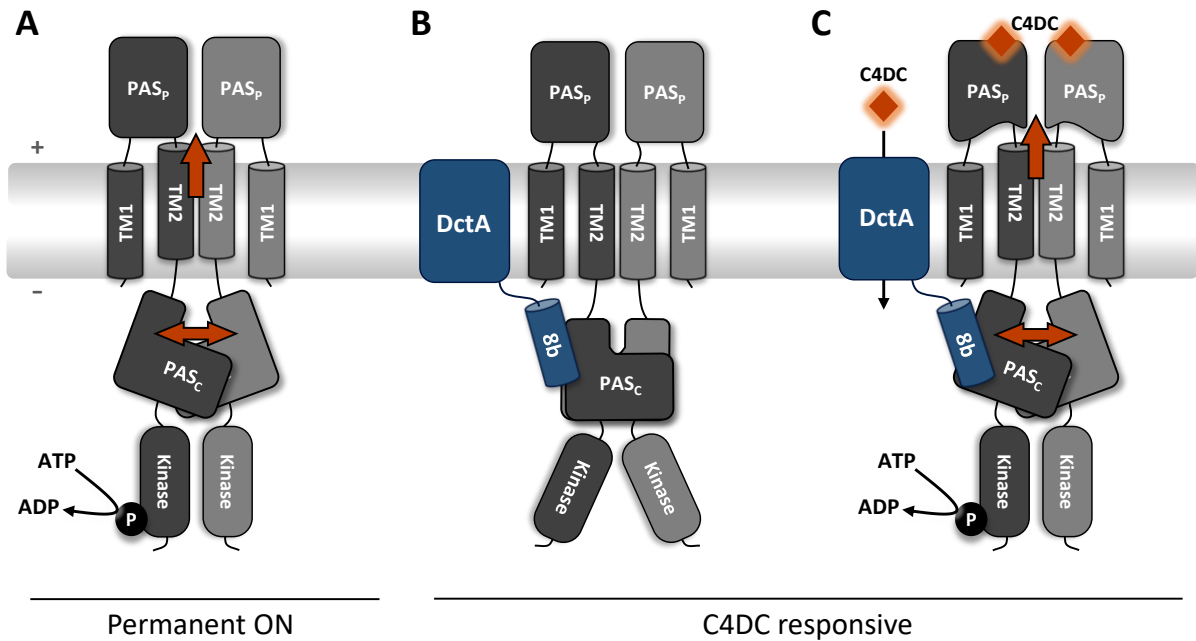
Figure 4. Model of dimeric DcuS signal transduction in the DcuS-DctA sensor complex. (A) DcuS dimer in the absence of DctA. C4DC-responsive DcuS-DctA sensor complex in absence (B) or presence (C) of C4DC. (Potential) Movements in DcuS signal transduction are indicated as orange arrows. For details see text. Figure modified according to Unden *et al*. 2016b.

2.5 Bacterial intramolecular signal transduction

The ability of sensor kinases to detect an external, periplasmic effector and to generate a corresponding cytoplasmic response requires a signal transfer. The physical separation of signal input and output by the membrane represents a special mechanical challenge. The highly dynamic nature of sensor kinases is essential for adopting to a stimulus by conformational changes enabling signal transduction. This nature of the proteins poses a challenge to structure elucidation and hinders progress in understanding molecular mechanisms. However, several insights in signal transduction of isolated domains or partial truncated sensor kinases have been obtained (Hendrickson, 2016).

In order to perceive an external stimulus an effector must be detected to initiate signaling. In the all-helical nitrate sensor NarX and the aspartate chemoreceptor Tar the ligand is bound within a four-helix bundle (Milburn *et al*. 1991; Cheung and Hendrickson, 2009). Structure comparison of the apo-state sensory domain with its corresponding ligand-bound state the of NarX indicate an axial displacement called "piston-type" shift of the C-terminal and N-terminal helices relative to each other (Cheung and Hendrickson, 2009).

In the related NarQ sensor kinase the signal transduction mechanism of the sensor domain was shown in a construct that also includes the TM domain and the adjacent cytoplasmic HAMP (Histidine kinases, Adenylate cyclases, Methyl accepting proteins, Phosphatases) domain. The

sensory periplasmatic 4-helical bundle is activated via a rotation together with a diagonal kinking, which is probably accompanied by a small piston-type shift of ~0.5 to 1 Å (Gushchin *et al.* 2017, 2020). The sensory PAS$_P$ domains from CitA sensor kinases undergo a compaction upon citrate binding, which leads to an uplift of the C-terminus. It is assumed that this is transferred directly to TM2 resulting in a piston-type shift (Sevvana *et al.* 2008; Salvi *et al.* 2017). The same suggestion was made for PAS$_P$ and TM2 of DcuS as a CitA family member (Cheung and Hendrickson, 2008; Monzel and Unden 2015; see section 2.4.2).

The typical structure of two TM helices in a dimeric sensor kinase enables a variety of TM signaling mechanisms (Gushchin and Gordeliy, 2018). A change of the position of TM1 and TM2 within a 4-helix bundle in a sensor dimer was examined in detail for the chemotaxis proteins Trg and Tar. Activation causes a changed position of the TM helices of a sensor monomer relative to one another (Chervitz and Falke, 1995; Hughson and Hazelbauer, 1996). In Tar this is a piston-type shift of about 1.0 to 1.6 Å of TM2 relative to TM1 within the monomer (Chervitz and Falke, 1996; Ottemann *et al.* 1999; Hall *et al.* 2011). A piston-type shift was also proposed for TM2 of DcuS and CitA (Monzel and Unden 2015; Salvi *et al.* 2017; see section 2.4.2) and for the single TM helix of BvgS from *Bordetella pertussis* (Lesne *et al.* 2017). Furthermore, rotation has also been described as a mechanism of TM signaling. A significant rotation by 90° of the signaling helices TM1 and TM5 represents the main mechanism of TM-signaling of the thermo- or fluidity sensor DesK. This restructuring is coordinated by two proline residues each within the two TM helices (Abriata *et al.* 2017). The signal transduction triggered by the binding of an effector by the *quorum sensing* membrane integral receptor LuxPQ represents a special case. The binding of Autoinducer-2 to the periplasmic binding protein LuxP causes an asymmetrical rotation within a TM four-helix bundle in the associated membrane integral LuxQ dimer (Neiditch *et al.* 2006). A combination of different movement mechanisms is described for the sensor kinase PhoQ. A change in the concentration of divalent cations triggers a tilting (scissors-like movement) of all the helices of a four-helix bundle in the sensor dimer, which is accompanied by a slight rotation at the C-terminus. It is assumed that a centrally located proline residue is driving the rearrangement in the signal transfer (Lemmin *et al.* 2013; Molnar *et al.* 2014). The investigation of the sensor kinase NarQ represents a unique case, since here it is possible to gain insight in its TM signaling mechanism directly by aligning the apo with a symmetrical holo (nitrate-bound) crystal structure of a construct consisting of the sensor, the TM domain, and the cytosolic HAMP domain. NarQ exhibits a combination of different conformational changes in TM signaling. Activation of NarQ causes a rotation in the periplasm/membrane interface combined with

scissoring of the TM helices and in the cytoplasm/membrane interface a piston-type shift of TM1 relative to TM2 (Gushchin *et al*. 2017).

Generally, another cytoplasmic domain is interposed between the TM domain and the actual kinase, which processes the incoming signal. Most frequently, these are HAMP, PAS or GAF (cGMP-specific phosphodiesterases, adenylate cyclases and FhlA) domains. Various models of HAMP domain signaling have been proposed, such as the dynamic bundles model, whereby the general stability of the dimer is influenced by the signaling state of the sensor (Parkinson *et al*. 2010; Sukomon *et al*. 2017), or the gearbox model that is based on a change in the packing within the coiled coil of the four-helix bundle (Hulko *et al*. 2007, 2011). The TM piston-type signal of NarQ is converted to helical rotation of the cytoplasmic HAMP domain by a proline hinge between TM2 and the AS1 helix of the HAMP domain (Gushchin *et al*. 2017). Cytoplasmic PAS domain signaling is less well studied than in HAMP domains but few signaling mechanisms have been proposed. In NifL it is assumed that a signal is transmitted from PAS1 to the immediately adjoining PAS2 domain by a change in the quaternary structure in the homo-dimer (Salvany *et al*. 2010). A similar mechanism by an overall weakening of PAS_C homo-dimerization in DcuS and CitA is proposed to transduce the signal to their C-terminal kinase domain (Etzkorn *et al*. 2008; Monzel *et al*. 2013; see section 2.4.2).

2.6   Thesis objectives

The C4DC dependent regulation and C4DC transport of *E. coli* has been extensively studied and DcuSR represents a well understood TCS. DcuSR and the related transport of L-aspartate and L-malate by the anerobic Dcu transporters for fumarate respiration was even recently shown to be promotive in *Salmonella typhimurium* gut-lumen colonization in mice (Nguyen *et al*. 2020). However, due to their physical nature, structural data of membrane proteins, especially sensor histidine kinases, are underrepresented in the overall scientific data situation and their signaling mechanisms are still poorly understood (Hendrickson, 2016; Gushchin *et al*. 2017).

No structural data are available for full-length DcuS, especially for the TM domain. For DcuS TM signaling TM2 was identified as the main TM signal transducer. The data were limited, however, to α6 of PAS_P and the N-terminus of TM2. Thus, the postulated piston-type parallel displacement of TM2 is verified only for this region. TM1 showed only minor changes in membrane position and was not investigated further (Monzel and Unden, 2015).

Therefore, the structure of TM2, the adjacent cytoplasmic linker, and the N-terminus of PAS_C (with focus on α1) as well as TM1 in the DcuS dimer will be analyzed by oxidative *in vivo*

cysteine cross-linking (Cys CL) of DcuS single Cys variants. In this way the significance of the SxxxGxxxG motif in TM2 for the homo-dimerization will be tested and verified. Time-resolved Cys CL should reveal position (domain) dependent different CL dynamics representing conformational changes of DcuS upon fumarate activation to provide more detailed insight into DcuS TM signaling. It will also be examined how a DctA deficiency affects the dynamic of the DcuS CL reaction in different domains in order to gain structural information on how DcuS is converted into the C4DC-responsive state in the DcuS-DctA sensor complex.

The adaption of C4DC metabolism on the transcriptomic level is well studied, but a comparative study of the effect of C4DC, especially fumarate, on the aerobic and anaerobic proteome is lacking. Therefore, the effect of fumarate on the aerobic and anaerobic *E. coli* proteome was examined with a 'shotgun proteomics' approach. This should contribute to a broader understanding of the regulation of the C4DC metabolism through the direct, DcuSR-dependent regulation as well as potential indirect, DcuSR-independent regulation.

3 Experimental procedures

The experimental procedures of Surmann *et al*. (2020) and Stopp *et al*. (2021) are described in the publication, respectively. All additional experimental procedures that were used in the course of this study are described in the following.

3.1 Bacterial strains, plasmids and primers

Bacterial strains, plasmids and primers used in the course of this study are listed in Table 5, 6, 7, and 8 of the appendix.

3.2 Chemicals

The chemicals are listed in Table 9 of the appendix.

3.3 Media and buffers

All components were dissolved in demineralized H_2O. If necessary, all media, solutions and buffers have been autoclaved or sterile filtered, if indicated, before use.

3.3.1 General media and buffers

LB medium (Bertani (1951))

    10 g/l Tryptone

    5 g/l Yeast extract, 10 g/l NaCl

    10 g/l NaCl

A ready mix was used (Roth. L3022).

SOC medium (Hanahan, 1983)

    20 g/l Bacto tryptone

    5 g/l Yeast extract

    0.584 g/l NaCl

    0.19 g/l KCl

    2.03 g/l $MgCl_2$ x 6 H_2O

    2.46 g/l $MgSO_4$ x 7 H_2O

    3.96 g/l Glucose x H_2O

A ready mix was used (AE27.1, Roth) and glucose in the appropriate amount was added.

LB-Agar

LB medium

15 g/l Agar-Agar Kobe I

Enriched M9 (eM9) medium (Miller, 1992; Lehnen *et al*. 2002)

10 x M9 stock solution (pH = 7)   Supplements

75 g/l Na_2HPO_4 x 2 H_2O 10 ml/l 10 mM $CaCl_2$

30 g/l KH_2PO_4 1 ml/l 2 M $MgSO_4$

5 g/l NaCl   eM9 supplements (Lehnen *et al*. 2002)

10 g/l NH_4Cl 10 ml/l 10 % (w/v) AHC

5 ml/l 1 % (w/v) L-Tryptophan

Carbon source   Electron acceptor

50 mM Glycerol   20 mM Dimethyl sulfoxide (DMSO)

Effector

20 mM Fumarate

TSB buffer   **Glycerol-MOPS-buffer**

LB medium with added: 1 mM MOPS

100 g/l Polyethylene glycol (PEG) 6000   15 % (v/v) Glycerol

2.46 g/l $MgSO_4$ x H_2O

2.03 g/l $MgCl_2$ x 6 H_2O

100 ml/l DMSO

All ingredients were dissolved in H_2O and sterile filtered.

Agarose gel

1 % (w/v) Agarose

25 μl/l RedSafe[TM] Nucleic Acid staining solution

in 1x TAE-buffer

Antibiotics

The antibiotics used in this study are listed in Table 1.

Table 1. Antibiotics used in this study.

Antibiotics	Stock solution	Final conc. (medium)
Chloramphenicol	20 mg/ml in Ethanol	20 µg/ml
Kanamycin	50 mg/ml in H_2O	50 µg/ml
Tetracycline	15 mg/ml in Ethanol: H_2O 1:1	15 µg/ml

3.3.2 β-galactosidase assay (Miller, 1992)

β-galactosidase reaction buffer (pH = 7) (Monzel *et al*. 2013)

> 100 mM Potassium phosphate buffer
>
> 10 mM KCl
>
> 1 mM $MgCl_2$
>
> 8 mM Dithiothreitol (DTT)
>
> 0.005 % (w/v) Cetyltrimethylammonium bromide (CTAB)
>
> 0.0025 % (w/v) Sodium deoxycholate (SDC)

DTT was freshly added before use.

Solutions for the β-galactosidase assay

> 4 mg/ml ONPG
>
> 1 M Na_2CO_3

3.3.3 Oxidative *in vivo* Cysteine cross-linking (Cys CL)

Cu[II]-(1,10-phenanthroline)₃ (Cu-phenanthroline) solution

> 4 mM $CuSO_4$
>
> 3.33 mM Sodium phosphate buffer (pH = 7.4)
>
> 13 mM 1,10-Phenanthroline

For the time-resolved cysteine cross-linking (3.6.2) the concentrations of the components of the Cu-phenanthroline solution were adjusted as indicated in Table 4.

Stop solution/SDS loading buffer

> 20 mM Tris(hydroxymethyl)-aminomethane (Tris)
>
> 8 mM Sodium phosphate buffer (pH = 7.8)
>
> 12.5 mM Ethylenediamine tetraacetic acid disodium salt dihydrate (EDTA)
>
> 12.5 mM N-ethylmaleimide (NEM)
>
> 1.25 % (w/v) Sodium dodecyl sulfate (SDS)
>
> 12.5 % (w/v) Sucrose
>
> 0.2 % (w/v) Bromophenol blue

3.3.5 SDS-PAGE

Gradient separation gel (5 to 12 %)

Upper separation gel 5 % (3,0 ml)

> 1.70 ml H_2O
>
> 0.50 ml Acrylamide mix (30 % Acrylamide; 0.8 % Bisacrylamide)
>
> 0.75 ml Tris/HCl (1.5 M; pH = 8.8) (separation gel buffer)
>
> 30 µl 10 % SDS
>
> 7.5 µl N,N,N',N'-Tetramethyl ethylenediamine (TEMED)
>
> 12.5 µl 10 % (w/v) Ammonium persulfate (APS)

Lower separation gel 12 % (3,0 ml)

> 1.00 ml H_2O
>
> 1.2 ml Acrylamide mix (30 % Acrylamide; 0.8 % Bisacrylamide)
>
> 0.75 ml Tris/HCl (1.5 M; pH = 8.8) (separation gel buffer)
>
> 30 µl 10 % SDS
>
> 7.5 µl TEMED
>
> 12.5 µl 10 % (w/v) APS

Stacking gel (4 %)

    4.7 ml H_2O

    1.9 ml Acrylamide mix (30 % Acrylamide; 0,8 % Bisacrylamide)

    2.1 ml 0,5 M Tris/HCl, pH 6.8 (stacking gel buffer)

    0.081 ml SDS (10 % (w/v))

    20 µl TEMED

    40 µl 10 % (w/v) APS

Running buffer (x10)

    250 mM Tris

    1.92 M Glycine

    1 % (w/v) SDS

3.3.6 Buffers and solutions for the *semi-dry* Western blotting (Towbin *et al*. 1979)

Transfer buffer

    25 mM Tris

    192 mM Glycine

    20 % Ethanol (v/v)

Immunostaining

Blocking buffer

    5 % (w/v) Skimmed milk powder

    0.1% (v/v) Polyoxyethylene (20) sorbitan monolaurate (Tween 20)

    in 1 x PBS

    diluted from 10 x PBS-buffer (pH 7.5):   1.37 M NaCl

                                          27 mM KCl

                                          0.1 M Na_2HPO_4

                                          20 mM KH_2PO_4

Washing buffer   Antibody solution

     0.1 % (v/v) Tween 20   1 % (w/v) Bovine serum albumin (BSA)

     in 1 x PBS   0.1 % (w/v) Tween 20

                                 Antibody (diluted)

                                 in 1 x PBS

Primary antibody

Anti-DcuS-PD from rabbit, against the periplasmic DcuS domain (PAS_P) (Müller, 2007); dilution 1:10,000

Secondary antibody

Anti-IgG against rabbit, HRP conjugate (Anti-rabbit-HRP) (Sigma-Aldrich); dilution 1:10,000

Chemiluminescence detection

WesternBright^{TM} ECL HRP substrate (Advansta)

3.4   Growth of *Escherichia coli*

All strains of *E. coli* used in this study are listed in Table 5. *E. coli* was always grown in the presence of the appropriate antibiotics (Tab.1), unless otherwise stated.

Genetic purposes

For the purpose of genetic work, the cultures of the *E. coli* strains were incubated aerobically in test tubes filled with 5 ml LB medium at 37°C and 200 rpm for 16 h (Excella E24, New Brunswick Scientific). Aerobic pre-cultures were cultivated in the same way.

Production of electrocompetent cells (Farinha und Kropinski, 1990)

For production of electrocompetent cells 200 ml LB medium were inoculated with 2 % of an aerobic *E. coli* pre-culture of the respective strain (IMW260, C43, IMW660). The main culture was incubated aerobically in baffled flasks (V = 1.0 l) at 37°C and 160 rpm (Excella E24, New Brunswick Scientific) until an optical density at 578 nm (OD_{578nm}) of 0.5 to 0.8 was reached. Afterwards the cells were pelleted by centrifugation (6000 rpm, 5 min; Centrifuge 5403, Eppendorf) in sterile tubes at 4°C. This was followed by washing three times with 10 ml ice-

cold glycerol-MOPS buffer (5000 rpm, 10 min; Centrifuge 5403, Eppendorf). Finally, the cells were resuspended in 1/20 of the cell culture volume glycerol-MOPS buffer and aliquoted. The cells were stored at -80°C until further use.

Production of chemical-/heat-competent cells

The production of chemical-/heat-competent cells was carried out analogously to the production of electrocompetent cells (see above) with the exception that the main culture was inoculated with 4 % of an *E. coli* XL1-Blue culture. In addition the main culture was cultivated without antibiotics. After an $OD_{578nm} = 0.5$ to 0.8 was reached the cells were pelleted in sterile centrifuge tubes at 4°C (6000 rpm, 5 min; Centrifuge 5403, Eppendorf) and the cells were washed twice with 10 ml of ice-cold TSB buffer (6000 rpm, 7 min; Centrifuge 5403, Eppendorf). The cells were resuspended in TSB buffer equivalent to 1/100 of the cell culture volume. For storage at -80°C, the cell suspension was divided into 100 µl aliquots each.

Anaerobic *dcuB-lacZ* expression assay

For the anaerobic reporter gene assay based on the *dcub-lacZ* expression the DcuS deficient strain IMW260 was transformed with the derivatives of the plasmid pMW336. *E. coli* was grown in sterile 96-deep-well plates (VWR International) covered with aluminum foil. The 96-deep-well plates were filled with 1 ml enriched M9 (eM9) medium per well with 20 mM glycerol as carbon/electron source and 20 mM DMSO as electron acceptor. 20 mM fumarate was added as needed. The 96-deep-well plates of the pre-culture were inoculated with one colony of transformed IMW260 per well and were incubated at 37°C for 24 h. The main culture was inoculated with 1 % (with fumarate) or 10 % (without fumarate) of the cell suspension from the pre-culture. The plates were placed in an anaerobic jar (OXOID), evacuated for 15 min and gassed with nitrogen gas (1.2 bar, purity 99.999 %, Westfalengas). The main culture was incubated at 37°C for 32 h (without fumarate) or 16 h (with fumarate). Growth was checked (96-*well-reader*: EL808, Biotek; 315 µl) and *E. coli* cultures that reached an $OD_{570nm} = 0.25$ to 0.6 were used for the β-galactosidase assay.

Oxidative *in vivo* cysteine cross-linking (Cys CL)

For the *in vivo* cysteine cross-linking cells of the *E. coli* strain C43 were transformed with derivatives of the plasmid pMW336 encoding DcuS single Cys variants of the Cys free DcuS variant (DcuS$_{Cys0}$). Growth was carried out in sterile 48-well-plates with 700 µl LB medium per well. If the influence of an effector on DcuS was tested, 50 mM fumarate was added. The pre-cultures were inoculated with one colony per well and incubated aerobically for 16 h at 30°C under vigorous shaking (1050 rpm; Titramax 1000, Heidolph). The main culture was

inoculated with 2 % of the preculture and incubated also aerobically at 30°C and 1050 rpm for 6 h. The expression of the DcuS varaints was induced with 1 mM IPTG after 2 h.

Strain collection

5 ml of LB medium with an appropriate antibiotic in test tubes were inoculated with one colony each and incubated with shaking for 16 h (37°C, 200 rpm; Excella E24, New Brunswick Scientific). The cells were pelleted by at 4°C (6000 rpm, 5 min; Centrifuge 5403, Eppendorf) to remove the medium. For storage, the cells were resuspended in LB medium and 50 % (v/v) glycerol in a 1:1 ratio, transferred to sterile 1.5 ml tubes and stored at -80°C.

3.5   Molecular genetic methods

The isolation of plasmids was carried out with the GenElute^{TM} HP Plasmid Miniprep Kit (Sigma-Aldrich).

3.5.1 Transformation by electroporation

The transformation by electroporation was prepared by mixing 1 µl of plasmid solution (50 - 100 ng plasmid) with 50 µl of cell suspension in sterile electroporation cuvettes (1 mm electrode gap; PEQLAB). The cuvettes were pre-cooled and kept on ice as soon as they were pre-loaded with cells/plasmid until transformation. When the strain IMW260 was transformed, five times the amount of plasmid was used. The transformation was carried out by a pulse of 2500V for 6 ms (Eppendorf Eporator®). The entire batch was immediately transferred to 1 ml of preheated SOC medium and incubated at 37°C for 90 min at 1000 rpm (Thermomixer comfort®; Eppendorf) for regeneration. 50 to 200 µl of the suspension were plated on appropriate LB agar plates and incubated aerobically at 37°C for at least 16 h.

3.5.2 Transformation by heat-pulse

For the transformation by heat-pulse 50 µl of chemical-/heat competent XL1-Blue cells were mixed with 3 µl of DpnI-digested plasmid DNA in sterile 1.5 ml tubes. The transformation mixture was heated at 42°C for 45 s, followed by incubation on ice for 2 min. Then 1 ml of pre-warmed SOC medium was added to the transformation mix and the cells were incubated at 37°C for 90 min shaking at 1000 rpm (Thermomixer comfort®; Eppendorf). The entire batch was plated on LB agar plates with the appropriate antibiotic and incubated aerobically at 37°C for at least 16 h.

3.5.3 Polymerase chain reaction (PCR)

The polymerase chain reaction was used to amplify plasmid DNA in the site-directed mutagenesis (3.5.4) or DNA fragments for sequencing (3.5.6). The Phusion® High-Fidelity DNA polymerase (Thermo Scientific) was used for all applications and the corresponding composition of the PCR mixture and the PCR protocol are given in Tables 2 and 3. The primers for the amplification were synthesized by Eurofins MWG and Sigma-Aldrich and are shown in Table 7. The annealing temperature and the elongation time were adjusted to the respective primer and template. The protocols were run by the Thermocycler C1000 Touch Thermal Cycler (Bio-Rad) und MJ Mini-Cycler (Bio-Rad).

Table 2. Composition of the PCR reaction mixture.

Component	$Phusion^{®}$
HF Phusion buffer (5 x)	10 µl
dNTP Mix (10 mM)	250 µM
Primer	each 0.5 µM
DMSO	3 % (v/v)
Template DNA	50 ng
Polymerase	1 U
H_2O	ad 50 µl

Table 3. PCR protocol of the Phusion® polymerase.

Step	Temperature	Time
1) Initial denaturation	98°C	30 s
2) Denaturation*	98°C	10 s
3) Annealing*	$T_M + 3$°C	30 s
4) Elongation*	72°C	30 s/kb
5) Final elongation	72°C	10 min

* The steps 2 to 4 were repeated 30 times.

3.5.4 Site-directed mutagenesis

The DcuS single cysteine mutations in pMW336 were generated by site-directed mutagenesis using PCR (see section 3.5.3). The individual primers used to exchange the corresponding nucleotides for the construction of the DcuS single cysteine variants are listed in Table 7. After the amplification, the parental/template DNA was digested with the restriction enzyme DpnI (37°C, 1 h) and transformed into XL1-Blue cells (see section 3.5.2). The success of the mutagenesis was checked by sequencing.

3.5.5 Agarose gel electrophoresis of nucleic acids

The agarose gel electrophoresis was used to separate DNA molecules to verify the success of the PCR amplification. The agarose gels were prepared by dissolving 1 % agarose and Red-Safe[TM] Nucleic Acid Staining Solution in TAE buffer by boiling and then re-solidifying the agarose gel mixture in an agarose gel tray. 5 µl of the DNA from the PCR were mixed with 1 µl loading dye (Thermo Scientific) and applied to the agarose gel. The DNA was separated based on their size in the electric field at constant voltage (90 V) for 50 min.

3.5.6 DNA sequencing

All plasmids and DNA fragments were sequenced by LGC Genomics. The primers used for sequencing are listed in Table 8.

3.6   Biochemical methods

### 3.6.1   Quantitative β-galactosidase assay

The quantitative β-galactosidase assay was used to measure *dcub-lacZ* expression in IMW260 depending on complementation of the DcuS deficiency with DcuS single Cys variants (pMW36 derivatives). The activity was measured according to Miller (1992) by hydrolysis of the chromogenic substrate *o*-nitrophenyl-β-D-galactopyranoside (ONPG) to galactose and *o*-nitrophenol. The yellow-colored *o*-nitrophenol can be detected photometrically at 420 nm. A modified protocol of the quantitative β-galactosidase assay was applied (Griffith and Wolf 2002; Monzel *et al*. 2013). All measurements were performed in 96-well-microtiter plates (MTP) (Sarstedt) with the MTP-Reader (EL808, Biotek) with a total volume of 315 µl per well. After growth (see section 3.4) the optical density of the *E. coli* culture was measured at 570 nm ($\Delta OD_{570nm(culture)}$). 200 µl of the cell culture and 800 µl of β-galactosidase reaction buffer were transferred to 96-deep-well plates (VWR International) per well and the cells were disrupted by 15 cycles of the "mix function" of an automatic multi-channel pipette (E4 XLS Rainin, Mettler-Toledo). The mixture of disrupted cells and reaction buffer of each individual culture was divided into four wells (185 µl each) of a 96-well-MTP. and the detection reaction was started by adding 40 µl ONPG (4 mg/ml) per well. The reaction was stopped by addition of 90 µl NaCO$_3$ (1 M) per well. The extinction was measured at 415 nm (ΔE_{415nm}) as well as interference of cell debris ($\Delta OD_{570nm(debris)}$) with the MTP reader and the β-galactosidase activity in Miller units [MU] was calculated using Equation 1.

$$[MU] = \frac{1000 \cdot \left(\Delta E_{415nm} - \Delta OD_{570nm(culture)}\right)}{t[min] \cdot V_{sample}[ml] \cdot \Delta OD_{570nm(debris)}} \qquad \text{Equation 1}$$

3.6.2 Oxidative *in vivo* cysteine cross-linking

The sulfhydryl groups of two cysteine residues can be covalently cross-linked with one another via a disulfide bond by oxidation using a catalyst such as Cu[II]-(1,10-phenanthroline) (Cu-phenanthroline) (Bass *et al.* 2007). If two cysteine residues within two monomers each of a dimeric protein are in close proximity, they can be cross-linked with high efficiency (Fig. 1A). On the other hand, two cysteine residues that are located at a great distance from one another or on opposite sides of two monomers in the dimer cannot be cross-linked at all or can only be cross-linked with low efficiency (Fig. 1B).

For the *in vivo* cysteine cross-linking (Cys CL) of DcuS derivatives of the plasmid pMW336 (Scheu *et al.* 2010), which encodes the Cys free DcuS variant (C199S + C471S; DcuS$_{Cys0}$), were used. All single Cys variants of DcuS are listed in Table 6.
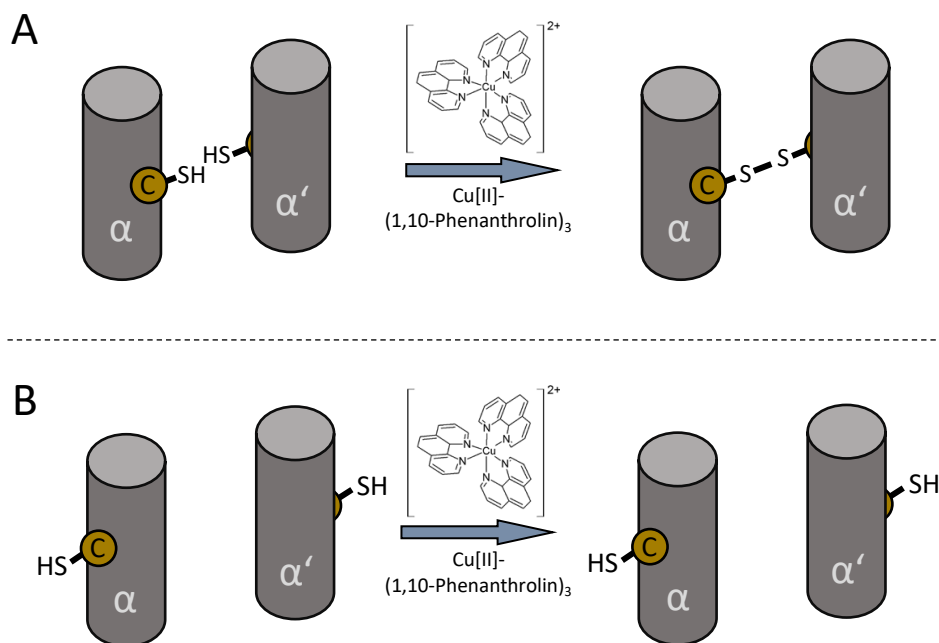
Figure 5. Scheme of the principle of Cys CL with Cu-phenanthroline using the example of dimeric α-helices. Individual cysteine residues (C) of the α-helices (α and α') are shown as yellow circles and their sulfhydryl groups are shown, respectivly. (A) illustrates the position of the cysteine residues in a shared interface of of the α-helices, whereas (B) shows α-helices whose cysteine residues are on opposite sides. For detailed information see section 3.6.2.

After cultivation (see section 3.4) 100 µl of the cell suspension were transferred to one well of a 48-well-plate (Sartdedt). The reaction was started by adding 100 µl of the Cu-phenanthroline solution to the cell suspension in the wells. The reaction mixture was incubated for 10 min at

25°C with vigorous shaking at 1050 rpm (Titramax 1000; Heidolph). The reaction was stopped by adding 50 µl of Stop solution/SDS loading buffer and subsequent shaking for 1 min at 1050 rpm. The samples were transferred to 1.5 ml tubes, boiled at 95°C for 5 min (Thermomixer comfort®; Eppendorf) and applied to SDS-PAGE (see section 3.6.3).

Time-resolved oxidative *in vivo* cysteine cross-linking

The time-resolved oxidative *in vivo* Cys CL was carried out in the same way as previously described for the oxidative *in vivo* Cys CL (see section 3.6.2). In order to obtain a course of the CL reaction as a function of the reaction time, the reaction conditions were optimally adapted for each individual variant in terms of the Cu-phenenathroline concentration and reaction temperature (Tab. 4). If a reaction was carried out at 4°C, the cell suspension was equilibrated after growth for 20 min at 4°C. For the actual CL reaction, 500 µl of cell suspension from exactly the same culture were distributed evenly into five wells of a 48-well plate, each with 100 µl, after growth. The reaction was stopped in one of the five wells after 0.5, 3, 10, 20 min, respectively. 100 µl of H_2O was added to the remaining well of the five wells and Stop solution was immediately added representing 0 min of CL reaction time.

Table 4. Optimized reaction conditions for individual single Cys variants in the time-resolved Cys CL. All concentrations refer to the (Cu-phenanthroline) solution. In the column DcuS variants single-Cys variants derivatives of DcuS$_{Cys0}$ are listed.

DcuS varaint	c(CuSO$_4$)	c(1,10-phenanthroline)	c(Na-PO$_4$) buffer	T
G190C	2 mM	6.5 mM	3.33 mM	4°C
G194C	0.5 mM	1.625 mM	3.33 mM	4°C
K206C	4 mM	13 mM	3.33 mM	25°C
I208C	0.5 mM	1.625 mM	3.33 mM	4°C
L209C	0.5 mM	1.625 mM	3.33 mM	4°C
E213C	0.5 mM	1.625 mM	3.33 mM	4°C
R224C	0.5 mM	1.625 mM	3.33 mM	4°C
L228C	0.5 mM	1.625 mM	3.33 mM	4°C
I231C	0.5 mM	1.625 mM	3.33 mM	4°C
G234C	0.5 mM	1.625 mM	3.33 mM	4°C

3.6.3 SDS-PAGE

The sodium dodecyl sulphate polyacrylamide gel electrophoresis (SDS-PAGE) enables a separation of a mixture of proteins based on their molecular weight in an electrical field. The Mini-PROTEAN system (Bio-Rad) was used for all experiments.

To produce a gradient gel (5 to 12 %), APS was added to the separately prepared solutions of the upper and lower separating gel concentrations. 2.5 ml each of the 5 % and 12 % solutions were taken up one after the other with a 5 ml serological pipette and were mixed gently by an

air bubble. The solutions were then poured between the glass plates of the Mini-PROTEAN®
Tetra Cell Casting Module (Bio-Rad). The pipette was gently moved back and forth across the
gap to distribute the solution evenly within the chamber. Finally, after the gradient separating
gel had polymerized, the stacking gel solution was poured onto it and allowed to polymerize
completely.

20 µl of all samples from the Cys CL (see section 3.6.2) were applied to gradient gels. The
proteins were separated by electrophoresis at constant voltage (150 V) for 120 min.

3.6.4 *Semi-dry* Western blotting, immunostaining and chemiluminescence detection

Semi-dry Western blot

For specific detection of proteins using appropriate antibodies, the proteins were transferred
from the polyacrylamide gels onto a nitrocellulose membrane (Amersham™ Protran™; Cytiva)
after SDS-PAGE. For this purpose, two layers of Whatman® chromatography paper (GE
Healthcare) were placed on the anode of the blotter (Semi-Dry-Blotter MAXI; Roth). The
nitrocellulose membrane (Amersham ™ Protran ™ 0.45 NC; Cytiva), the gel and finally two
layers of chromatography paper were placed on top. For equilibration, all components were
previously soaked in transfer buffer. After mounting the cathode, the proteins were transferred
at a constant current ($0.6 \, \text{mA/cm}^2$) within 90 min.

Immunostaining

After completion of the protein transfer the membrane was incubated in 20 ml of bocking buffer
at 4°C for 16 h on the tumble shaker (Polymax 1040; Heidolph). This saturates free binding
sites in the membrane and prevents non-specific binding of the antibodies. The membrane was
then incubated with the antibody solution of the corresponding primary antibody (Anti-DcuS-
PD) and secondary antibody (Anti-rabbit-HRP) for 60 min each at room temperature (RT) on
the tumble shaker. After each incubation step, excess antibody was removed by washing three
times for 5 min with 20 ml of washing buffer.

Chemiluminescence detection

DcuS protein on the membrane was detected via the „horseradish peroxidase" (HRP), which is
coupled to the secondary antibody. The membrane was incubated with 1 ml of the
WesternBright™ ECL HRP substrate (Advansta) between two layers of rigid foil for 4 min at
RT. Excess substrate was removed and an X-ray film (LucentBlue X-ray film; Advansta) was

exposed to the membrane for 10 s in a film cassette. The X-ray film was incubated in developer solution (GBX developer/replenisher) for 25 s. Immediately afterwards, the X-ray film was rinsed off with H_2O and incubated for 15 s in fixing solution (GBX fixer/replenisher). All work with the X-ray film was carried out in the darkroom.

3.5   Bioinformatics

Databases & Research

EcoGene:	http://www.ecogene.org
PubMed:	http://www.ncbi.nlm.nih.gov/pubmed/
OpenWetWare:	http://openwetware.org/wiki/Main_Page
Uniprot:	http://www.uniprot.org

Sequence alignment

BLAST:	http://blast.ncbi.nlm.nih.gov/Blast.cgi
Clustal Omega:	https://www.ebi.ac.uk/Tools/msa/clustalo/

3D structure prediction

QUARK ONLINE:	http://zhanglab.ccmb.med.umich.edu/QUARK/
I-TASSER	https://zhanglab.ccmb.med.umich.edu/I-TASSER/

3D structure visualization and manipulation

Chimera v. 1.14:	http://www.cgl.ucsf.edu/chimera/

Additional programs

Clone Manager:	http://www.scied.com/index.htm
FinchTV:	http://www.geospiza.com/Products/finchtv.shtml
ImageJ	https://imagej.nih.gov/ij/
Oligo Calc:	http://www.basic.northwestern.edu/biotools/oligocalc.html
Protein MW calculator:	http://www.sciencegateway.org/tools/proteinmw.htm
Translation:	http://web.expasy.org/translate/

4 Results

4.1 Transmembrane signaling by DcuS

In *E. coli* the DcuSR TCS regulates uptake and utilization of C_4-dicarboxylates (C4DC) (Unden *et al*. 2016a). The membrane integral sensor histidine kinase DcuS detects C4DCs like fumarate or malate as well as citrate at the periplasmic PAS_P domain. Stimulus perception causes a cytoplasmic autophosphorylation of a conserved histidine residue at the kinase domain (Janausch *et al*. 2002b). Therefore, the physical separation of periplasmic signal input and cytoplasmic autophosphorylation requires a signal transfer mechanism across the membrane. The TM region of DcuS is formed by two TM helices, TM1 and TM2 that were assigned to the positions 20 to 40 (TM1) and 182 to 201 (TM2) by Cys accessibility studies. A piston-type movement of TM2 plays an important role in TM signaling of DcuS whereas TM1 was essentially static (Monzel and Unden 2015). In order to solve the roles of TM1 and TM2 in TM signaling, the characteristics of the TM helices (in particular of TM2) and their contribution to TM signaling were analyzed. By Cys scanning and cross-linking (CL) of the full TM domains and an adjoining linker region, the α-helicity and dimerization was characterized, both in the inactive and the fumarate activated state. The data allowed to integrate previous interaction and dimerization studies of TM2 (Steinmetz, 2014) in a detailed model for TM signaling of TM2 and the linker region.

4.1.1 TM signaling and cytoplasmic signal conversion by TM2 and the linker

The data have been published (Stopp *et al*. 2021) and are only briefly described.

Oxidative *in vivo* cross-linking of single Cys variants in TM2 and the adjacent cytoplasmatic region

In DcuS TM2 and a short linker connect PAS_P and PAS_C. For TM2 a piston-type movement in the direction of the periplasm was identified as a major movement upon fumarate activation. Initial experiments suggested a parallel DcuS dimer of α6 of PAS_P and the N-terminal part of TM2 up to residue Ser186 (Monzel and Unden, 2015).

To further analyze DcuS dimerization and to gain information on the structure of TM2 and the linker a complete set of single Cys variants of DcuS was used up to residue Glu213, which is located on the cytoplasmic side in the N-terminus of the α1-helix in PAS_C. Each amino acid was individually replaced genetically by a Cys residue in the plasmid-encoded Cys-less variant ($DcuS_{Cys0}$). In $DcuS_{Cys0}$, the wildtype Cys199 and Cys471 are replaced by Ser, without a loss

in DcuS sensitivity and only a moderate decrease in DcuS fumarate stimulation (Scheu *et al.* 2010; Monzel and Unden, 2015; Stopp *et al.* 2021).
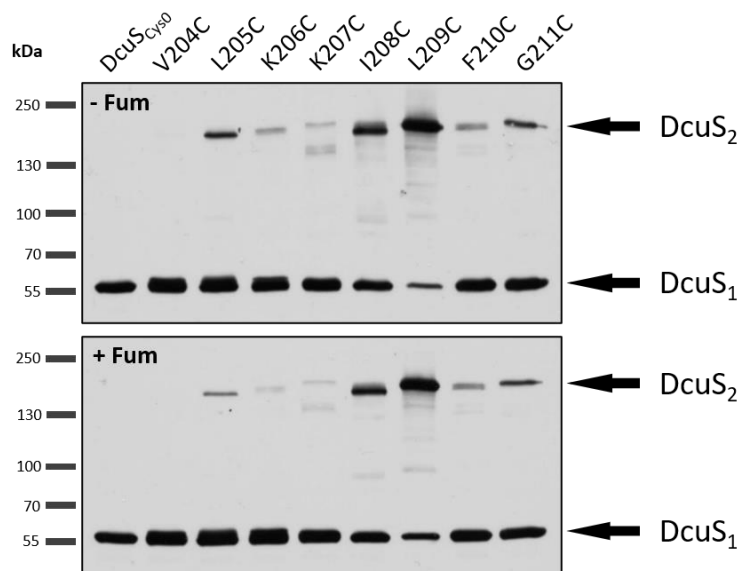
Figure 6. Detection of DcuS after oxidative *in vivo* Cys disulfide CL. CL *E. coli* C43 cells containing expressed DcuS single-Cys variants was performed by adding Cu^{2+} phenanthroline to the reaction mixture in the absence of fumarate (- Fum) and in the presence of 50 mM fumarate (+ Fum). The CL samples were separated in non reducing SDS-PAGE and DcuS monomers (DcuS$_1$) and CL products (DcuS$_2$) were detected by chemiluminescence after Western blotting. The scans of the X-ray films of CL of DcuS single Cys variants at positions Val204 to Gly211 Cys-less control (DcuS$_{Cys0}$) are shown as an example. Molecular weight marker: PageRuler^{TM} Plus Prestained Protein Ladder (Thermo scientific). Figure modified according to Stopp *et al.* (2021).

Oxidation of single Cys variants is a well-established method to study protein dimerization (Bass *et al.* 2007). Cys residues in proximity can be oxidized to a disulfide with high efficiency and thus enable statements to be made about the structure. The role of TM2 and the adjacent cytoplasmic region in DcuS homo-dimerization was analyzed in aerobically grown *E. coli* cells, i.e. in the native context with DctA by Cys CL using membrane-permeant copper(II)-(1,10-phenanthroline)$_3$ (Cu^{2+} phenanthroline) as a catalyst (Lee *et al.* 1995; Hughson and Hazelbauer, 1996; Monzel and Unden 2015). Cys CL of the DcuS single Cys variants was visualized by non-reducing SDS-PAGE and Western blotting with DcuS specific antisera, which allowed us to separate DcuS monomers (calculated mass = 62 kDa; apparent mass ~55 kDa for His$_6$-DcuS) from cross-linked DcuS homo-dimers (calculated mass = 124 kDa; apparent mass ~170 kDa) (Fig. 6). The plot of the *in vivo* oxidative Cys CL is shown in Figure 7.
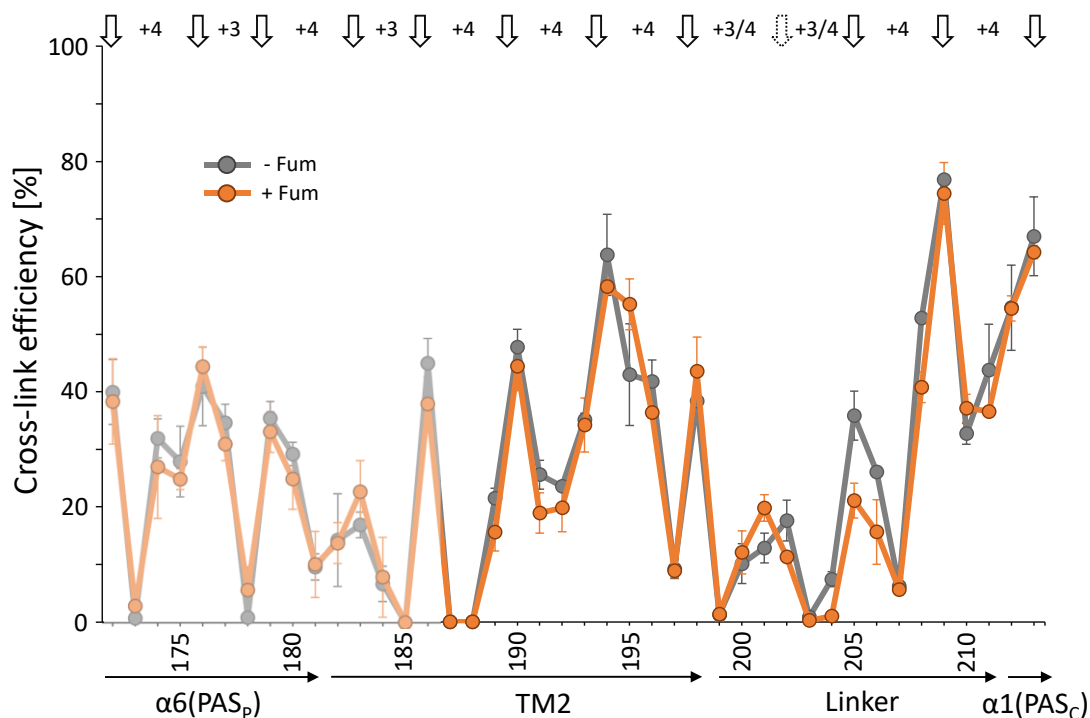
Figure 7. Oxidative *in vivo* Cys disulfide CL in the α6(PASₚ)-TM2-linker-α1(PASc) region of DcuS. CL was performed by adding Cu^{2+} phenanthroline to the reaction mixture in the absence of fumarate (-Fum) and in the presence of 50 mM fumarate (+ Fum). The ratio of the CL product to total DcuS was calculated by scanning the Western blots and quantitatively evaluating the signal in ImageJ software by measuring the band intensities. The CL efficiency for each individual Cys residue was determined in three independent experiments and the arithmetic mean plotted. The maxima of the CL efficiency are highlighted by arrows and their spacing indicated. Values for Val172 to Ser186 (presented in light lines) from Monzel and Unden (2015) are included for completeness. Figure modified according to Stopp *et al*. 2021.

The CL efficiency ranged from 0 to 74 %. The CL efficiency was lower at the membrane/water interfaces on the periplasmic (residues Trp181 to Trp185) and cytoplasmic (Cys199 to Lys207) sites, whereas the CL efficiency peaks in the TM2 core area, the periplasmic α6 of PASₚ and the cytoplasmic α1 of PASc were higher. The local maxima of the CL efficiency occur for almost the whole analyzed region in a +3 or +4 spacing indicating a characteristic periodicity of a dimeric α-helical interface. In addition, the CL pattern is retained for non-activated and fumarate activated DcuS, with the maximum difference in CL efficiency of 12 % between the signaling states. This spacing is only indistinct in the transition area to the cytoplasm (residues Leu201/Val202). In general, this area from position Leu201 to Lys206 shows the relatively highest fumarate-dependent change in CL efficiency compared to the adjacent areas. Overall, the results suggest a continuous α-helix ranging from α6 of PASₚ through the complete TM2 to α1 of PASc.

## The S₁₈₆xxxGxxxG₁₉₄ motif of TM2 in DcuS function and dimerization

The DcuS single Cys retained 87 % to 118 % of DcuS_Cys0 activity in *dcuB-lacZ* expression and induced *dcuB-lacZ* in a fumarate-dependent manner as the wild-type. However, there was a striking drop in fumarate induced *dcuB-lacZ* expression in a coherent stretch of seven amino

acids (F189 to L195) (Stopp *et al.* 2021). Noticeably this functional peculiarity coincides with a GxxxG motif in this TM2 core area. This GxxxG motifs are frequently involved in mediation of TM α-helical interaction (Senes *et al.* 2000; Kleiger *et al.* 2002) and are commonly extended or replaced by amino acids with small side chains (Ala, Ser, Thr) described as (small)xxx(small) motif (Dwason *et al.* 2002; Schneider and Engelman, 2004) or glycine-zipper-like motif (Kim *et al.* 2005). Therefore, a $S_{186}xxxGxxxG_{194}$ motif in TM2 was identified and tested for its impact on DcuS function. Since Ala replacements of GxxxG motifs are known to disrupt α-helical interaction, if they are critical for TM dimerization, the TM2 motif residues and adjacent residues were substituted with Ala or Cys (for Ser) and tested for impact on DcuS function in a *dcub-lacZ* reporter gene assay in a DcuS-deficient background. The S186C and the G190A variants almost resembled the DcuS wildtype activity, but G194A variant caused a decrease in fumarate stimulated activity to 44 % of wildtype DcuS. The *dcuB-lacZ* expression was further reduced by introducing the motif double variants S186C+G190A and G190A+G194A. Other substitutions of adjacent residues and even the mutation of the Thr198 position, which was noted with a locally high CL efficiency and whose +4 CL spacing to position Gly194 of the motif could indicate a participation in the TM2 dimer interface, did not significantly affect DcuS function (Stopp *et al.* 2021). This data suggests that the $S_{186}xxxGxxxG_{194}$ motif in TM2 is crucial for DcuS function.

Due to the functional impairment of DcuS by TM2 motif variants the impact of the $S_{186}xxxGxxxG_{194}$ motif on DcuS homo-dimerization was tested in the bacterial two-hybrid (BACTH) system. In the BACTH system the genetically separated T18 and T25 domains of the *Bordetella pertussis* adenylate are fused to the proteins of interest. Interaction of the proteins can restore cyclase activity and can be measured as cAMP/CRP dependent β-galactosidase expression/activity (Karimova *et al.* 1998; Karimova *et al.* 2000). Full-length DcuS was fused with either T18 or T25 at the N-terminus (Scheu *et al.* 2012) and caused a high β-galactosidase activity when co-expressed. Individual mutations of the signature residues Gly190 and Gly194 of the $S_{186}xxxGxxxG_{194}$ motif decreased the reporter activity (DcuS homo-dimerization dependent *lacZ* expression) to ~70 % (G190A) and ~55 % (G194A) of wildtype DcuS. No significant decrease was detected for the S186C variant and the combination with the variant G190A did not lead to any further effect beyond single variant G190A affected reporter gene activity. In contrast, the double variant G190A+G194A reduced the β-galactosidase activity close to the background level. The $G_{190}xxxG_{194}$ element within the $S_{186}xxxGxxxG_{194}$ motif is important for homo-dimerization of DcuS.

Potential interfering effects of other DcuS domains on TM2 homo-dimerization were eliminated by application of the GALLEX two-hybrid system. Isolated TM domains are fused C-terminally genetically to the maltose binding protein ensuring proper TM membrane integration. The N-terminus of each fusion construct is fused to the LexA DNA-binding protein. Interaction of the TM helices promotes LexA dimerization enabling binding to the *sulA* promoter, which is located upstream of the LacZ gene. Therefore, TM interaction can be measured as a decrease in β-galactosidase activity (Schneider and Engelman, 2003). In comparison with the strong homo-dimerizing TM1 of the human Gylcophorin A (GpA) and the weak interacting GpA variant GpA G83I (Schneider and Engelman, 2003) a TM2 fusion construct of a length of 16 amino acids (Ile183 to Thr198) inhibited β-galactosidase activity to 70 % of the GpA wildtype fusion construct representing a strong homo-dimerization. Introducing both double variants S186C+G190A and G190A+G194A to the TM2 fusion construct caused less inhibition reporter activity than the TM2 wildtype even less than the GpA G83I variant. Therefore, a strong impairment of TM2 homo-dimerization by the $S_{186}xxxGxxxG_{194}$ motif's variants is indicated (Stopp *et al*. 2021).

In summary the affected homo-dimerization of DcuS by the double variant G190A+G194A is in line with its impact on TM2 homo-dimerization. The double variant S186C+G190A is comparatively critical for isolated TM2 homo-dimerization, but full length DcuS is still able to stabilize its overall interaction indicated by the BACTH test results.
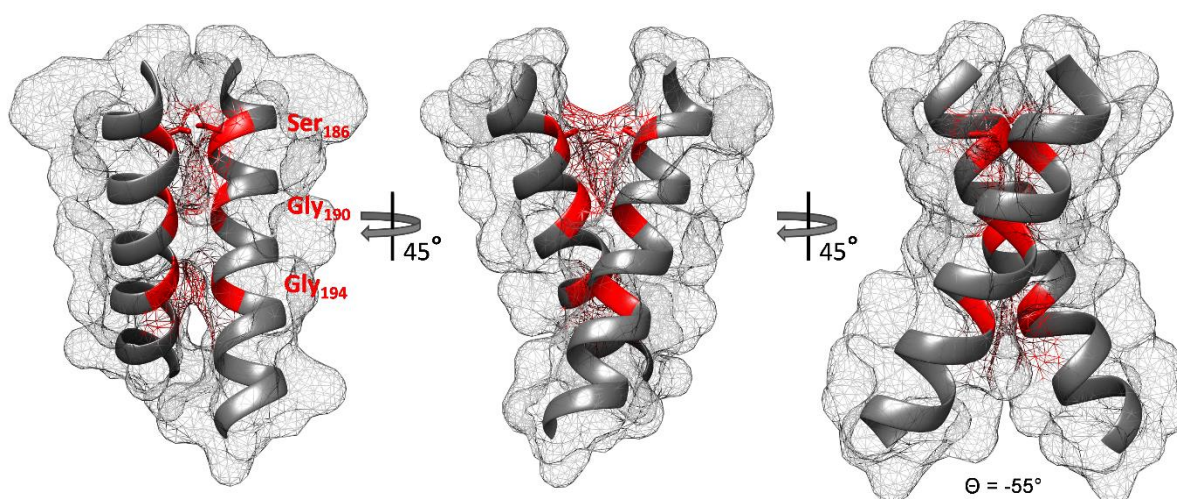
Figure 8. Model of the TM2 homo-dimer and the location of Ser186, Gly190, and Gly194 of the $S_{186}xxxGxxxG_{194}$ motif. The structural model of a TM2 homo-dimer was generated using the PREDDIMER web-tool (47) with the input sequence from DcuS position Ile176 to Phe210. The helices are limited to residues Ser182 to Leu201. The membrane-water interfaces at the periplasmic and cytoplasmic sides are at Ser182 and Cys199, respectively. The positions of Ser186, Gly190, and Gly194, as well as the predicted contact sites of Ser186, Gly190, and Gly194 in the surface projections of the TM2 homodimer interface are marked in red. The crossing angle of the predicted TM2 homo-dimer (Θ) is shown below the right projection. Figure from Stopp *et al*. 2021.

TM dimers are also predictable *in silico* by the PREDDIMER web-tool (Polyansik *et al*. 2014). provided as one of the top-scoring structures a TM2 homo-dimer with an interface of dimerization that involves exactly the residues of the $S_{186}xxxGxxxG_{194}$ motif (Fig. 8). Together with the initial Cys CL and the studies on homo-dimerization this model strongly suggests TM2 being a right-handed helix forming a homo-dimer with a crossing angle of -55° that is stabilized by the $S_{186}xxxGxxxG_{194}$ motif. Within that the $G_{190}xxxG_{194}$ motif in particular is crucial for both TM2 homo-dimerization and DcuS dimeric function.

The TM2-PAS$_C$ linker is involved in regulation of DcuS activity

The C-terminus of TM2 and the N-terminus of α1 of PAS$_C$ are connected by a short linker ($C_{199}ILVKVLKKILFG_{211}$) (Etzkorn *et al*. 2008; Monzel and Unden, 2015; Weisenburger *et al*. 2017). It includes the LxxxLxxxL sequence within which the residues Leu205 and Leu209 attracted attention. Upon activation of DcuS by fumarate, Leu205 becomes inaccessible and Leu209 accessible to labeling by hydrophilic reagents, which was interpreted to reflect structural reorganization such as a move into or out of the hydrophobic membrane core region (Mozel and Unden, 2015). Furthermore, three Lys residues are part of the linker, which is consistent with their cytoplasmic location as a demarcation from TM2 and the positive inside rule (von Heijne, 2006). In the Cys CL the linker showed a comparatively lower CL efficiency but a relatively large change of CL efficiency between the DcuS signaling states (Fig. 7). To further investigate the function of the linker, Ala substitutions of all linker positions were generated and analyzed for their impact on DcuS function in the *dcub-lacZ* reporter gene assay.

For variant L209A a major loss of fumarate stimulated DcuS function was observed in the *dcub-lacZ* reporter gene assay. To a lower extent the F210A variant of the adjacent Phe210 position was also impaired in fumarate activated function. In contrast, substitution of Lys206 by Ala resulted in a clear ON phenotype in the absence of fumarate, which was not observed when mutating the remaining residues, apart from a weak ON phenotype of the V202A substitution (Stopp *et al*. 2021). Strikingly, a similar ON phenotype for Trp substitutions of positions Val202 and Lys206 was observed when analyzing the impact of Trp residues on TM2 membrane topology in TM signal transduction (Monzel, 2014). Remarkably, the Cys substitutions in the linker used for the CL assay were not conspicuous in the *dcub-lacZ* reporter gene assay (Stopp *et al*. 2021), suggesting that Cys substitutions are more neutral than Ala substitutions in this region. Cys replacements in the region connecting the TM region of the chemotaxis protein Tsr

with the signal transducing HAMP domain, or 'control cables', also showed a remarkable tolerance to Cys substitutions (Kitanovic *et al*. 2011).

The strong effects observed upon mutation of Lys206 and Leu209 suggest the importance of the linker for controlling DcuS activity, which is supported by a relatively large change in CL efficiency in the linker (Cys199 to Lys207) in the presence and absence of fumarate (Fig. 7).

Cross-linking dynamics of TM2 and the linker

Cys CL of TM2 and the linker was performed under relatively strong oxidizing conditions (Lee *et al*. 1995; Molnar *et al*. 2014) to obtain clear information of the dimeric structure focusing on α-helicity. However, the linker showed a higher deviation relative to TM2 in the CL efficiency between the DcuS signaling states and an overall lower CL efficiency (Fig. 7). This leads to the question of whether the distinct areas show different behavior in DcuS signal transduction. To this end for each residue optimal oxidation conditions were adjusted by optimizing the concentration of Cu^{2+} phenanthroline and temperature to achieve a decrease in oxidative reactivity (see 'experimental procedures' section). This enabled monitoring CL efficiency over time and comparison for the presence or absence of fumarate. DcuS variants with high CL yield (Fig. 7) were chosen for analysis to enable quantitative evaluation even under weakened oxidizing conditions.

For the TM2 region the single Cys variants of positions Ser186, Gly190, Gly194, and Thr198 were selected. For the single Cys variants G190C, G194C, and T198C high CL levels were observed within short time (< 1min) after addition of the oxidant, and the kinetics were not affected by the presence of fumarate. An exception is the reactivity of the single Cys variant S186C, with fumarate reflecting the reactivity of the other TM2 positions, but without fumarate showing slow increase in CL efficiency (Fig. 9A).

The CL kinetics of the linker are clearly distinguishable to TM2. For single Cys variants L205C, I208C, and L209C, the CL efficiency was very low after 0.5 to 3.0 min in the presence of fumarate, and only slightly increased, if at all, within 20 min. However, in the absence of fumarate, the CL efficiency was also low initially, but increased over time by factor 2 to 7 in the absence of fumarate compared to the fumarate activated state, which is particularly evident for the C-terminal linker positions Ile208 and Leu209 (Fig. 9B). At position Leu201, which is close to the membrane/cytoplasm interface, the CL response was different from those seen for other positions in the linker. CL in the presence of fumarate was low but reached near maximal levels early after 0.5 min (Fig. 9B), similar to the neighboring TM2 region (Fig. 9A). But in the absence of fumarate almost no CL product was detected (Fig. 9B).
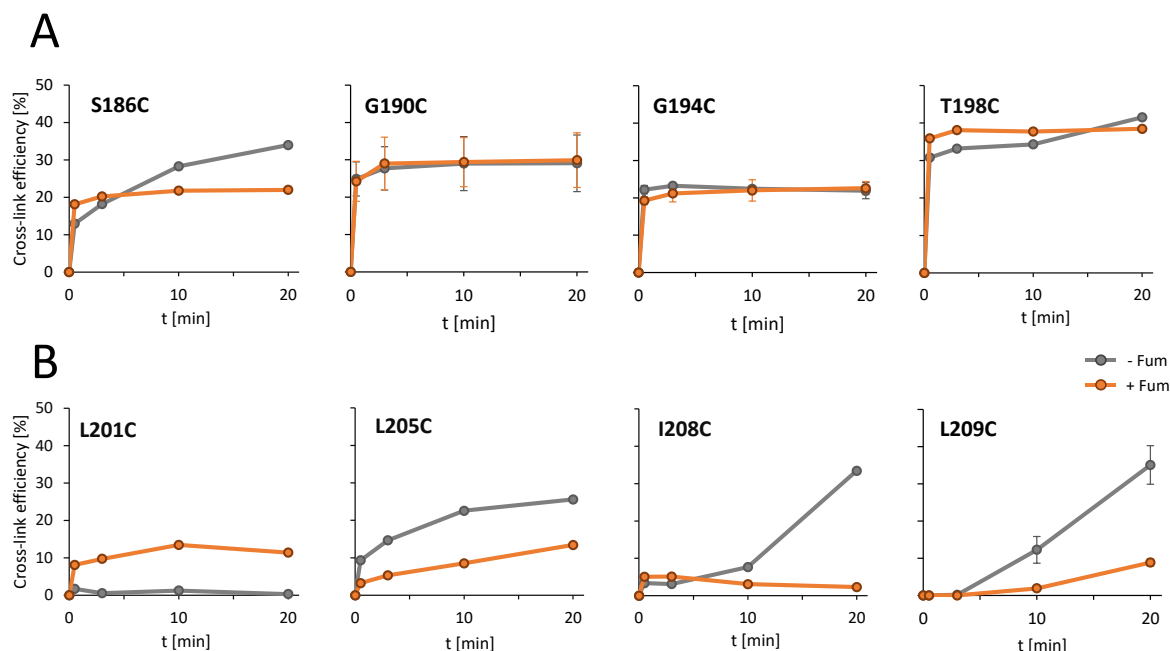
Figure 9. The effect of fumarate on oxidative Cys CL of sites in TM2 (A) and the linker (B): Time-resolved CL. The bacteria for the *in vivo* CL assay were grown in the presence (orange) or absence (gray) of fumarate. Oxidative CL was performed under optimized conditions with respect to Cu^{2+} phenanthroline concentrations and temperature (see experimental procedures section) with and without fumarate. For key residues G190C, G194C, and L209C the CL kinetics was performed in repeat and error bars are given. The ratio of CL products to the total amount of DcuS was calculated after scanning the anti-DcuS Western blots and evaluating the band intensities with ImageJ software. Figure from Stopp *et al*. 2021.

Therefore, the data suggest major differences for homo-dimerization of TM2 and the linker region, as residues of the linker region (Leu201, Leu205, Ile208, and Leu209), but not the TM2, exhibited a marked fumarate-induced difference in CL efficiency. These findings suggest fumarate-induced effects on helix dimerization and restructuring of (at least) the extra-membranous part of the linker.

4.1.2 Dimerization and signal transduction by the DcuS PAS$_C$ domain

Upon activation of histidine kinases by periplasmic stimuli the signal is intracellularly forwarded often by via cytoplasmic PAS or HAMP domains to the kinase domain (Etzkorn *et al*. 2008; Parkinson, 2010; Gushchin *et al*. 2017).

Positions 212 to 320 of DcuS comprise a domain, that shows the characteristic folding of cytoplasmic PAS domains including a central five-stranded β-sheet framework interspersed by α-helices (Etzkorn *et al*. 2008; Weisenburger *et al*. 2017). In DcuS PAS$_C$ acts as the interconnector of TM2/linker and the kinase domain. Consequently, PAS$_C$ has been considered to convert the signal incoming from TM2/linker to cause kinase rearrangement and stimulating autophosphorylation (Etzkorn *et al*. 2008). As part of the previous studies PASc has been extensively analyzed for functional mutants identifying a surface area of concentration of

fumarate-insensitive DcuS ON-variants. This showed the importance of the PAS$_C$ dimer for DcuS function and suggested a participation in signal transduction by change in the dimerization state of PAS$_C$ in the DcuS dimer (Monzel *et al*. 2013).

Meanwhile structure elucidation of the closely related CitA sensor kinase PAS$_C$ domain has progressed (Weisenburger *et al*. 2017), but detailed information on the role of PAS$_C$ in signal transduction are still lacking. Hence, PAS$_C$ will be further characterized by Cys scanning mutagenesis (Lee *et al*. 1998; Monzel and Unden, 2015; Stopp *et al*. 2021) involving *dcuB-lacZ* reporter gene test and oxidative *in vivo* Cys CL. For this purpose a set of plasmid encoded DcuS single Cys variants was generated. DcuS contains two Cys residues (C199, C471), which can be replaced by Ser residues without loss in DcuS sensitivity (Scheu *et al*. 2010; Monzel and Unden, 2015; Stopp *et al*. 2021). The variants start directly behind the TM2-linker region and range from positions Pro214 to Arg241. This region comprises a long α-helical region (α1) and the first β-strand (β1) of PAS$_C$ (Fig. 10).
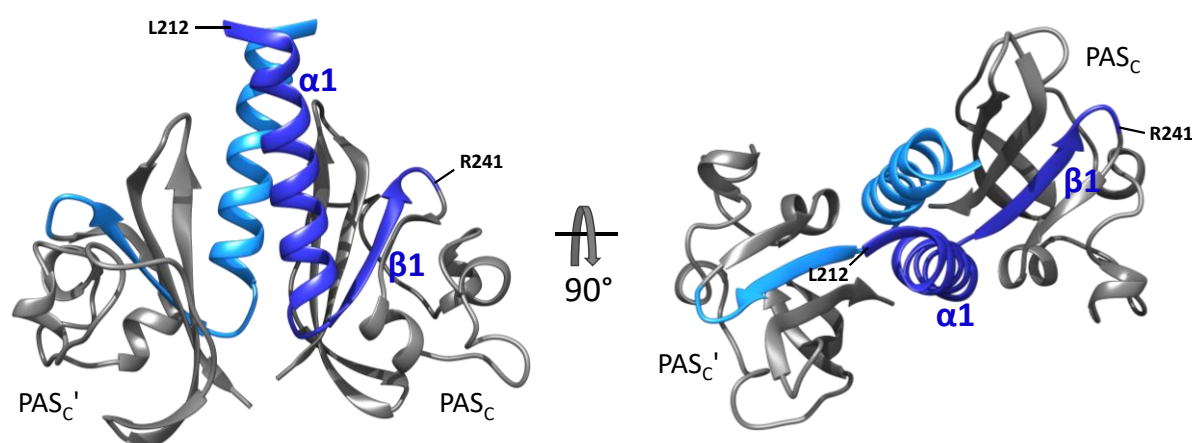
Figure 10. Model of the DcuS PAS$_C$ homo-dimer. The PAS$_C$ dimer structure was modeled using the structure of CitA from *G. thermodenitrificans* as a template (PDB ID: 5FQ1). The area analyzed by a continuous set of single Cys variants is highlighted in the respective monomers PAS$_C$ (blue) and PAS$_C$' (light blue) and the positions delimiting this area are marked. Positions Leu212 and Glu213 were already tested in Stopp *et al*. (2021).

Functionality of single Cys variants in the PAS$_C$ α1/β1 region

The activities of the *dcuB-lacZ* reporter gene assay are shown in Figure 11. All DcuS single Cys variants of DcuS in this region showed an increase in *dcuB-lacZ* expression, when fumarate was added as an electron acceptor, indicating that fumarate sensitivity was retained. But the level of expression varied clearly between the variants. Variants DcuS P214C, I217C, S218C, Q225C, and V235C of DcuS retained a fumarate stimulated activity of 32 to 46 % of Cys-free DcuS (DcuS$_{Cys0}$). A significant increase in activity, however, was observed for variants L220C, E223C, R224C, L228C, E233C, V235C, and A237C, which increased to 150 to 170 % of DcuS$_{Cys0}$.
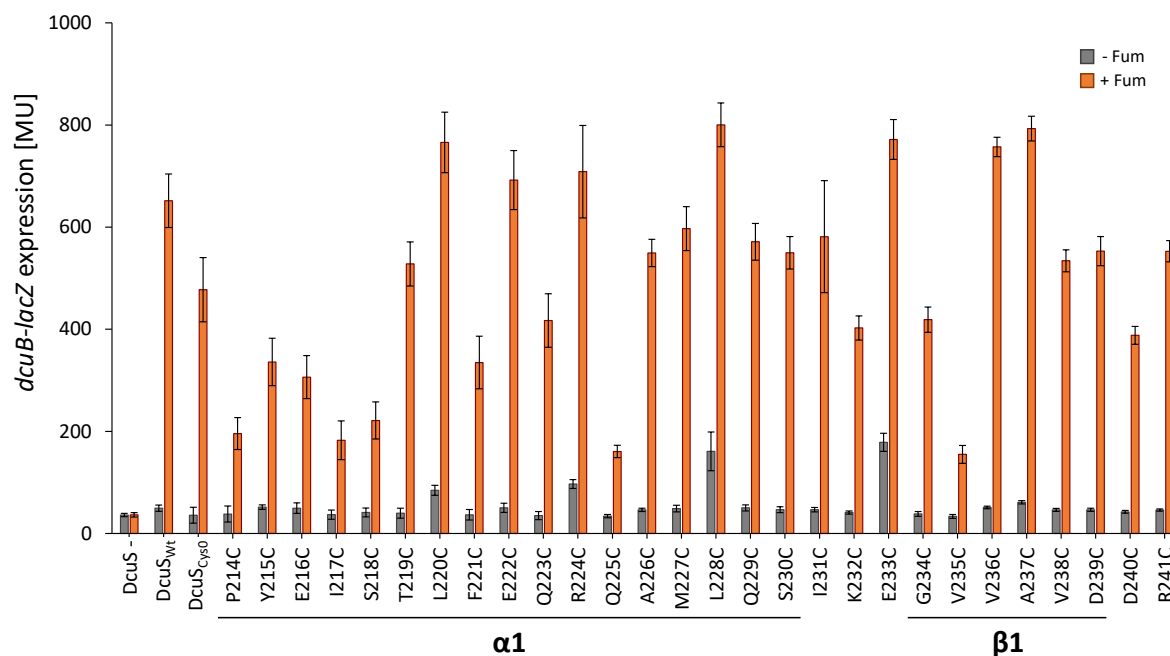
Figure 11. **Effect of DcuS cysteine substitutions in the PAS$_C$ α1/β1 region on *dcuB-lacZ* expression.** Expression of *dcuB-lacZ* and effect of the substitutions was tested in the *dcuS* negative strain IMW260 (DcuS -) complemented with plasmid (pMW336)-encoded Cys-less DcuS (DcuS$_{Cys0}$) and derivatives of DcuS with single Cys substitutions. Growth was performed under anaerobic conditions in eM9 medium with glycerol plus 20 mM DMSO with or without 20 mM di-sodium fumarate. Secondary structural elements are marked below the corresponding residues according to Etzkorn *et al*. (2008) and Weisenburger *et al*. (2017).

Notably, among the DcuS Cys variants with an increase in fumarate stimulated *dcuB-lacZ* expression, variants L220C, R224C, L228C, and E233C also exhibited an increase in *dcuB-lacZ* activity without fumarate of factor 3.4 to 7.8 compared to DcuS$_{Cys0,}$ but without the loss of fumarate stimulation. All other variants resembled in their *dcuB-lacZ* expression the strain with DcuS$_{Cys0}$.

The residues Ile217, Phe221, Leu228, Glu233, and Val235 of the PAS$_C$ α1/β1 region attracted attention, since the substitutions L228A, E233A, and V235A caused a fumarate-independent ON-phenotype, whereas I217A and F221A caused substitutions an OFF phenotype (Degreif-Dünnwald, 2011; Monzel *et al*. 2013). Therefore, residues Ile217, Leu228, Glu233 are generally susceptible to functional impairment (decreased or OFF phenotype and increased activity or ON phenotype), indicating their importance for PAS$_C$ function. Interestingly, all DcuS single Cys variants do not cause a clear ON- or OFF-phenotype and are more tolerable in terms of DcuS function. This has already been observed for single Cys variants of the DcuS PAS$_P$(α6)-TM2-linker region (Monzel and Unden, 2015; Stopp *et al*. 2021). The phenotypes of variants Q225C, R224C, L220C have not been observed for any other DcuS variant so far (Monzel *et al*. 2013).

Oxidative *in vivo* cross-linking of single Cys variants in the PAS$_C$ α1/β1 region

Single Cys replacement variants of the region were used to study changes in the CL-link pattern and potential changes in the dimerization interface.

Cys CLwithin the PAS$_C$ domain is shown in Figure 12. In the α1-helix of PAS$_C$ the CL efficiency without fumarate ranged from 6 % of variant Q229C to 77 % of variant L220C, whereas the addition of fumarate led to a CL efficiency in between 13 % of variant E222C and 74 % of L220C. In the β1-strand of PAS$_C$ the minimum and the maximum were each clearly assigned to a variant independent of the effector fumarate. The minimal CL efficiency was found for D239C with 27 % and 20 % CL efficiency and the highest CL efficiency of 84 % and 66 % without and with fumarate, respectively, was observed for DcuS G234C.
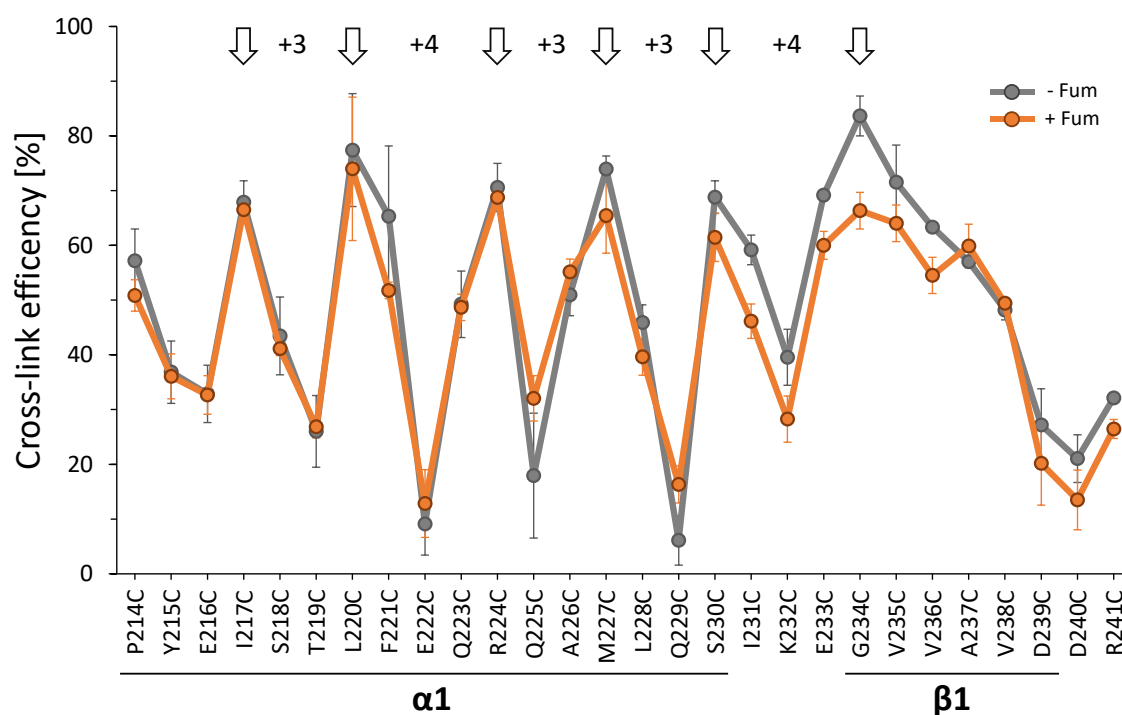
Figure 12. Oxidative *in vivo* Cys CL in the PAS$_C$ α1/β1 region of DcuS. *E. coli* C43 cells transformed with DcuS single Cys variants at positions Pro214 to Arg241 and were grown in the absence of fumarate (-Fum) and in the presence of 50 mM Na$_2$fumarate (+ Fum). CL was performed by adding Cu^{2+} phenanthroline to the reaction mixture. The ratio of the CL product to total DcuS was calculated by scanning the Western blots and quantitatively evaluating the signal in ImageJ software by measuring the band intensities. The CL efficiency for each individual Cys residue was determined in three independent experiments (two repeats for positions 236 to 241) and the arithmetic mean plotted. The maxima of the CL efficiency are highlighted by arrows and their spacing is indicated. Secondary structural elements are marked below the corresponding residues according to Etzkorn *et al*. (2008 and Weisenburger *et al*. (2017). The complete set of Western blots for the Cys variants from positions Pro214 to Arg241 are shown in Fig. 29 and 30.

For the complete α1-helix of PAS$_C$ a +3 or +4 spacing of local maxima of CL efficiency was observed, indicating a typical bi-α-helical interaction. This double helix extends from Ile217 to Ser230. In a consolidated view with the data form Monzel and Unden (2015) and Stopp *et al*. (2021) the +3 or +4 periodicity extends from the periplasmic α6-helix of PAS$_P$, through TM2, the linker, and the adjoining α1-helix of PAS$_C$, clearly showing a continuous double helix from

Val172 to Ser230. Another α-helical extension to Gly234 within the +3 or +4 pattern is conceivable, but due to the structural alignment of DcuS with the PAS$_C$ domain of CitA (Weisenburger *et al.* 2017) a localization of Gly234 in the β-strand (β1) is more plausible.

Overall, the CL efficiency in the PAS$_C$ α1/β1 region did not differ largely with and without fumarate and no change of the periodicity was observed. The maximal change in CL efficiency was in variant F221C (15.5 %) for the α1-helix, in variant G234C (17 %) for the β1-fold. Strikingly, there is a clear loss of periodicity at Gly234 where the β1 fold starts.

Cys Cross-linking dynamics of PAS$_C$ α1/β1 (time-resolved Cys CL)

As already applied to TM2 and the linker in Stopp *et al.* (2021), relatively strong oxidizing conditions were used in the Cys CL of the PAS$_C$ α1/β1 region to obtain information on α-helicity or structure in general. Due to the minor changes in CL efficiency of inactivated and fumarate activated DcuS single Cys variants optimal oxidation conditions were adjusted for selected DcuS single Cys variants by optimizing the concentration of Cu^{2+} phenanthroline and temperature. This should lead to a decrease in oxidative reactivity enabling monitoring of the CL efficiency over time and visualization of potential fumarate-dependent changes in CL dynamics caused by structural rearrangement.

For this purpose the moderate to high reactive single Cys variants E313C (Stopp *et al.* 2021), R224C, and L228C as PAS$_C$ α1 representatives, and I231C and G234C as representatives of PAS$_C$ β1 and the α1/β1 transition area (Fig. 12) were selected. The results of the time-resolved Cys CL are shown in Figure 13.

The CL kinetics of the two α1 representative positions Glu213 and Leu228 was clearly affected by the addition of fumarate. Both Cys variants were relatively rapidly cross-linked, but fumarate caused a decrease in oxidative reactivity. Noticeable, E213C showed a slight DcuS disulfide formation without the addition of an additional oxidant other than oxygen (0 min), but Cu^{2+} phenanthroline driven increase of Cys reactivity was more decisive. However, E213C reactivity was generally higher. The CL kinetics α1 position Arg224 were different. Unlike E213 and L228C, R224C showed no initial reactivity and still was very low after 10 min, but after 20 min the reactivity was strongly increased. In addition, there was no significant reduction in the Cys reactivity by fumarate.
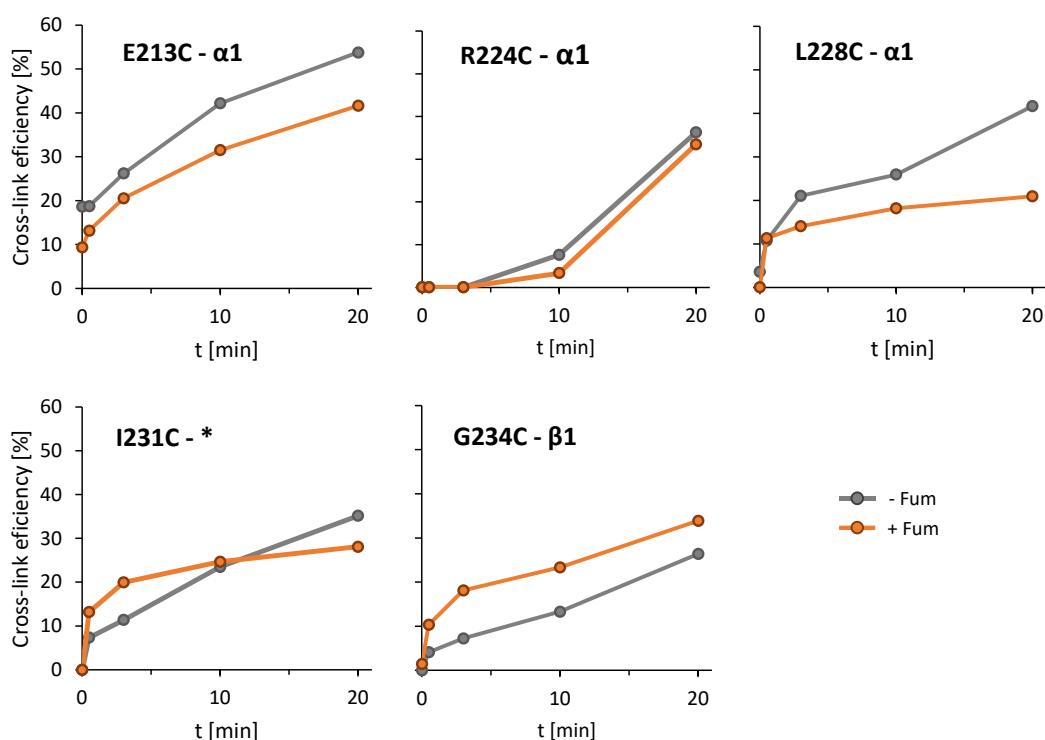
Figure 13. The effect of fumarate on oxidative Cys CL of sites in the PAS$_C$ α1/β1 region: Time-resolved CL. The C43 *E. coli* cells for the *in vivo* CL assay were grown in the presence (orange) or absence (gray) of fumarate. Oxidative Cys CL was performed under optimized conditions with respect to Cu^{2+} phenanthroline concentrations and temperature (see 'experimental procedures' section) with and without fumarate. The ratio of CL products to the total amount of DcuS was calculated after scanning the anti-DcuS Western blots and evaluating the band intensities in ImageJ software. In the top position of each plot the corresponding variant and the associated secondary structures of PAS$_C$ are listed. *Variant I231C is presumably located in the α1-β1 linker. The Western blots are shown in Figure 31.

For position Ile231, presumably located in the PAS$_C$ α1-β1 linker, the CL efficiency increased in an almost linear course without fumarate. Fumarate activated variant S231C, however, showed a more rapid initial CL reaction, but the reactivity slowed down and the maximal CL efficiency achieved was lower after 20 min compared to the non-fumarate activated condition. The kinetics of position Gly234 was also different from that of the positions located in α1. An increase in CL efficiency was evident under both conditions, but variant G234C CL's efficiency was clearly higher upon fumarate activation overall.

Interestingly, the CL reactivity without fumarate was faster in all α1 positions, even if it was almost similar for the variant R224C with the addition of fumarate. This fumarate response in Cys CL dynamics is opposed by the kinetics of variant G234C. Furthermore, the α1/β1 transition area located variant I231C also represents a transition area in dynamics of Cys CL, because the fumarate dependence of the reactivity does not convey a clear profile. Overall, the of Cys CL dynamics of DcuS PAS$_C$ single Cys variants are much more variable compared to the TM2 and linker variants (Stopp *et al*. 2021; Fig. 9).

4.1.3 TM1: The role in DcuS function and dimerization potential

DcuS is anchored in the membrane via the two TM helices TM1 and TM2. Both TM1 and TM2 frame the periplasmic stimulus receiving PAS$_P$ domain. But only TM2 is covalently connected to the cytoplasmic domains of DcuS. For TM2 it has been shown that a piston-type displacement of a rigid TM2 homo-dimer has a major role in signal transduction across the membrane (Monzel and Unden, 2015; Stopp *et al*. 2021). The position of TM1 shifted only slightly and predictions of apparent free energy changes of TM1 membrane insertion support a fixed position of TM1 (Monzel and Unden, 2015).

To explore the function of TM1 in more detail, TM1 was targeted to mutation to analyze TM1 homo-dimerization and its role for DcuS and function. Data from Steinmetz (2014) are shown in Figure 14, which complement the CL and functional studies performed here.

GxxxG and (small)xxx(small) type sequence motifs often act as a framework of TM helical interaction (Senes *et al*. 2000; Russ and Engelman, 2000). TM1 exhibits the Ala$_{27}$xxxSer$_{31}$ motif of the (small)xxx(small) type. Therefore, mutations of the sequence motif were tested for their effect on DcuS function in the *dcuB-lacZ* reporter gene assay. Further two adjacent positions (Met24 and Ser26) were tested as a control. All three variants M24A, S26A as well as the double variant A27G+S31C can complement the DcuS deficiency of the reporter strain. The slight increases in reporter activity did not affect DcuS fumarate sensitivity indicating no critical impact on DcuS function (Fig. 14A).

The effect of TM1 positions that are part of a potential (small)xxx(small) motif were tested with the BACTH interaction assay (Karimova *et al*. 1998; Karimova *et al*. 2000). The genetically separated adenylate cyclase domains T18 and T25 were fused to DcuS. Restored adenylate cyclase activity depending on DcuS homo-dimerization was measured in analogy to the interaction assay for TM2 (Stopp *et al*. 2021; compare 4.1.1). The substitutions of S26A and A27G+S31C had minor effects on DcuS interaction. The variant S26A reduced DcuS interaction slightly to 70 % of the DcuS Wt. The double variant A27G+S31C had an even less effect, suggesting the Ala$_{27}$xxxSer$_{31}$ motif has little or no impact on the stability of the DcuS homodimer (Fig. 14B).
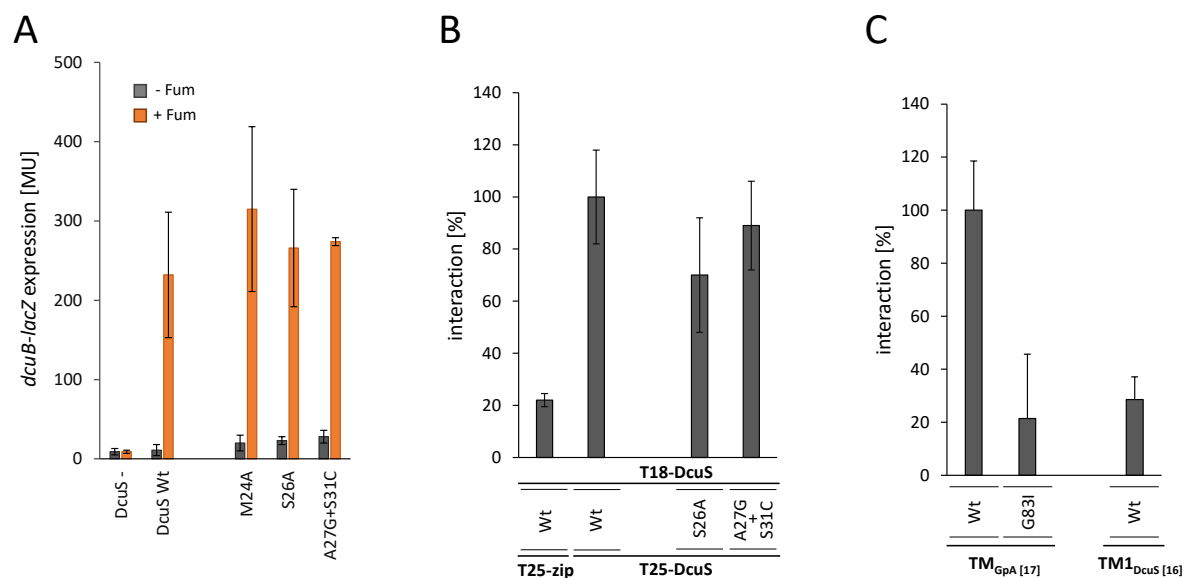
Figure 14. Effect of TM1 variants on DcuS function and homo-dimerization and homo-dimerization of isolated TM1.
(A) Effect of DcuS TM1 varaints on *dcuB-lacZ* expression. The DcuS variants were tested in *dcuS*-negative *E. coli* strain IMW260 (DcuS-) complemented with plasmid (pMW181)-encoded wild-type DcuS (DcuS Wt). The bacteria were grown under anaerobic conditions in eM9 medium with glycerol plus DMSO with or without 20 mM di-sodium fumarate. (B) DcuS homo-dimerization in the BACTH system: *E. coli* BTH101 cells were co-transformed by plasmid pairs encoding T18-DcuS (pMW429), T25-DcuS (pMW426), and its derivatives. The cells were grown aerobically to an OD_{578} of 0.5 to 0.7 and the β-galactosidase activity was assayed. All values were normalized to the value for the interaction between the T18-DcuS and T25-DcuS Wt pair. The activity of the non-interacting T25-Zip and T18-DcuS pair was defined as the background. (C) TM homodimerization in the GALLEX system: *E. coli* SU101 was transformed with GALLEX construct encoding TM1 of DcuS with a length of 16 amino acids ($TM1_{DcuS\ [16]}$). The bacteria were cultivated aerobically in LB to an OD_{578} of 0.5 and β-galactosidase activities were assayed. The constructs $TM_{GpA\ [17]}$ (Wt) and $TM_{GpA\ [17]}$ (G83I) served as controls for interaction in the GALLEX system (Schneider and Engelman, 2003). The dimerization of $TM_{GpA\ [17]}$ (Wt), which exhibited the strongest inhibition of β-galactosidase expression, was set to 100 % and all other values were normalized accordingly. Figure modified according to Steinmetz (2014).

In order to check, whether TM1 has any potential to homo-dimerize, isolated TM helices were tested in the GALLEX system. The TM helices are fused to the LexA binding domain, whose dimerization upon homodimerization of the TM helices inhibits *lacZ* reporter gene transcription (Schneider an Engelman, 2003). The experiments were carried out analogously to Stopp *et al*. (2021). The TM1 fusion constructs of a length of 16 amino acids (Ile22 to His37) inhibited β-galactosidase activity by 20 % of that for the TM1 GpA fusions constructs. The latter served as a control for strongly homodimerizing TM helices. Furthermore, the inhibition was only slightly higher than for the weak interacting G83I GpA variant indicating only a weak homo-dimerization of TM1 (Fig 14C). Thus, the homodimerization of TM1 is significantly weaker than that of TM2 (Steinmetz, 2014; Stopp *et al*. 2021; see section 4.1.1).

Functionality of TM1 single Cys variants

The BACTH and GALLEX interaction studies suggest no crucial role of a (small)xxx(small) motif in TM1 for DcuS function and homo-dimerization. Like DcuS the osmo-sensor kinase EnvZ is anchored in the membrane via two TM helices, whereby the N-terminal TM1 is not directly connected to the cytoplasmic kinase domain. Cys variants of EnvZ in TM1, which are

involved in homo-dimerization, result in a significant increase in the signal output at low osmolarity (Heiniger *et al.* 2016). Single Cys variants of the PAS$_C$ domain and TM2 of DcuS have been successfully used to examine the influence of individual residues on the function (Stopp *et al.* 2021; see sections 4.1.1, 4.1.2). This functional test was also applied to TM1 and the surrounding periplasmic and cytoplasmic areas in the *dcuB-lacZ* reporter gene assay (Fig. 15). Upon addition of fumarate as stimulus of the DcuSR TCS *dcuB-lacZ* expression was clearly increased for all single Cys variants compared to the non-activated state. The level of fumarate stimulation was comparable to DcuS$_{Cys0}$ for almost all positions with exception of position Val28. The single Cys variant V28C reporter activity decreased to 69 % of DcuS$_{Cys0}$, but without affecting fumarate sensitivity.
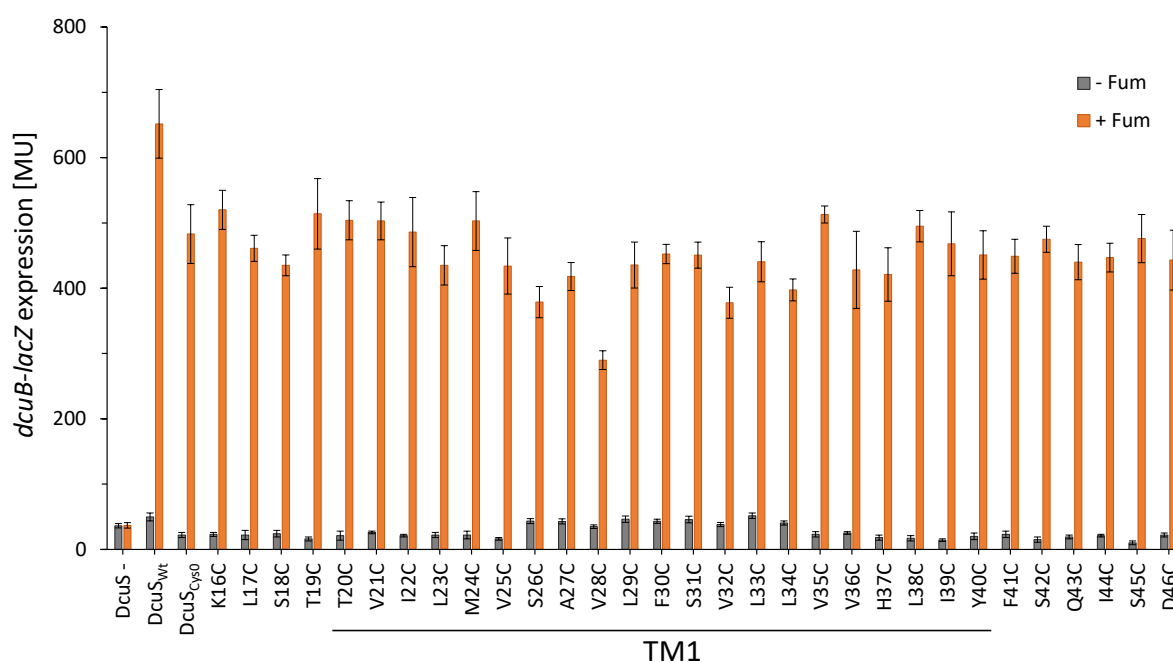
Figure 15. Effect of singlr cysteine substitution of DcuS TM1 and adjacent regions on *dcuB-lacZ* expression. Expression of *dcuB* and effect of the substitutions was tested in the *dcuS* negative strain IMW260 (DcuS -) complemented with plasmid (pMW336)-encoded Cys-less DcuS (DcuS$_{Cys0}$) and derivatives of DcuS with single Cys substitutions. Growth was performed under anaerobic conditions in eM9 medium with glycerol plus 20 mM DMSO with or without 20 mM di-sodium fumarate. All activities were normalized to the wildtype control of DcuS in the fumarate activated state. Variants K16 - V25 and 196 - 213 have been tested earlier (Monzel and Unden, 2015) without presenting the data.

Oxidative *in vivo* cross-linking of single Cys variants in TM1

The oxidative Cys CL (Lee *et al.* 1995; Monzel and Unden, 2015; Stopp *et al.* 2021) was applied to TM1 in order to check, whether there is TM1 homo-dimerization in full length DcuS as indicated by isolated TM1 constructs (Fig. 16). Furthermore, the Cys CL can provide information on TM1 structure.

The positions Leu23 and Ser26 represented the residues with the minimal and maximal CL efficiency for both the non-activated DcuS and the fumarate-stimulated state. The CL efficiency without fumarate ranged from 0 % for variant S26C to 55 % for variant L23C, and with fumarate from 0 % (S26C) to 56 % (L23C). By far the highest CL efficiency was shown by the periplasmic single Cys variant I44C with 89 % (- Fum) and 86 % (+ Fum). The CL efficiency in the TM1 region did not differ largely for the various maxima. Maximal effect in CL efficiency upon fumarate activation was 13 % for Cys variant I22C. The local maxima of CL efficiency of position Leu23 to Leu34 represent a typical bi-α-helical +4+3+4 pattern. However, the distances between the CL efficiency maxima in the adjacent regions were larger and increased to +5/+5 and +6 in the C- and N-terminal transition regions to the periplasmic and cytoplasmic areas, respectively. This clearly points to a homo-dimerization of TM1 in the DcuS dimer, which, however. corresponds only in the central TM region to a typical TM double α-helix. Additionally, around positions Leu33 to Tyr40 CL efficiency did not differ in a high extend between the individual single Cys variants, except for H37C representing a plateau of reactivity. This reinforces the assumption that TM1 has not a typical α-helical structure with a broader interaction surface in the homo-dimer.
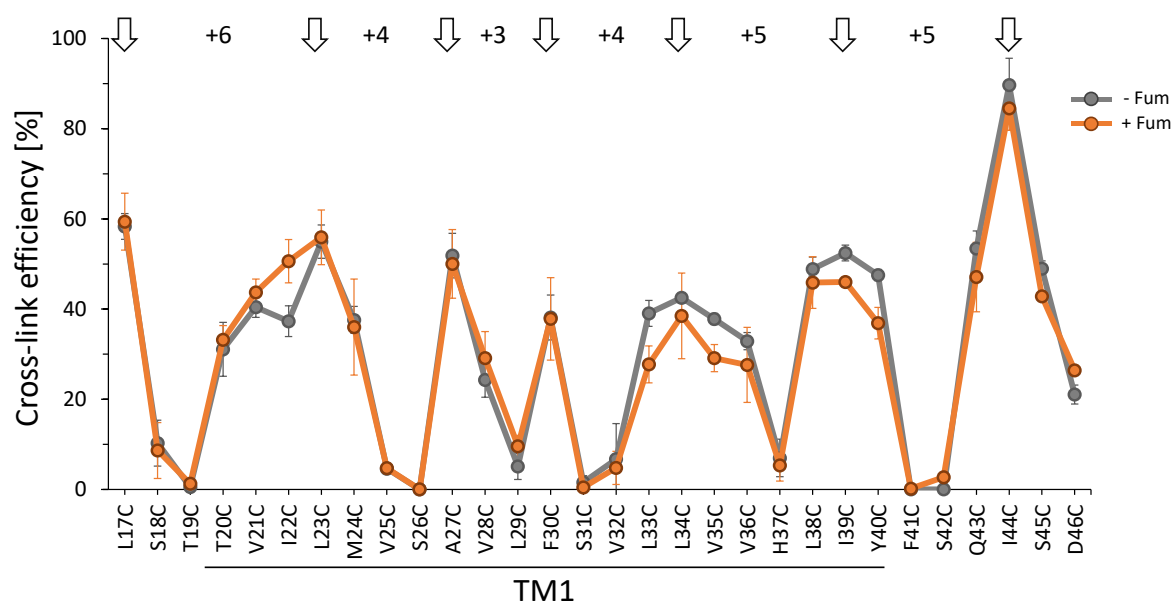
Figure 16. Oxidative *in vivo* Cys CL of TM1 of DcuS. *E. coli* C43 cells transformed with DcuS single-Cys variants at positions Leu17 to Asp46 and were grown in the absence of fumarate (-Fum) and in the presence of 50 mM Na$_2$fumarate (+ Fum). CL was performed by adding Cu^{2+} phenanthroline to the reaction mixture. The ratio of the CL product to total DcuS was calculated by scanning the Western blots and quantitatively evaluating the signal in ImageJ software by measuring the band intensities. The CL efficiency for each individual Cys residue was determined in three independent experiments and the arithmetic mean plotted. The maxima of the CL efficiency are highlighted by arrows and their spacing is indicated. The complete set of Western blots for the Cys variants from positions Leu17 to Asp46 are shown in Figures 32 and 33.

4.1.4 Co-regulation of DctA on a structural level in DcuS signal transduction

The DcuSR TCS regulates the expression of the genes of the C4DC metabolism, including the aerobic symporter DctA and the anaerobic antiporter DcuB (Zientz *et al*. 1998; Golby *et al*. 1999). Both DctA and DcuB interact with DcuS (Kleefeld *et al*. 2009; Witan *et al*. 2012) and are required as co-regulators of the sensor kinase converting DcuS to the C4DC-receptive state (Steinmetz *et al*. 2014; Wörner *et al*. 2016). Since the transporters do not have a co-sensory function and DcuS represents the only signal input site, it is obvious that the transporters must interfere in the signaling mechanism by interaction with DcuS.

Time-resolved CL enabled the visualization of oxidative Cys CL dynamics depending on the signaling state of DcuS in different domains (Stopp *et al*. 2021; Fig. 9 and 13). Thus, the time-resolved Cys CL was performed *in vivo* in presence and absence of DctA for both signaling states of DcuS to evaluate effects of DctA deficiency on Cys CL kinetics, that can represent rearrangements in the signaling mechanism.

Single Cys variants of positions in different domains of DcuS that were already considered to reflect signal transduction dynamics, were selected to capture a broad range of DctA dependent effects on the Cys CL kinetics. The DcuS single Cys variants were expressed in the strain IMW660, a C43 derivative with inactivated *dcuS* and *dctA* genes, where expression of single Cys variants is not affected (Schubert, 2018). Time-resolved oxidative Cys CL was performed by addition of the catalyst Cu^{2+} phenanthroline under optimized conditions (Stopp *et al*. 2021; see sections 4.1.1, 4.1.2). The results are described below, sorted by location of the selected positions.

TM2: Effect of DctA deficiency on time-resolved CL dynamics

TM2 is the main transducer of the periplasmic signal by a piston-type displacement across the membrane after activating DcuS by C4DC binding at the PAS_P domain (Monzel and Unden, 2015; Salvi *et al*. 2017). The TM2 positions Gly190 and Gly194 are part of a homo-dimer stabilizing $S_{186}xxxGxxxG_{194}$ motif (Stopp *et al*. 2021). Both single Cys variants G190C and G194C reacted rapidly after Cu^{2+} phenanthroline addition and high CL levels were observed within 0.5 min, which did not increase much further after 20 min (Fig. 9A). In the absence of DctA (-DctA/-DcuS) the kinetics of the variant G194C were the same as for the wildtype conditions (Wt) including the lack of a fumarate effect on the kinetics. This also applied to the variant G190C. The kinetics in the absence of DctA resembled the wildtype conditions in high extent, but the CL efficiency was constantly lower (up to 9 %) than under wildtype conditions. In addition, the CL efficiency after 0.5 min without fumarate was 8 % higher than fumarate

activated, which indicates a slightly faster reaction (Fig. 17). Overall, the DctA deficiency had no or minor effects of the Cys CL kinetics of the TM2 representative positions Gly190 and Gly194. The rapid reaction of the variants is therefore independent of the DcuS-DctA interaction, which indicates that the close proximity and stability of the TM2 homo-dimer is retained in the $S_{186}xxxGxxxG_{194}$ region in the absence of DctA.
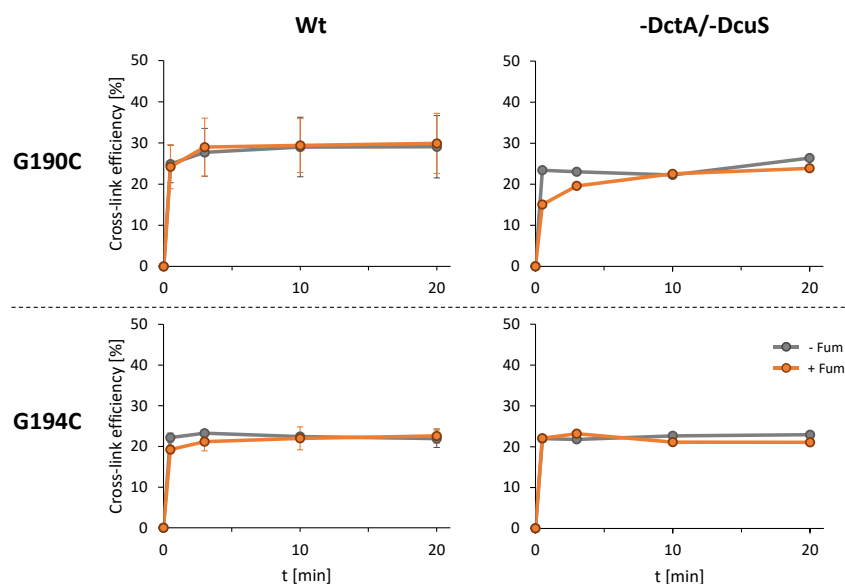
Figure 17. The effect of DctA deficiency on time-resolved oxidative Cys CL of DcuS variants G190C and G194C of TM2. For the *in vivo* CL assay the bacteria of the *E. coli* strains C43 (Wt) and IMW660 (-DctA/-DcuS) were grown in the presence (orange) or absence (gray) of fumarate. Oxidative CL was performed under optimized conditions with respect to Cu^{2+} phenanthroline concentrations and temperature (see 'experimental procedures' section) with and without fumarate. The ratio of CL products to the total amount of DcuS was calculated after scanning the anti-DcuS Western blots (Fig. 34) and evaluating the band intensities in ImageJ software. The plots of the Wt conditions are already published in Stopp *et al*. (2021) (Fig. 9A) and are added for comparing purpose.

Linker: Effect of DctA deficiency on time-resolved CL dynamics

The Linker connects TM2 with the cytoplasmic PAS_C domain of DcuS ($C_{199}ILVKVLKKILFG_{211}$). The linker has a significant influence on the function of DcuS and shows in the Cys CL a behavior that stands out compared to other regions and was consequently considered a separate domain (Stopp *et al*. 2021). The TM2/PAS_C linker CL dynamics showed high sensitivity to fumarate (Stopp *et al*. 2021). The CL efficiency of the single Cys variants I208C and L209C expressed in the wildtype was still low after a few minutes independent of fumarate, but increased sharply in the absence of fumarate, whereas upon fumarate activation the CL efficiency remained significantly lower within 20 min (Fig. 9B). When the Cys CL was carried out in the DctA deficient strain, a drastic effect was observed for both variants. Regardless of fumarate activation, no DcuS CL was detectable for the variant L209C within 20 min and DcuS expression was not impaired (Fig. 18 and 35). The DctA deficiency had a

comparable effect on variant I208C, but the low CL efficiency in the wildtype strain was retained, when fumarate was added.
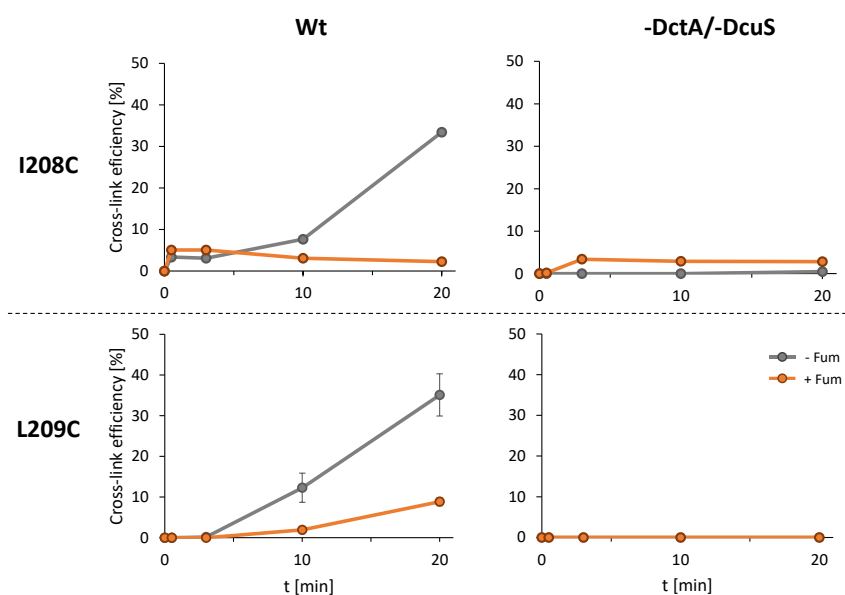

Figure 18. The effect of DctA deficiency on time-resolved oxidative Cys CL of DcuS variants I208C and L209C in the Linker. For the *in vivo* CL assay the bacteria of the *E. coli* strains C43 (Wt) and IMW660 (-DctA/-DcuS) were grown in the presence (orange) or absence (gray) of fumarate. Oxidative CL was performed under optimized conditions with respect to Cu^{2+} phenanthroline concentrations and temperature (see 'experimental procedures' section) with and without fumarate. The ratio of CL products to the total amount of DcuS was calculated after scanning the anti-DcuS Western blots (Fig. 35) and evaluating the band intensities in ImageJ software. The plots of the Wt conditions are already published in Stopp *et al*. (2021) (Fig. 9B) and are added for comparing purpose**.**

Aditionally the single Cys variant K206C that is also located in the linker region, was examined in the time-resolved CL. Lys206 is one of three Lys residues within the linker and represents a contrast to the apolar residues of the positions Ile208 and Leu209 (Fig. 18). In the wildtype strain variant K206C showed a CL efficiency of 23 % after 0.5 min that did not increase further over time. With fumarate, the CL efficiency was already lower from the beginning (0.5 min) and atypically decreased further by factor 0.4 after 20 min. In the absence of DctA, the CL efficiency of the K206C variant was only 7 %, which was lower than in the wild-type strain and even decreased within 20 min to the limit of detectability. If fumarate was added the initial CL efficiency was relatively high (24 %, 0.5 min), but the clear decrease in CL efficiency by factor 0.1 was stronger compared to the wildtype. In the absence of DctA the atypical behavior of variant K206C was intensified (Fig 19). The reason for this behavior is not clear.
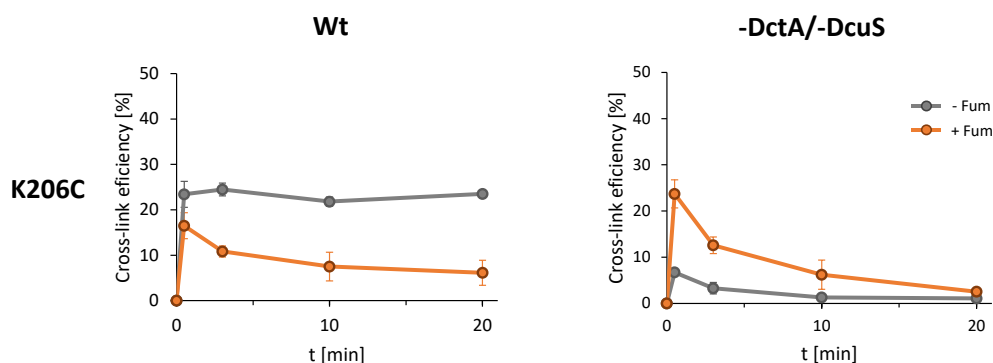
Figure 19. Time-resolved oxidative Cys CL of the linker variant K206C. For the *in vivo* CL assay the bacteria of the *E. coli* strains C43 (Wt) and IMW660 (-DctA/-DcuS) were grown in the presence (+ Fum, orange line) or absence (- Fum, gray line) of fumarate. Oxidative CL was performed under optimized conditions with respect to Cu^{2+} phenanthroline concentrations and temperature (see 'experimental procedures' section) with and without fumarate. The ratio of CL products to the total amount of DcuS was calculated after scanning the anti-DcuS Western blots (Fig. 36) and evaluating the band intensities in ImageJ software. The results of two individual experiments are plotted and error bars are shown.

These results indicate restructuring in the linker of non-activated DcuS in absence of the coregulator DctA. It seems that the linker represents a dynamic element in DcuS, whose structure depends on the interaction with DctA.

PAS$_C$ α1: Effect of DctA deficiency on time-resolved CL dynamics

PAS$_C$ dimerization was already identified to be critical for DcuS function (Monzel *et al*. 2013) and is part of the signal transduction mechanism in DcuS. For inactivated DcuS the CL kinetics of variant R224C are similar to the variants I208C and L209C (compare Fig. 9 and 13), which were clearly influenced by the absence of DctA in case of the Linker variants (Fig. 18). Therefore, Arg224 located in α1 of PAS$_C$ was selected as a representative for effects of DctA deficiency on the *in vivo* time-resolved Cys CL (Fig. 20).

The CL efficiency of variant R224C under wildtype conditions was very low within the first 10 min, but after 20 min the reactivity was strongly increased regardless of fumarate addition. This reactivity was also observed for variant R224C in the DctA deficient strain, but the CL efficiency was even lower after 10 min. After 20 min the CL efficiency increased sharply in the wildtype strain to 36 % (- Fum) and 34 % (+ Fum). But in the absence of DctA the oxidation of R224C resulted in a decreased CL efficiency after 20 min of 21 % (- Fum) and 12 % (+ Fum). Therefore, DctA deficiency clearly effects the dynamics of Cys CL reaction of position Arg224, but less rigorous than for the linker positions Ile208 and Leu209. This shows that α1 of PAS$_C$ just as the linker is subject to restructuration in the absence of DctA.
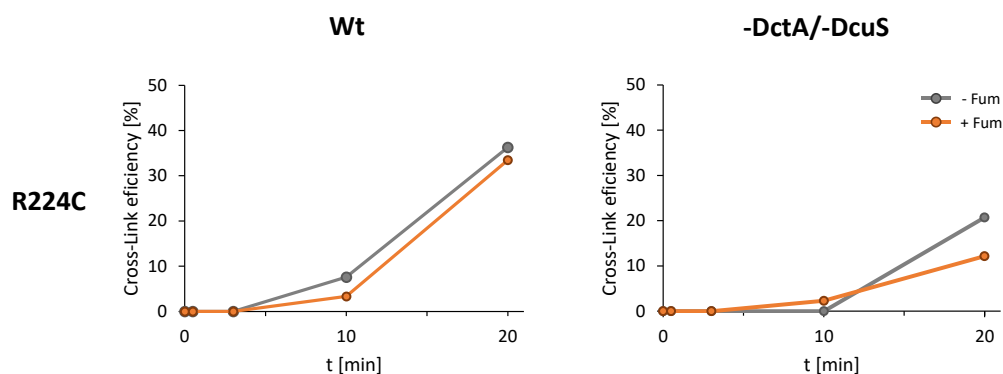
Figure 20. Time-resolved oxidative Cys CL of the PAS$_C$ α1 variant R224C. For the *in vivo* CL assay the bacteria of the *E. coli* strains C43 (Wt) and IMW660 (-DctA/-DcuS) were grown in the presence (+ Fum, orange line) or absence (- Fum, gray line) of fumarate. Oxidative CL was performed under optimized conditions with respect to Cu^{2+} phenanthroline concentrations and temperature (see 'experimental procedures' section) with and without fumarate. The ratio of CL products to the total amount of DcuS was calculated after scanning the anti-DcuS Western blots (Fig. 37) and evaluating the band intensities in ImageJ software. The plot of the Wt condition is already described in section 4.1.2 (Fig 13) and is added for comparing purpose.

4.2   The fumarate proteome of aerobic and anaerobic *E. coli*

The results in this chapter have already been published in Surmann *et al*. (2020) and are only briefly described.

C4DCs represent important substrates for energy and carbon metabolism of *E. coli* (Unden *et al*. 2016). Under aerobic conditions C4DCs are channeled in the TCA cycle and completely oxidized to CO$_2$ to form the redox equivalents ubiquinol and NADH. Reoxidation of those in the respiratory chain generates an electrochemical proton gradient that is used for energy conservation by the ATP-synthase (Maloney *et al*. 1979).

In absence of oxygen the TCA cycle is interrupted and succinate cannot further be metabolized. Therefore, C4DCs are used in the fumarate respiration. Fumarate serves as a terminal electron acceptor requiring electron donors like glycerol and is reduced directly by the fumarate reductase FrdABCD to succinate. Other C4DCs must be converted to fumarate first. L-Malate is dehydrated by the fumarase FumB and aspartate is desaminated the by the aspartase AspA to fumarate (Unden *et al*. 2016; Guest *et al*. 1984).

According to their impact on *E. coli* metabolism, C4DC uptake and utilization require specific control. The DcuSR TCS perceives a variety of C4DC and activates transcription of genes linked to C4DC catabolism. The expression of the *dctA* gene, encoding a C4DC symporter, is stimulated by DcuSR in presence of C4DCs. Under anaerobiosis DcuSR activates the transcription of *frdABC*, *fumB*, and *dcuB* encoding enzymes required for fumarate respiration (Zientz *et al*. 1998; Golby *et al*. 1999) as well as transcription of the citrate fermentation TCS genes *citAB* (Scheu *et al*. 2012).

The adaption of C4DC metabolism on transcriptomic level has been extensively studied, but a comparative study of the effect of C4DC, especially fumarate, on the aerobic and anaerobic proteome is lacking. In this study the changes in protein abundance of *E. coli* were addressed using a global proteomic approach. For this purpose *E. coli* wildtype strain W3110 was cultivated in eM9 medium (Krämer *et al*. 2007) under aerobic conditions (glycerol + O_2) or with fumarate (fumarate + O_2) as carbon source. Anaerobic growth was performed with (glycerol + DMSO + fumarate) or without (glycerol + DMSO) fumarate as electron acceptor. The enrichment of the membrane fraction and integration of membrane proteins into the list of cytosolic proteins should allow a broader view on the global proteomic effects. This experiments primary aim for the revelation of the proteomic response to fumarate under aerobic and anaerobic conditions.

Over all conditions a total of 1657 proteins were detected and assigned to their function in *E. coli* metabolism. After aerobic growth with fumarate as the sole carbon source 211 proteins displayed alterations in protein level more than 2-fold compared to growth with glycerol. The addition of fumarate as a terminal electron acceptor besides DMSO (glycerol + DMSO vs. glycerol + DMSO + fumarate) influenced the intensities of 76 proteins. The abundances found are classified in the following sub-chapters.

4.2.1 Fumarate effect on proteins directly related to the C4DC metabolism

Fumarate is a stimulus molecule for the DcuSR TCS and thus can induce the transcription of some C4DC metabolism specific genes (Zientz *et al*. 1998; Golby *et al*. 1999). This regulatory process is displayed in the proteomic changes. Complementary, the levels of other proteins of the C4DC metabolism are affected. The changes in protein abundances are described in the following two sections and are shown in Figure 21.
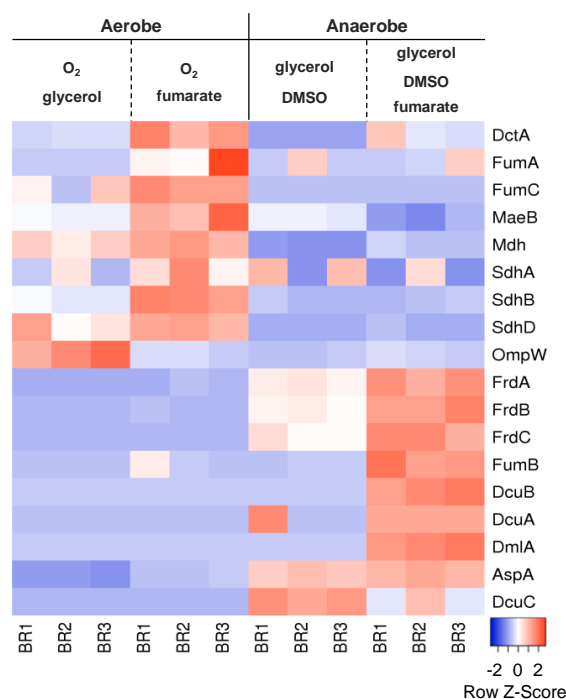
Figure 21. Heatmap visualizing intensity distributions of proteins assigned to the C4DC metabolism. (q < 0.05, ratio > 1.5 or < 0.67 in at least one comparison) prepared with Heatmapper (Babicki *et al*. 2016). Intensities of three biological replicates (BR1-3) per condition are visualized (blue, relatively decreased; red, relatively increased). Figure modified according to Surmann *et al*. (2020).

Specific alterations of the aerobic C4DC metabolism

Among the proteins, whose level was significantly affected by fumarate, the DcuSR regulated aerobic C4DC symporter DctA was increased. The abundance of further proteins of the C4DC metabolism increased in the presence of fumarate. The aerobic fumarases FumA and FumC, the NADP-dependent malic enzyme MaeB, the malate dehydrogenase Mdh, and the succinate dehydrogenase subunits SdhB and SdhD showed elevated protein levels in at least one comparison. Despite the generally lower level under aerobic conditions compared to the anoxic conditions the aspartate ammonia-lyase AspA showed a significant fumarate driven increase in protein level. An opposite effect of fumarate could be observed for the outer membrane protein OmpW. Although OmpW can bind fumarate and is connected to the C4DC metabolism (Xiao *et al*. 2016), fumarate caused a decrease in OmpW level.

Specific alterations of the anaerobic C4DC metabolism

The adaption to fumarate under anoxic conditions included changes in abundance of proteins that are directly linked to C4DC metabolism. This includes the C4DC antiporter DcuB, the anaerobic fumarase FumB, and the fumarate reductase FrdABC that are directly regulated by DcuSR (Zientz *et al*. 1998). Furthermore, the level of the D-malate/3-isopropylmalate dehydrogenase DmlA, which is essential for growth on D-Malate (Lukas *et al*. 2010), increased

significantly under aerobic conditions. Both DcuC and the C4DC antiporter DcuA showed a fumarate-dependent trend (DcuC decreased, DcuA increased) of their protein levels under anaerobic conditions that has not been observed on the transcriptional level (Zientz *et al*. 1998; Golby *et al*. 1998; Zientz *et al*. 1999).

4.2.2 Aerobic adaptations of the TCA cycle and related pathways to fumarate as the only carbon source

Many proteins, whose abundance has been affected by fumarate under aerobic conditions, are part of the TCA cycle. Almost all TCA cycle proteins increased upon replacment of gylcerol by fumarate as the carbon source. This effect was also observed for a broad range of enzymes of the feeding and the bypass reactions (Fig. 22). The aerobic C4DC symporter DctA as major fed-pathway for external fumarate increased in level (see section 4.2.1), whereas no significant change was detected for the transporter DauA shutteling C4DC at a pH = 5 (Karinou *et al*. 2013). The malic enzyme MaeB and PEP-carboxykinase PckA participating in the PEP/pyruvate bypass and gluconeogenesis as well as the glyoxylate bypass enzyme malate synthase AceB were increased as a response to fumarate replacing glycerol as the carbon source. Remarkably, a broad range of 33 proteins involved in amino acid synthesis or degradation were decreased in the presence of fumarate (Surmann *et al*. 2020). As a major part of this group of proteins the branched-chained amino acids (IlvABCDEH and LeuAB) and methionine (MetACFKL) pathways were decreased in level. The inverse effect was observed for succinate-semialdehyde dehydrogenase GabD and 4-aminobutyrate aminotransferase GabT proteins, which provide succinate from arginine degradation and were increased in level, when fumarate was the carbon source. The same was valid for tryptophanase TnaA and alanine racemase DadX, which feed the TCA cycle by producing pyruvate from tryptophan or alanine. Another group of enzymes with an increase in protein level contributing to TCA cycle anaplerosis are involved in fatty acid degradation by β-oxidation producing acetyl-CoA. Although FadI and FadJ are prevalent in anaerobic β-oxidation of *E. coli*, grown on various fatty acids, and serve parallel function to FadA and FadB (Campbell *et al*. 2003), all of them showed increased protein levels aerobically grown on fumarate as a sole carbon source (Fig. 22).
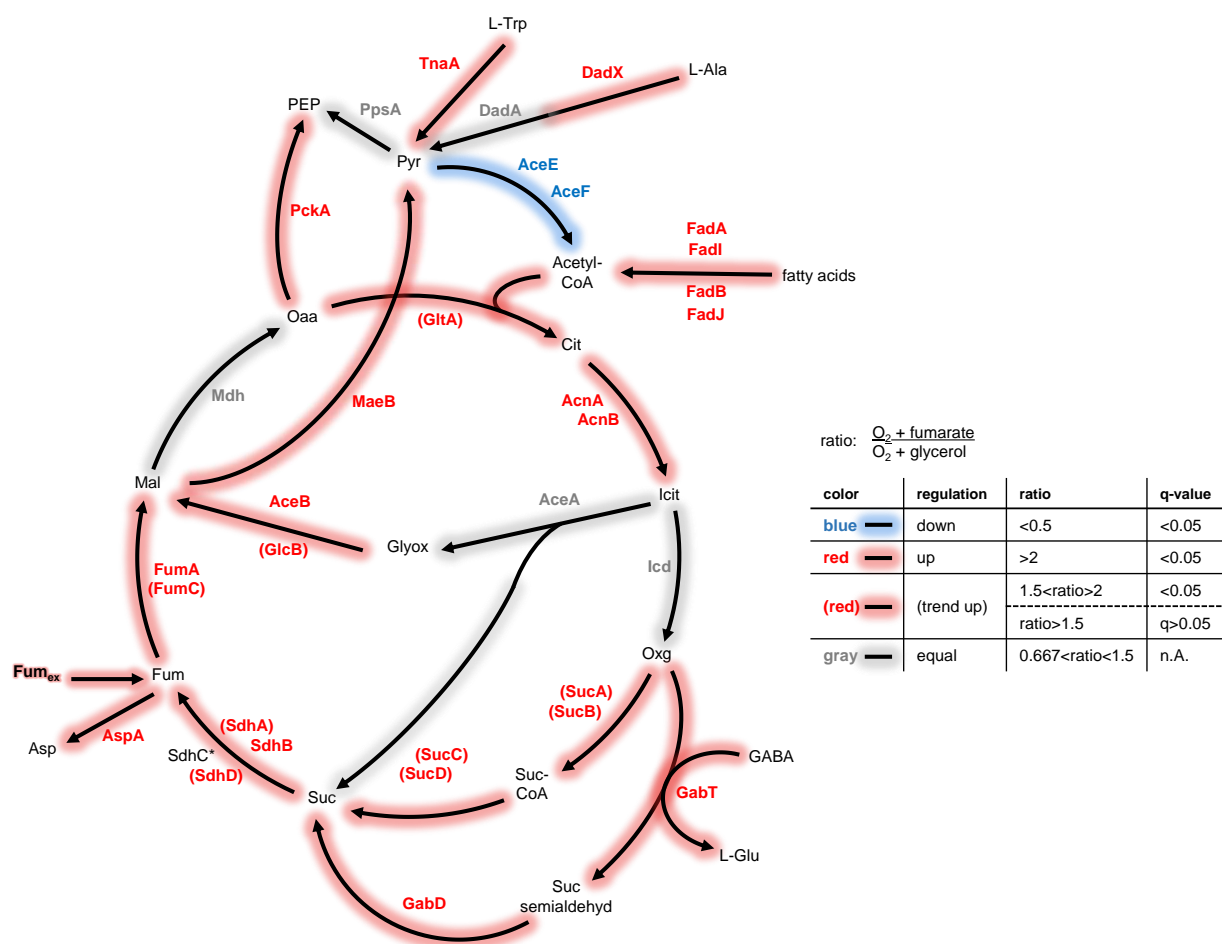
Figure 22. Effects of fumarate on the TCA cycle during aerobic growth. Alteration in protein levels of the TCA cycle and related pathways are highlighted. Proteins that significantly increased in level (ratio > 2 & q < 0.05) are shown in red letters. Proteins, which show a trend in regulation (1.5 < ratio > 2 & q < 0.05 or ratio > 1.5 & q > 0.05), are shown in red letters as well with additional red parentheses. Blue letters indicate proteins that significantly decreased in level (ratio < 0.5 & q < 0.05). Proteins that showed no trend in regulation (equal, 0.667 < ratio < 1.5) are shown in gray letters. *Protein SdhC was not detected. Figure modified according to Surmann *et al.* (2020).

Complementary to an almost complete increase in the level of TCA enzymes the level of the NADH-quinone oxidoreductase Nuo complex was increased, whereas the non-coupling respiratory enzymes glucose dehydrogenase Gcd, GlpD, and NADH dehydrogenase Ndh were decreased (Surmann *et al.* 2020).

The pyruvate dehydrogenase subunits AceE and AceF represent the only TCA cycle associated enzymes, whose protein level deacresed (AceE 0.45-fold, AceF 0.46-fold) upon replacing glycerol as the sole carbon source by fumarate (Surmann *et al.* 2020).

4.2.3 Anaerobic enhancement of motility and chemotaxis by fumarate

Among the 76 proteins with a significant change in protein abundance and excluding the already mentioned C4DC-specific abundancy alterations of proteins involved in fumarate respiration and C4DC transport (see section 4.2.1), a significant number of proteins is involved in motility and chemotaxis. A large part of the Fli and Flg proteins that are part of the flagella (synthesis),

the flagellar motor, the flagellar basal body as well as the chemotaxis proteins (CheY and CheZ) showed a significantly increased protein level (fold change > 2) in presence of fumarate. In addition to these proteins eleven other proteins of this functional group displayed a trend in regulation (q-value < 0.05; fold change > 1.5, < 2), including the methyl-accepting chemotaxis proteins (Tsr, Trg, Tar, Tap) and CheA and CheW. Overall, the motility and chemotaxis proteins generally appeared in higher abundance under anaerobic than aerobic conditions (Surmann *et al*. 2020).

4.2.4 CRP and DcuR effects on TCA cycle regulation and related pathways

The proteomic analysis of the fumarate effect revealed many changes in level of proteins under aerobic and anaerobic conditions that are not controlled by the DcuSR C4DC TCS. Conspicuously, enzymes of the TCA cycle and associated anaplerotic and bypass reactions (glyoxylate shunt, pyruvate bypass) and of gluconeogenesis are increased in protein level (see section 4.2.2), but only DctA is shown to be regulated by DcuSR in presence of oxygen within this coherent group of proteins yet (Zientz *et al*. 1998; Golby *et al*. 1998; Unden *et al*. 2016). Many of the fumarate-induced, but DcuS-DcuR independent genes are preceded by cAMP receptor protein (CRP) binding sites (summarized in Surmann *et al*. 2020). Strikingly, also levels of proteins like the transcriptional regulator MalT or the periplasmic binding proteins of maltose and xylose catabolism MalE and XylF were strongly increased during growth on fumarate (Surmann *et al*. 2020).

To test the supposed regulatory connection plasmid encoded fusions of the *lacZ* gene and the complete intergenic upstream promoter region of selected TCA, cycle-related genes were generated. The expression of the *lacZ* reporter gene was tested in *E. coli* BW25311 derived strains containing inactivated *dcuR* (JW4085) or *crp* (JW5702) genes (Baba *et al*. 2006). The results are shown in Fig. 23. In a wildtype background the expression of *lacZ* was stimulated by factor 2.8 by fumarate compared to glycerol representing an established model for DcuSR regulated expression (Fig 23A). The *aspA*, *pckA*, *fumA,* and *sdhC* promoter region caused a fumarate stimulated increase of *lacZ* reporter gene by factor 2.0 - 2.3. (Fig. 23B to E), which is consistent with the increase in protein level (see section 4.2.2). In a DcuR deficient background the fumarate driven effect was lost for all promoter-*lacZ* fusions. Notably, the expression of *aspA$_P$*, *fumA$_P$*, and *sdhC$_P$* reporter gene fusions was slightly increased compared to the Wt strain, when glycerol was the carbon source (Fig. 23C to E). The CRP deficient strain caused a loss of the fumarate effect in parallel with a generally very low *lacZ* expression (Fig. 23) indicating an over-riding regulation by CRP in the TCA cycle context.
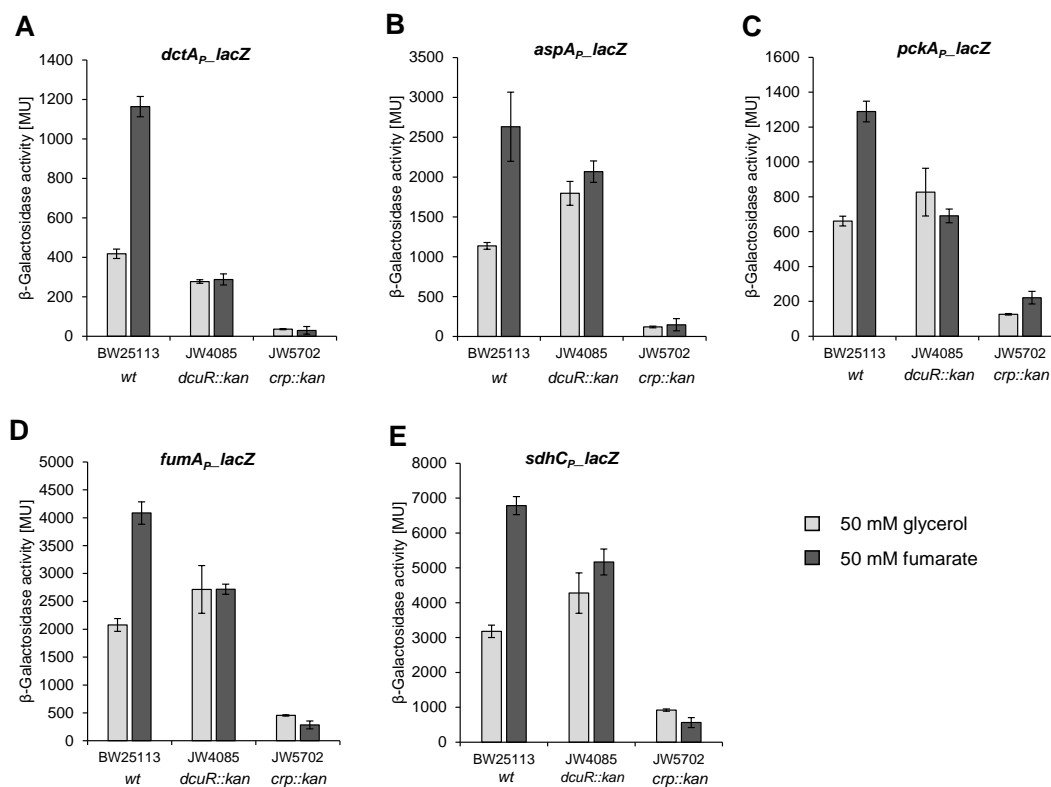
Figure 23. Effect of fumarate on the expression of promoter-*lacZ* fusions depending on DcuR and CRP regulation. Each strain was transformed with the plasmids harboring the *lacZ* fusions with the upstream intergenic region of *dctA* (pMW103, A), *aspA* (pMW2498, B), *pckA* (pMW3037, C), *fumA* (pMW3038, D), and *sdhC* (pMW3039, E). Aerobic cultivation was performed in 48-well plates in eM9 with glycerol (50 mmol/l) or fumarate (50 mmol/l) as carbon source to an OD_{578} of 0.4 - 0.7. Figure modified according to Surmann *et al*. (2020).

For almost all genes of enzymes with a clear increase in protein level by feeding on fumarate as a sole carbon source (see section 4.2.2) a CRP binding site has already been shown or has been annotated based on the CRP binding consensus sequence (summarized in Surmann *et al*. 2020). Remarkably, this also applies to the genes *frdA*, *dcuB,* and *fumB* of anoxic fumarate respiration, which are specifically controlled by DcuSR (Zientz *et al*. 1998; Golby *et al*. 1998; Unden *et al.* 2016). Motif analysis revealed potential CRP binding sites for *frdA* and *dcuB*/*fumB* with a match in sequence identity of 50 to 55 %. However, comparing the promoter regions of the genes *citAB*, *dctA*, *dcuB*, and *frdA* carrying verified DcuR binding sites, the upstream intergenic regions of *aspA* and *pckA* contained conserved sequences that could represent DcuR binding sites (Surmann *et al*. 2020). This indicates a potential parallel regulation of aerobic and anaerobic C4DC metabolism by DcuSR and cAMP/CRP.

5 Discussion

5.1 Signal transduction by the sensor kinase DcuS

The membrane integral sensor histidine kinase DcuS perceives various C4DCs and citrate at the periplasmic PAS_P domain (Kneuper *et al*. 2005; Krämer *et al*. 2007). C4DC binding results in autophosphorylation at the cytoplasmic kinase domain (Janusch *et al*. 2002b). The physical separation of signal input and autophosphorylation, especially by the membrane, requires a signal transfer mechanism by structural reorganization. Binding of a stimulus molecule at PAS_P causes compaction of the central β-sheet at the binding pocket causing an uplift or shortening of the C-terminal β-strand in CitA and presumably the homologous DcuS (Sevvana *et al*. 2008; Monzel and Unden, 2015; Salvi *et al*. 2017). This forces the α6 of PAS_P and the N-terminal part of TM2 to follow this uplift in axial direction described as a piston-type movement (Monzel and Unden, 2015). The experimental evidence for the piston-type movement was limited to the N-terminal part of TM2. The aim of this study was to investigate the structure of the complete TM domain and the C-terminally adjacent domains of DcuS with biochemical methods under *in vivo* conditions gaining an advanced insight in the signaling mechanism of DcuS upon activation by C4DCs.

5.1.1 A membrane spanning continuous double helix connects DcuS signal input and output

In DcuS TM2 was shown to represent the major structure in signal transduction from the periplasm to the cytoplasmic domains of DcuS due to its change of the relative positioning within the membrane (Monzel and Unden, 2015). The signal input domain PAS_P and N-terminal part of TM2 are connected by a joint α-helix of α6 (PAS_P) and TM2 comprising the positions Val172 - Ser186 including four starting residues of TM2. A more complete understanding of the signaling mechanism requires detailed knowledge of the full secondary structures crossing the membrane.

DcuS is *in vivo* a dimer or higher oligomer, regardless of the signaling state (Scheu *et al*. 2010b), enabling structure examination by an oxidative Cys cross-linking (Pakula and Simon, 1992). Hence, single Cys variants of subsequent positions Val187 to Arg241 were oxidatively cross-linked *in vivo*. Over the whole distance the single Cys variants showed a variation in CL efficiency from 0 to 86 %. The spacing of the local maxima of the CL-efficiency can be described as Val_{172}-4-3-4-3-4-4-4-(3/4)-(3/4)-4-4-4-3-4-3-3-4-Gly_{234} (Fig. 9 and 12) in a joint projection of Monzel and Unden (2015) and Stopp *et al*. (2021). Canonical α-helices have a rise of 1.5 Å per residue and 3.6 residues per turn (Pauling and Corey, 1951; Pauling *et al*. 1951).

Consequently, by a spacing of +3/+4 residues are located on the same side of the α-helix resulting in the same periodicity of contact sites in a canonical dimer. α-Helical dimers are often organized as coiled coils, whose interaction is determined by a +3/+4 periodicity of predominantly apolar residues in a heptad repeat of two helical turns (Crick, 1953). In DcuS, however, the pattern of local maxima of CL efficiency fits the periodicity of a canonical coiled coil only partially. The pattern of the core region of TM2 and of the entire linker shows mostly a spacing of +4 (Ser_{186}-4-4-4-(3/4)-(3/4)-4-4-Glu_{213}), representing an average period of 3.86 ($\pm$ 0.22) residues per turn. Notably, there is a switch in the spacing from a 4/3 to a 3/4 pattern in the membrane-cytoplasm transition region Thr_{198}-X(7)-Leu_{205} upon fumarate activation. There was no change in the spacing of labeling maxima on other position regardless the DcuS signaling state (Fig. 9 and 12).

Therefore, DcuS contains no canonical α-helical homo-dimer for the full length from Val172 to Gly234. The pattern of +3 or +4 spacing with an average period of 3.63 ($\pm$ 0.45) residues per turn, however, strongly indicates a helical dimer that is stable in both inactivated and fumarate activated DcuS. This is supported by the crystal structure of dimeric α1 in the PAS_C dimer of the DcuS homologous CitA (Weisenburger *et al*. 2017) and is in line with the α-helical structure of α6 in PAS_P, even though this domain was crystallized as a monomer, when the isolated domain was used (Sevvana *et al*. 2008; Cheung and Hendrickson, 2008). Additionally, the comparison of DcuS PAS_C with the CitA PAS_C structure (Weisenburger *et al*. 2017) strongly indicates that Gly234 is part of the β-strand (β1), rather than part of the continuous helix ending at position Ser230 of α1 in PAS_C.

Based on the biochemical experiments and the structures of PAS_P and PAS_C a model of the DcuS dimer was created that contains a double helix ranging from position Val172 to Ser230. The helix therefore connects PAS_P as the signal input domain via TM2 and the linker with α1 of PAS_C, which represents the cytoplasmic signal output site (Fig. 24).
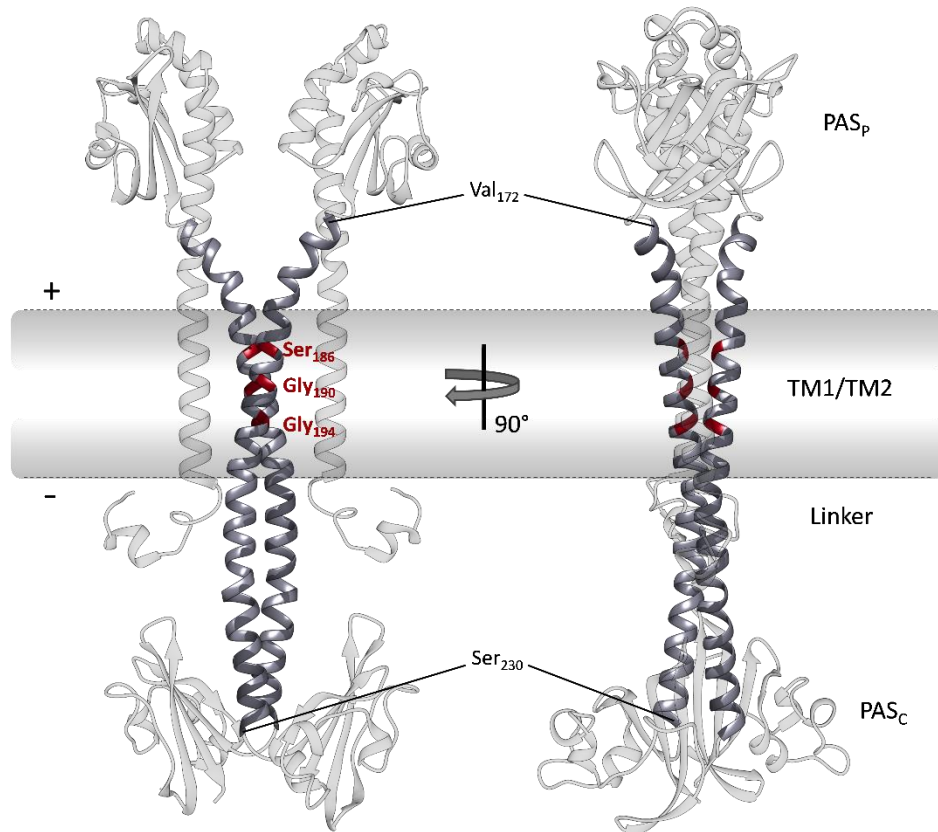
Figure 24. Model of dimeric DcuS with an emphasis on the bi-helical TM2 region extending from α6 of PAS$_P$ into α1 of PAS$_C$. The positions of Ser186, Gly190, and Gly194 are highlighted in red. other domains of both DcuS monomers are grayed out. DcuS was modeled as a composition of the structures of PAS$_P$, PAS$_C$, and modelled TM2 and the linker from CL studies. UCSF Chimera was used to fuse the structures obtained by (homology) modeling (PAS$_P$, PAS$_C$) and predicted structures (TM2, linker). The PAS$_P$ structure of DcuS was used (malate bound) (PDB ID: 3BY8). The PAS$_C$ dimer structure was modeled using the structure of CitA as a template (PDB ID: 5FQ1). The helix dimer from Val172 to Glu213 was derived by structural analysis of the C-terminal region of PAS$_P$ (α6) and the N-terminal region of PAS$_C$ (α1) (Cheung and Hendrickson, 2008; Etzkorn *et al*. 2008; Weisenburger *et al*. 2017), and the CL data (Monzel, 2014; Monzel and Unden, 2015; this work) for Val172 to Ser230. The cytoplasmic N-terminal coil, TM1, and the TM2-PAS$_C$ linker were predicted as single subdomains by the online tool I-TASSER (Yang *et al*. 2015). The kinase domain is not shown. The model is adapted from Stopp *et al*. (2021).

The S$_{186}$xxxGxxxG$_{194}$ motif in TM2 stabilizes the dimeric helix

TM2 of DcuS harbors a combined version of a GxxxG and a (small)xxx(small) sequence motif that was described as the S$_{186}$xxxGxxxG$_{194}$ tandem motif (Steinmetz, 2014; Stopp *et al*. 2021). GxxxG as well as (small)xxx(small) motifs are over-represented in TM helices (Senes *et al*. 2000; Kleiger *et al*. 2002) and mediate interaction of α-helices in general (Russ and Engelman, 2002; Schneider and Engelman, 2004). In the homo-dimer of the human membrane protein glycophorin A the GxxxG motif allows close contact by forming a plain site serving as dimerization surface for a ridge from the residues of the complementary GpA monomer (MacKenzie *et al*. 1997; Smith *et al*. 2001). The interaction of GpA with a focus on the impact of the GxxxG motif for GpA homo-dimerization was studied extensively with mutational approaches (Lemmon *et al*. 1992; Langosch *et al*. 1996; Schneider and Engelman, 2003).

Therefore, the influence of the TM2 motif on the homo-dimerization of DcuS and especially of the isolated TM2 was investigated (Steinmetz, 2014; Stopp *et al*. 2021).

With the GALLEX system (Schneider and Engelman, 2003) the homo-dimerization of isolated TM2 with a length of 16 amino acids was tested. The wildtype TM2 fusion construct showed a strong interaction, whereas both double variants S186C+G190A and G190A+G194A decreased the interaction drastically. Therefore, TM2 is a homo-dimer that is stabilized by the residues of the $S_{186}xxxGxxxG_{194}$, which fits perfectly with the local maxima of the CL efficiency (Fig. 7). In the bacterial two-hybrid (BACTH) system (Karimova *et al*. 1998; Karimova *et al*. 2000) full length DcuS showed strong interaction, which was also decreased in the G190A+G194A double variant. Therefore, $G_{190}xxxG_{194}$ of the $S_{186}xxxGxxxG_{194}$ motif is essential for DcuS homo-dimerization.

Since TM2 is part of the continuous double helix (Fig. 24), it is concluded that the $S_{186}xxxGxxxG_{194}$ motif is a stabilizer of the TM2-TM2' homo-dimer, and the $G_{190}xxxG_{194}$ motif stabilizes the entire double helix, which is important for signal transduction.

5.1.2 A rigid TM2 dimer and a dynamic linker accomplish transmembrane signaling in DcuS

In sensor kinases TM signaling is still enigmatic, but piston-type movement, scissor-like kinking, and helical rotation are proposed as unique or combined mechanisms of TM signaling (Molnar *et al*. 2014; Monzel and Unden, 2015; Gushchin *et al*. 2017). Gushchin and Grodeliy (2018) discuss further structural rearrangements of sensor kinases with four TM helices during activation.

In DcuS the double helix ranging from PAS_P into PAS_C is the physical connection of periplasmic signal input and cytoplasmic signal conversion and output, which depends on structural rearrangements. Oxidative Cys CL is known as an effective method for detecting conformational changes in sensor kinases signal transduction (Lee *et al*. 1995; Hughson and Hazelbauer, 1996; Molnar *et al.* 2014). Cys CL was applied to DcuS, focusing on α-helical changes with monitoring of CL efficiency over time and the effect of fumarate.

Time-resolved Cys CL of residues Gly190, Gly194 and Thr198 in TM2 showed a rapid reaction that was not altered by the signaling state of DcuS. The response of Ser186 differed by the slowly increasing CL efficiency in the inactivated state (Fig. 9A). Therefore, the TM2 homo-dimer persists after activation with possibly a slight rearrangement at the N-terminal region close to the periplasm. This stability of the $S_{186}xxxGxxxG_{194}$ motif is essential for the function of DcuS in fumarate-stimulation (Steinmetz, 2014; Stopp *et al*. 2021). The piston-type shift was

demonstrated for the N-terminal part of TM2 (Monzel and Unden, 2015) and the data of this work strongly suggests a piston-type shift of the entire TM2 dimer.

The stability of the TM2 dimer argues against major contribution by other types of mechanisms, such as rotation and scissors-like movements. Proline residues in TM helices lead to kinks or non-helical structures (Riek *et al.* 2001; Rigoutsos *et al.* 2003; Senes *et al.* 2004) and can form hinge-like structures in a scissors-like movement (Lemmin *et al.* 2013; Molnar *et al.* 2014). TM2, however, does not contain any proline residues, and rotation should show detectable changes in the CL that were not observed.

The linker connects TM2 with PAS_C. The linker differs from TM2 in the extent of helical spacing indicating a structural response to activation of DcuS by fumarate. In the time-resolved Cys CL fumarate had a clear impact on CL efficiency at positions Leu201, Leu205, Ile208, and Leu209 (Fig. 9B) delimiting the linker from TM2 as a separate domain with distinct properties. At the C-terminal end the linker is defined by the start of PAS_C from DcuS and CitA (Etzkorn *et al.* 2008; Weisenburger *et al.* 2017). The sequence of the linker can thus be defined as $C_{199}ILVKVLKKILFG_{211}$. The decrease of Cys reactivity at positions Leu205, Ile208, and Leu209 implies structural rearrangements of the linker upon fumarate addition, which could involve attenuated helix interactions or separation of the helical region in the presence of fumarate. The impact of fumarate differed between the N- and C-terminal part of the linker represented by position Leu201. The reactivity of L201C resembled somehow the TM2 CL dynamics in the fumarate activated state, but the clear difference between the signaling states speaks for a clear distinction to TM2. Therefore, it is assumed that the membrane/cytoplasm transition area acts as a switch between the rigid TM2 dimer and the flexible linker within the continuous double helix.

The importance of the linker for DcuS function is further supported by functional assays of DcuS linker Ala variants (Stopp *et al.* 2021). Thus, mutation of L209A from the $L_{201}xxxLxxxL_{209}$ sequence affected the activity of DcuS, whereas mutation K206A and V202A did not. In Monzel and Unden (2015) the Leu205 and Leu209 were shown to be sensitive to changes in accessibility to labeling by hydrophilic reagents upon activation of DcuS by fumarate. Leu205 becomes inaccessible and Leu209 accessible, complementing the model of a complex rearrangement of the linker. It can be suggested that Leu205 moves into the hydrophobic membrane core region as result of the piston-type uplift (Monzel and Unden, 2015) and Leu209 becomes accessible due to separation of the helices.

In summary a recent model for signal transduction by DcuS is based on the continuous double helix in the DcuS dimer (Fig. 25).
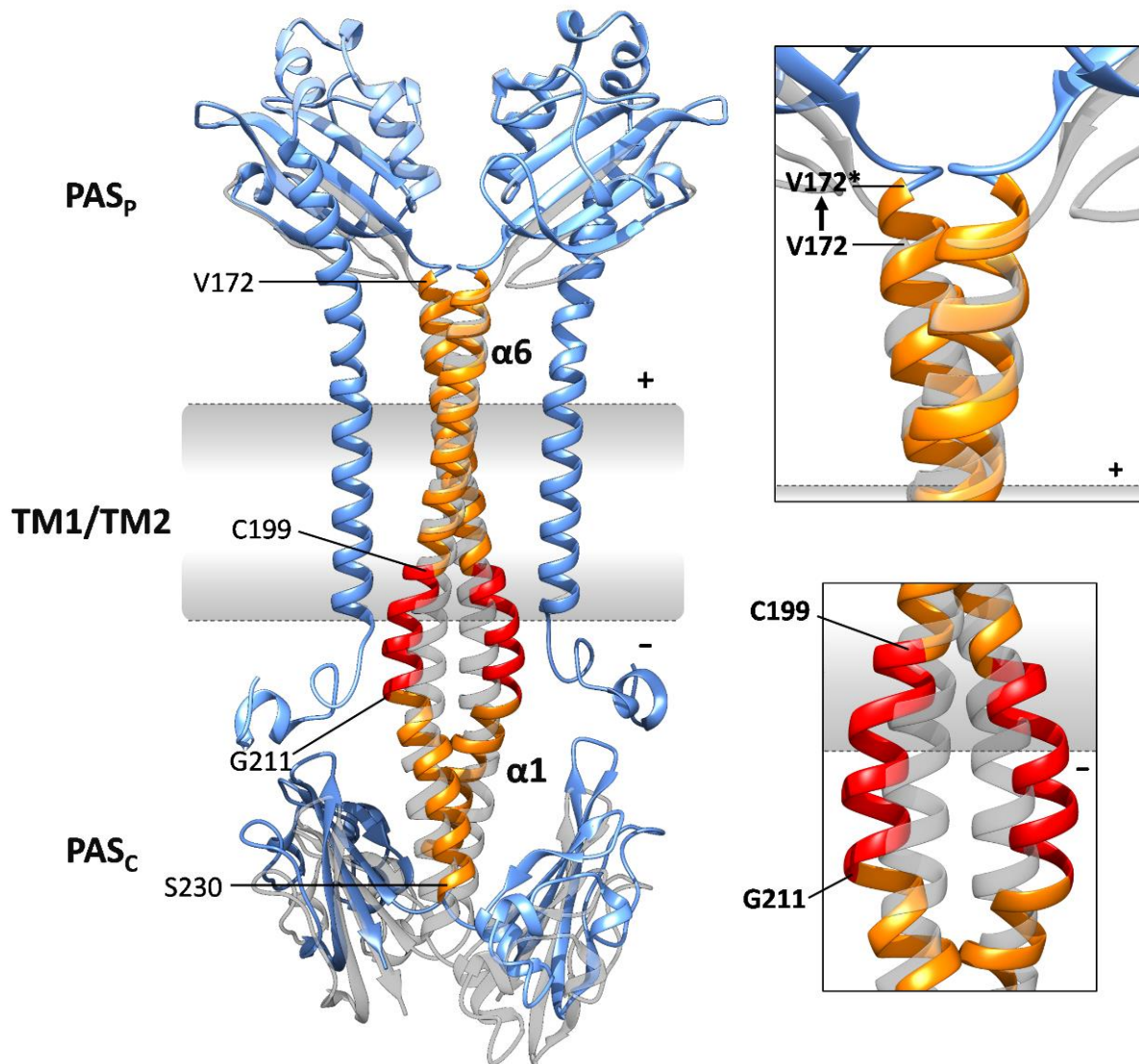
Figure 25. Model of dimeric DcuS with an emphasis on the bi-helical TM2 region extending from α6 of PAS$_P$ into α1 of PAS$_C$ and its role in TM signaling. Dimeric DcuS with the homo-dimeric α6(PAS$_P$)-TM2-linker-α1(PAS$_C$) helix in the presence (orange or red) or absence (grayed out) of fumarate. α6, α1, and amino acid residues delineating domains are shown: Val172 as the start site for α6, Val172/Cys199 as the limits of the rigid α6(PAS$_C$)-TM2 helix, Cys199/Gly211 as the linker region, and Gly211/Ser230 as α1. The structures of PAS$_P$, PAS$_C$, and TM1 are shown in light blue. The piston movement of TM2 upon fumarate activation (Monzel and Unden, 2015) is presented in the top magnification box by the movement of residue Val172 (V172) to the periplasmic position (V172*) in the fumarate-activated state. Val172 marks the starting point of the helix, and Cys199 and Gly211 the approximate starting and endpoints of the linker. The supposed movement of the linker monomers upon fumarate activation is shown in the bottom magnification box. The model was created as described in Fig. 24 and adaptation to the activated state was modeled with UCSF Chimera (Pettersen *et al*. 2004). The structure of the apo PAS$_P$ monomer was obtained using the structure of DcuS homolog CitA as a template (PDB ID:2V9A). Figure from Stopp *et al*. (2021).

In the DcuS homologous CitA binding of citrate to the PAS$_P$ domain causes a compaction of the central β-sheet around at the binding pocket and an uplift or shortening of the C-terminal β-strand (Sevvana *et al*. 2008; Salvi *et al*. 2017). This triggers an axial uplift of α6 of PAS$_P$, which initiates the piston type movement (Monzel and Unden, 2015) as the basis of TM signal transduction in DcuS. As a driving force the piston lifts the entire continuous double helix, whereby TM2 remains a stable homo-dimer as the signal crosses the membrane. On the

cytoplasmic side the TM2 piston movement is perceived by the linker. In the transition region the stability of the helical structure is modified, resulting in reorganization or the separation of the helices from one another. Thus, the uplift by the piston mode is diminished (Fig. 25). The structural changes in the linker are passed on via the C-terminal part of the continuous double helix (α1 of PAS$_C$) and are supposed to subsequently reorganize the PAS$_C$ dimer, which then controls the kinase domain and activity as suggested previously (Etzkorn *et al*. 2008; Monzel *et al*. 2013).

Signal transduction by the PAS$_C$ domain is further discussed in section 5.1.3.

Transmembrane signaling of DcuS in the context of mechanisms in other sensor kinases

In dimeric sensor kinases, comprising four TM helices the piston-type shift, helical rotation, and scissoring were discussed as actually possible rearrangements upon activation. Other model mechanisms have been suggested but are purely theoretical. However, it becomes clear that various combined mechanisms can occur in TM siganling. (Bhate *et al*. 2015; Gushchin and Grodeliy, 2018).

The PhoQ sensor kinase of enterobacteria, capable of sensing divalent cations and osmotic upshift (Véscovi *et al*. 1996; Yuan *et al*. 2017), displays a counterpart to DcuS signal transduction. PhoQ TM signaling is achieved by a combination of rotation and scissors-like kinking that is promoted by a central Pro kink (Lemmin *et al*. 2013; Molnar *et al*. 2014). Furthermore, a polar interaction in the TM domain by an Asn residue is sensitive to apolar substitutions and stabilizes the PhoQ TM domain (Goldberg *et al*. 2010).

Structural data of the nitrate/nitrite sensor NarQ revealed a merged mechanism of TM signaling that is somehow related to DcuS signal transduction by involving a piston-type shift. Binding of nitrate causes shifts in TM1 to the periplasmic site and helical rotation and diagonal scissoring promoted by a Pro residue in TM2. This rearrangement in the antiparallel four-helix coiled coil in the membrane triggers rearrangement in the cytoplasmic HAMP domain in a lever-like mechanism (Gushchin *et al*. 2017, 2020), showing that piston-typ shifts can be part of a complex mechanism in TM signaling.

In the *E. coli* chemoreceptors Tsr and Tar the mechanisms of TM signaling appear more closely related to those of DcuS. Upon activation a TM2 piston-type uplift of small amplitude is the major mechanism in TM signaling (Ottemann *et al*. 1999; Hall *et al*. 2011). In Tsr a highly conserved linker of 5 amino acids in the membrane/cytoplasm transition region (called 'control cable') mediates conversion of a TM signal to the cytoplasmic HAMP domain (Kitanovic *et al*. 2011, 2015). These similarities between Tsr and DcuS suggest that piston-like shifts and signal conversion by linker-like structures are common and present in unrelated sensor kinases. In

BvgS from *B. pertussis* similar linker structures are found. In BvgS a piston-type uplift is suggested for the TM2 homo-dimer in BvgS that is followed by a highly dynamic helical linker in the cytoplasm. BvgS comprises of a single TM helix (Lesne *et al*. 2017).

Regardless of the mechanism for TM signal transduction, no sequence motif comparable to the $S_{186}xxxGxxxG_{194}$ motif of DcuS TM2 is described for other sensor kinases. Even within the DcuS/CitA orthologs the motif or even parts of it are poorly conserved (Stopp *et al*. 2021). Only in the chemoreceptor Tsr a polar QxxS motif is known to contribute to TM domain interaction (Sal-Man *et al*. 2004). This indicates a mostly unrecognized and possibly unique mechanism in stabilization of a TM signaling domain in DcuS. The sensor kinases discussed here, with exception of BvgS, contain HAMP domains as cytoplasmic converters, representing a major difference to the PAS_C domain of the DcuS/CitA family serving this function.

5.1.3 The PAS_C domain is a dynamic signal transducer

PAS domains are widespread in sensor kinases and frequently involved in signal integration and transduction (Möglich *et al*. 2009). PAS domains have a high tendency to homo-dimerize as described for FixL from *Bradyrhizobium japonicum* (Ayers und Moffat, 2008) and VicK from Streptococcus mutants (Wang *et al*. 2013). In NifL from *Azotobacter vinelandii* a changed redox status in the first PAS domain causes in direct consequence a weakened dimerization of the second PAS domain, which suggests a signal relay in NifL due to changes in the quaternary structure and dimerization of the second PAS domain (Salvany *et al*. 2010).

In DcuS binding of C4DC at PAS_P generates a signal that is transduced through TM2 and the linker. The signal reaches PAS_C via the α1 helix in the N-terminal part of PASc. PAS_C plasticity was proposed to be essential in signal transduction (Etzkorn *et al*. 2008). Furthermore, mutagenesis studies of PAS_C revealed a cluster of ON-variants on the surface of the PAS_C monomer. Many of these fumarate-insensitive variants showed impaired homo-dimerization of DcuS suggesting that PAS_C controls kinase activity by dimerization (Monzel *et al*. 2013). By using individual Cys variants of DcuS, PAS_C was investigated further in to gain insight in signal transduction by PAS_C.

The Cys CL of single Cys variants showed that α1 of PAS_C is part of the continuous double helix and ends at position Ser230 (see section 5.1.1).

CL efficiency was high for the α1 adjoining positions Glu233, Gly234 and Val236 (> 60 %) (Fig. 12) indicating a large contact site in the dimer. Close contacts of Gly234 and Val235 with their corresponding residues in the second monomer conflicts with the homology structure of the PAS_C dimer as suggested by CitA from *G. thermodenitrificans* (Weisenburger *et al*. 2017;

Fig. 26). However, the plasticity of PAS$_C$ might support high disulfide formation under oxidizing conditions. The CL efficiency decreased from position Val236 to Asp240 continuously, corresponding to their proposed position in the β1 strand in the PAS$_C$ model, in which Asp239 is the outermost position (Fig. 26). The differences of the CL efficiency between both signaling states were relatively high at positions Ile231 to Val236. However, a higher reactivity with fumarate was observed for the positions Ile231 and Gly234 in the time-resolved CL (Fig. 13) and does not correspond to the structural Cys CL approach, in which the CL efficiency was higher without fumarate (Fig. 12). The difference can be partly artificial under strongly oxidizing conditions and is possibly a misleading effect. Nevertheless, this can also be an indication of the flexibility and restructuring of the PAS$_C$ domain in the β-sheet upon activation of DcuS.

The time-resolved Cys CL provides information on structural rearrangements during signal transduction (see. section 5.1.2). Fumarate had a clear influence on the CL efficiency kinetics of all tested variants (except R224C) (Fig. 13), reflecting structural changes upon activation. This confirms the assumption that PAS$_C$ is a highly dynamic domain and that its plasticity is essential in signal transduction (Etzkorn *et al*. 2008; Monzel *et al*. 2013). The fumarate responses are different in α1 and β1.

The Cys reactivity of α1 variants E213C and L228C became less rapid by fumarate activation and CL efficiency was overall lower in the time range from 3 min to 20 min. This could result from a comparable reactivity within the linker (compare 5.1.2; Fig. 9; Stopp *et al*. 2021). The data suggests that the α1 helices in the dimer diverge as part of the continuous double helix. A similar suggestion was made based on hydrogen-deuterium exchange mass spectrometry (HDX-MS) of truncated PAS$_C$-kinase constructs, as α1 became more accessible in ON-variant N304D. (Strecker, 2018). However, a rotational reorganization cannot be ruled out. Variant R224C showed little to no fumarate effect in the kinetics, suggesting that α1 has both dynamic and more static areas in signal transduction.

In the β1 strand the kinetics of variant G234C displayed a fumarate effect that was opposed to that of E213C and L228C. The overall higher reactivity represents a closer contact of the Gly234 position in the dimer after fumarate activation. These changes in the PAS$_C$ structure are not in line with a general dissociation of the corresponding regions in the PASc homodimers (Etzkorn *et al*. 2008; Monzel *et al*. 2013). The changes rather suggest that the β1 sheets are getting in closer contact in the dimer. The compaction in the β sheet core, observed in the HDX-MS (Strecker, 2018), supports this assumption. The Cys CL dynamics of variant I231C can neither be assigned to that of α1 nor that in position Gly234 of β1. The data suggest the location

of Gly234 in a short linker between α1 and β1 (Ile231 to Glu233). Therefore, the linker could act as a hinge and convert the signal.

The identification of regions with different dynamics within PAS_C enables an assessment of various functional variants in the context of signal transduction. In α1 the single Cys variants cause both a decrease in fumarate stimulated DcuS activity output or an increase in inactivated DcuS activity, depending on the variant (Fig. 11). These variants are located in the dimerization interface of the double helix or the water-exposed outside of the helical dimer, the α1/β1 linker and β1 (Fig 26). A disturbance of the interaction or steric effects are likely to be the cause. Taken together, the changes in interaction are supposed to reflect the structural reorganization during signal transfer and conversion in PAS_C.
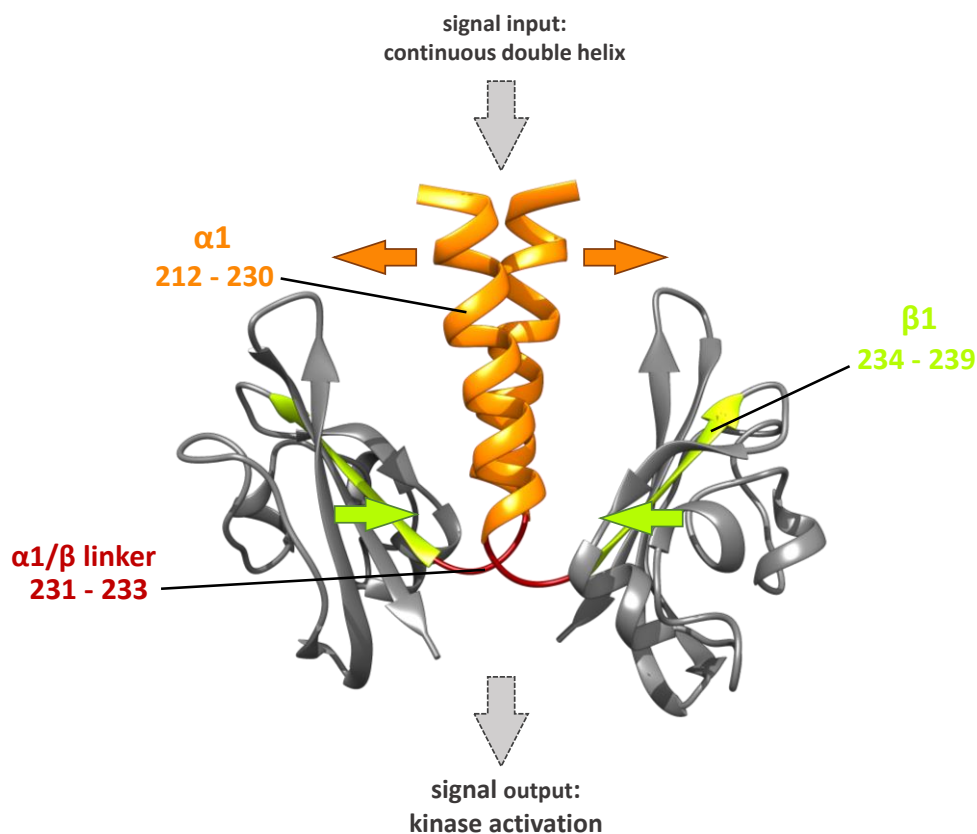
Figure 26. Model of signal transduction in the PAS_C homo-dimer of DcuS. The distinct structures are colored according to their different behavior in signal transduction and their respective positions are indicated. An incoming signal causes divergence of the α1 helices (orange) in the dimer (orange arrows). The α1/β1 linker (red) converts the α1 motion that results in approaching (green arrows) of the β1 strands (green) in the PAS_C dimer. The changes initiated in the β-sheet core are transduced to the kinase domains, which are activated thereby. The PAS_C dimer structure was modeled using the structure of CitA from *G. thermodenitrificans* as a template (PDB ID: 5FQ1).

The effects of the single Cys variants L228C, E233C, and V235C on DcuS function are observed in a similar way for variants L228A, E233A, and V235A that cause an ON-phenotype of DcuS (Etzkorn *et al*. 2008; Monzel *et al*. 2013). The residues are supposed to hydrogen bond

residue Asn248, which is highly conserved in PAS domains (Taylor and Zhulin 1999). Glu233 was postulated to interact with Asn248 and to structure PAS_C by a hinge-like movement (Etzkorn *et al.* 2008; Monzel *et al.* 2013). This fits perfectly to its position in the α1/β1 linker and its Cys CL dynamics that suggests a role for restructuring PAS_C after fumarate activation. Overall, the dynamics of the α1 and β1 region in signal transduction correlate with the occurrence of DcuS functional variants. Therefore, a more advanced model of the signal transduction mechanism of the highly dynamic PAS_C dimer can be proposed. An incoming signal, derived from the piston-type shift and rearranged by the linker, reaches PAS_C via the long continuous double helix extending into α1 of PAS_C. Restructuring of α1 includes a decrease in the interaction within the homodimer interface due to diverging helices (Fig. 26). In the model the short linker between α1 and β1 acts as a hinge by interaction with Asn248. The linker transfers the signal to the core of the β-sheet framework, leading to an approximation of the β1 sheets (Fig. 26). Overall, the rearrangement within the PAS_C dimer is proposed to cause a decrease in interaction controlling the kinase activity (Monzel *et al.* 2013).

For BvgS the mechanisms of signal transduction in the TM domain and a linker appear to be comparable to those in DcuS (see section 5.1.2). BvgS also contains a dimeric PAS domain that is directly connected to its linker, for which a weakening of the dimerization was suggested upon activation (Lesne *et al.* 2017). Hence, weakened interaction of DcuS PAS_C for kinase activation can be suggested despite the approximation of β1.

5.1.4 The atypical TM1 homo-dimer is not crucial for transmembrane signaling

The DcuS TM domain comprises the two TM helices TM1 and TM2. TM2 was shown to be the main signal transducer through the membrane. A ridged TM2 homo-dimer is uplifted in a piston-type shift as part of the continuous double helix (Monzel and Unden, 2015; Stopp *et al.* 2021). Contrary, TM1 shows marginal changes in membrane position, but these changes could not be assigned to any clear direction of movement (Monzel and Unden, 2015).

To gain insight into the role of TM1 in DcuS function, initial investigations were carried out in Steinmetz (2014). DcuS variants of a potential (small)xxx(small) motif in TM1 were examined for their impact on DcuS function. None of the variants were impaired in function. Furthermore, the TM1 variants showed a wildtype phenotype, when homo-dimerization was investigated with the BACTH assay, and the isolated TM1 constructs in the GALLEX system showed only a moderate potential for homo-dimerization. The TM1 $A_{27}xxxS_{31}$ sequence motif is therefore not essential for function and homo-dimerization of DcuS, nevertheless a TM1 homo-dimerization occurs.

The oxidative Cys-CL was carried out for single Cys variants of the entire TM1 (Thr20 to Tyr40) and the adjacent regions in order to obtain structural information about the potential of TM1 to homo-dimerize. The spacing of the local maxima of the CL-efficiency reflets a pattern of Leu_{17}-6-4-3-4-5-5-Ile_{44} that can be assigned to a canonical α-helical dimer in the TM1 core region (Leu_{23}-4-3-4 -Leu_{34}) and confirms the assumption that TM1 is a homo-dimer. In the transition regions to the periplasm and cytoplasm the distances between the CL maxima were wider and especially the C-terminal area Leu33 to Tyr40 shows a relatively constant CL efficiency (Fig. 16). This suggests a helix for TM1 that comprises wider turns than that of a canonical α-helix (Pauling and Corey, 1951; Pauling *et al.* 1951). In the helix with wider periodicity a broader dimerization interface is expected at positions Leu33 to Tyr40. The region Leu_{34}-5-5-Ile_{44} with higher periodicity could represent π- or 'wide turn' helices, which usually exhibit a backbone intrahelical hydrogen bonding pattern of $i + 5$ (Riek *et al.* 2001; Kim and Cross, 2004). π-Helical structures are often driven by aromatic residues preceding a Pro residue (Riek *et al.* 2001). His37 could represent a wide turn critical residue, even if an associated proline residue is missing. Non-Pro wide turns are known for TM helices (Riek *et al.* 2008). Overall, TM1 can be described as a TM helix that forms a dimer through a partially atypical helical structure.

From the Cys replacement mutations only the variant V28C showed a slight reduction in reporter gene expression (Monzel, 2014; Monzel and Unden, 2015; Fig. 15). In contrast to the situation with TM2, Cys variants of TM1 and the variants in the potential (small)xxx(small) motif had no significant effect on DcuS function, indicating that TM1 has no essential role in TM signaling. Appearance of π-helical structures is often linked to specific functions (Coolex *et al.* 2010, Weaver, 2000) which might have been overlooked so far in DcuS. Nevertheless, TM1 is a partially atypical homo-dimer, which most probably has little or no critical importance for DcuS TM signal transduction.

The comparison of TM1 from DcuS with TM1 in EnvZ appears interesting. In EnvZ TM1 and TM2 flank a sensory periplasmic domain and TM1 is not linked to a cytoplasmic domain like TM1 of DcuS. TM1 of EnvZ homodimerizes, but here the Cys substitutions within the interaction area clearly influence the signal output of EnvZ (Heininger *et al.* 2016). Therefore, signal transfer in EnvZ and DcuS likely depends on homo-dimerization of TM helices.

5.1.5 DcuS signal modulation and regulation by DctA

The regulation of DcuSR dependent C4DC gene expression is inextricably linked to the associated transporters (Unden *et al.* 2016b). DctA interacts with DcuS via the amphipathic

helix 8b (Witan *et al.* 2012) and transfers DcuS to its C4DC-responsive state. Since the transport function of DctA is decoupled from its regulatory function on DcuS, DctA is described as a co-sensor forming the DcuS/DctA sensor complex (Steinmetz *et al.* 2014). Based on the basal *dcuB* expression and the quantified absolute amounts of DcuS and DctA (DcuB) in the *E. coli* cell, it was suggested that small amounts of free DcuS are not integrated in the sensor complex and ensure the basal transcription of the C4DC transporters (Wörner *et al.* 2018). The mechanism for the modulation of the signal transfer in the sensor complex by DctA and of the control of the activity state of free DcuS is unknown. Therefore, the impact of DctA on the structure of the DcuS homodimer in signal transfer was examined with the time-resolved Cys-CL at representative positions of TM2, the linker, and PAS_C.

The CL kinetics of the TM2 single Cys variants G190C and G194C were basically not affected by the absence of DctA and a fumarate effect was not observed either (Fig. 17). Hence, DctA has no influence on the TM2 homo-dimer and its stability. It is assumed therefore that DctA does not modulate signaling of DcuS via the dimeric state of TM2.

In contrast, the absence of DctA changed the reactivity of the linker single Cys variants I208C and L209C drastically, which strongly resembles the C4DC sensitive state in the presence of fumarate (Fig. 18). Therefore, it can be assumed that the homo-dimerization at position Leu209 is abrogated or at least greatly reduced as concluded from the lack of Cys reactivity regardless of the DcuS signaling state. Since the reactivity at position Ile208 in the inactivated state is completly lost, this also indicates a significant weakening of homo-dimerization for position Ile208, which is even more pronounced than by activation by fumarate in the presence of DctA. The reactivity of I208C remained unchanged with fumarate. Although the reaction of the variant K206C cannot be explained (Fig. 19), the effect of the DctA deficiency indicates that a loss of DcuS-DctA interaction causes a drastic reorganization of the linker, which leads to the loss or at least significant weakening of the dimerization.

Furthermore, the DctA deficiency results in a decreased reactivity of the PAS_C α1 representative R224C single Cys variant both with and without fumarate (Fig. 20). This suggests the conformational changes in α1 to be different compared to both signaling states of DcuS in presence of DctA. However, the overall homo-dimerization of α1 is also weakened by the lack of interaction between DctA and DcuS. Consequently, α1 also responds with an altered conformation to the absence of DctA. However, the conformational changes are minor compared to the linker.

If these observations are summarized and transferred to the DcuS signal transduction mechanism, it can be assumed that the homo-dimerization of the linker is significantly

weakened in the absence of DctA (Fig. 27A), comparable to activation by fumarate with an intact DcuS-DctA sensor complex (Fig. 27C). The effect on the linker appears to be even more intense. Due to the drastic structural changes in the linker it appears likely that the lack of DcuS-DctA interaction and the linker reorganization affects as a consequence the stability of the α1 homo-dimer. In α1 the conformational changes due to the absence of DctA appears to be slightly different from the fumarate-activated state in presence of DctA, but the homo-dimerization is also weakened overall. This causes a downstream signaling effect by changing the core structure of PAS$_C$ and activating the kinase domain of DcuS, whereby DcuS is in the permanent ON state (Fig. 27A).
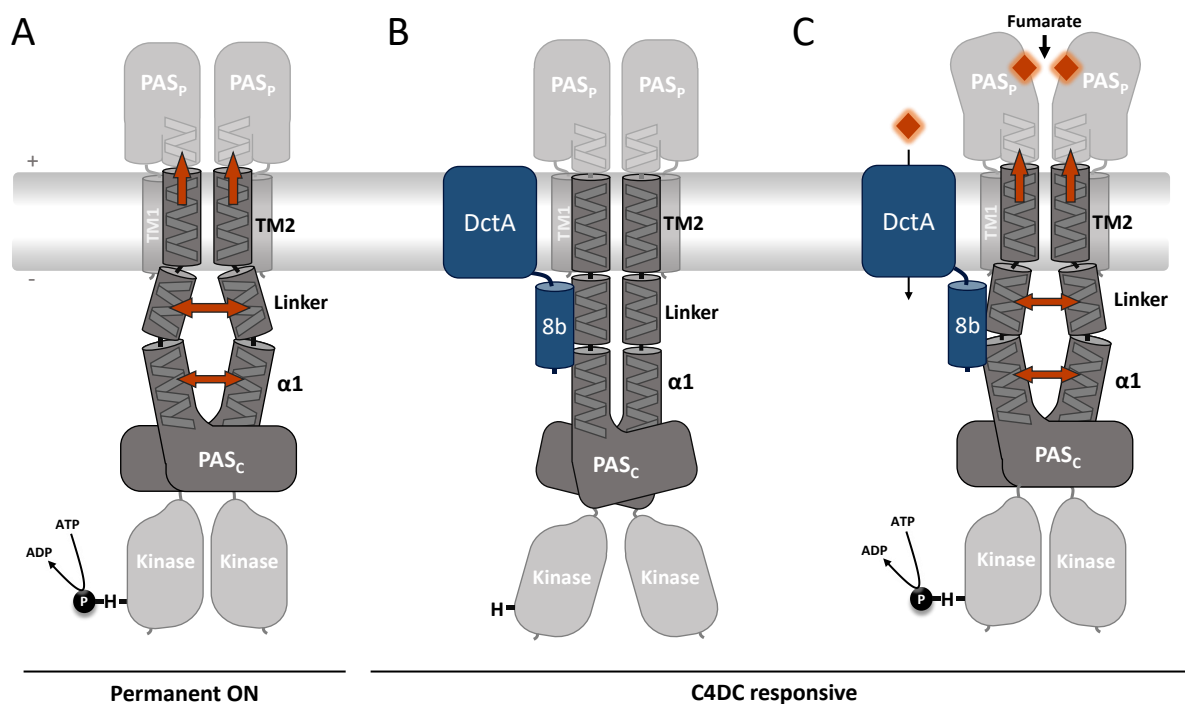
Figure 27. Scheme of DcuS signal transduction and activity state in absence (A) or presence of DctA (B, C). (A) In absence of DctA the lacking DctA-DcuS interaction causes a weakening/loss of dimerization in the linker and α1 of PAS$_C$ (orange arrows). This is accompanied by a TM2 piston-type shift (Monzel, 2014; Unden *et al.* 2016b). The subsequent restructuring in PAS$_C$ is transferred to the kinase, which adopts an active conformation and gets autophosphorylated representing the DcuS permanent ON state. (B, C) DctA interacts with DcuS via the helix 8b and stabilizes the dimeric structure of the cytoplasmic parts of the continuous double helix. This transfers DcuS to the C4DC (fumarate)-responsive state in the DcuS-DctA sensor complex. (B) Without external fumarate (orange rhomb) thight interaction of the continuous double helix and overall PAS$_C$ silences the kinase. (C) If external fumarate is available, fumarate is transported into the cell by DctA and independently triggers DcuS signal transduction (see sections 5.1.2, 5.1.3). The weakening of homo-dimerization of the linker might be more pronounced in the absence of DctA than upon fumarate activation (compare orange arrow thicknesses in (A) and (C)). Domains, whose representative positions were subject to Cys CL (see section 4.1.4), are colored opaque; other domains are grayed out.

In addition, there are indications that TM2 shows a piston-type shift in the absence of DctA just as upon fumarate activation in the intact DcuS-DctA sensor complex (Monzel, 2014) and a corresponding model has been proposed (Unden *et al.* 2016b) (Fig. 4). This is in line with the almost unchanged Cys reactivity within TM2, indicating a stable TM2 homo-dimer that is also shifted in axial periplasmic direction in the absence of DctA. It remains unclear whether the

positioning of TM2 in the OFF state of DcuS (Fig. 27B) in contrast to the positioning in the activated DcuS states (Fig. 27A, C) is also due to the stabilizing interaction of the helix 8b with DcuS in the cytoplasm. A yet unknown interaction of DcuS and DctA within the membrane is also conceivable.

Overall, DctA stabilizes the cytoplasmic parts of the continuous double helix by direct interaction of the helix 8b (Fig. 27B, C) and converts DcuS to its C4DC-responsive state (Steinmetz *et al*. 2014; Unden *et al*. 2016b).

The helix 8b of DctA is essential for the interaction in the DcuS-DctA sensor complex (Witan *et al*. 2012) and PAS$_C$ was suggested as the DcuS counterpart. However, the DcuS constructs used for the interaction studies were truncated behind position Lys206 (Witan *et al*. 2012; Monzel *et al*. 2013) and lack therefore essential parts of the linker (positions Cys199 to Gly211). In combination with the fact that the DctA deficiency caused the most drastic changes in the linker and moderate changes in α1, DctA helix 8b can be suggested to interact with the linker or both the linker and α1 of PAS$_C$ (Fig. 27B, C). Furthermore, the linker contains the $L_{201}xxxLxxxL_{209}$ sequence. Lxx(L)L motifs often mediate protein-protein interaction (Plevin *et al*. 2005). The separation of the apolar residues of $L_{201}xxxLxxxL_{209}$ upon DcuS activation (Fig. 25; see section 5.1.2) exposes the residues to the hydrophilic surrounding. This exposure requires stabilization, which makes a dynamic interaction of DctA with the linker even more conceivable, since the Leu residues of the $L_{405}xxxLxxxL_{414}$ motif in the helix 8b of DctA were identified to be essential for interaction with DcuS (Witan *et al*. 2012).

Similar to the regulatory interaction of the C4DC (Dct/Dcu) transporters in *E. coli* and *B. subtilis* with the DcuS-like sensor kinases several other examples of membrane proteins and transporters are known that influence kinase function (Alvardo *et al*. 2019). The small membrane protein MrgB regulates dynamic target gene expression of the PhoQP TCS in a negative feedback loop by interaction with the PhoQ sensor kinase (Salazar *et al*. 2016). Interaction of the Lys permease LysP and the membrane-integrated pH-sensitive transcriptional regulator CadC is required for a response to acidic stress (Tetsch *et al*. 2008). Lys dependent changes upon substrate binding or transport of LysP are suggested to control CadC regulated target gene expression via conformational changes in LysP/CadC interaction in the periplasmic and TM region (Rauschmeier *et al*. 2014). Consequently, the modes of regulation of sensory proteins by auxiliary proteins appear to be different, although no specific mechanisms have yet been proposed. In contrast to DcuSR, the closely related CitAB TCS does not require any auxiliary transporters for the regulation of citrate fermentation (Scheu *et al*. 2012; Graf *et al*. 2016).

5.2 Impact of fumarate on the aerobic and anaerobic *E. coli* proteome

5.2.1 Validation of the proteomics by C4DC specific regulation

E. coli can utilize C4DCs under aerobic and under anaerobic conditions. Aerobically C4DCs are channeled into the TCA cycle, whereas under anaerobic conditions C4DCs are converted to fumarate and used in fumarate respiration (Unden *et al*. 2016a). Specific transcriptional regulation of the genes of C4DC utilization is accomplished by the DcuSR TCS (Zientz *et al*. 1998; Golby *et al*. 1999). The effect of fumarate on the protein level has only been investigated to a limited extent (Wörner *et al*. 2018). Schmidt *et al*. (2016) have already determined a quantitative *E. coli* proteome for various conditions including 2359 *E. coli* proteins. However, the proteomics were exclusively designed for aerobic growth conditions and the composition of the respective growth media was not explicitly designed for a fumarate-focused comparative study. In addition, the enrichment of the membrane fraction enables a precise determination of membrane integral proteins (Wörner *et al*. 2018). Therefore, the influence of fumarate on the aerobic and anaerobic *E. coli* proteome was examined with a 'shotgun proteomics' approach (Surmann *et al*. 2020).

The significant increase in the levels of the C4DC transporter DctA under aerobic conditions and DcuB under anaerobic conditions, when cultivated with fumarate, confirms the results of the absolute quantification (Wörner *et al*. 2018). In addition, the transcriptional regulation of the C4DC-specific genes of fumarate respiration *fumB* and *frdABC* (Zientz *et al*. 1998) was confirmed at the protein level (Fig. 21; Surmann *et al*. 2020). However, the fumarate effect reaches further than the known regulation by DcuSR, as the level of further C4DC metabolism-associated proteins was increased in the presence of fumarate.

Particularly noticeable are the trends in regulation of the C4DC transporters DcuC and DcuA (DcuC decreased, DcuA increased) that are not seen on the transcriptional level (Zientz *et al*. 1998; Golby *et al*. 1998; Zientz *et al*. 1999). Therefore, the changes must be subject to another level of regulation that is not yet known. In contrast to the redox shuttling by DcuB, DcuA acts as a nitrogen shuttle for the uptake of L-aspartate. After deamination by AspA, fumarate is exported in an antiport by DcuA (Strecker *et al*. 2018). Since aspartate serves as a high-quality nitrogen source for *E. coli* (Schubert *et al*. 2020), this may be related to the upregulation of DcuA (and AspA under aerobic conditions), but the exact reason and the regulatory mechanism are unclear.

5.2.2 Adaptions of the *E. coli* aerobic metabolism to fumarate as a poor carbon and energy source

As a glucophilic bacterium, *E. coli* prefers glucose or hexoses as a carbon or energy source. C4DCs represent alternative substrates for the energy and carbon metabolism under aerobic conditions (Unden *et al.* 2016a). Hence adaptation of the central metabolism to fumarate is necessary. Expression of the aerobic C4DC transporter DctA by DcuSR is already known as a very specific adaptation to the availability of C4DC (Zientz *et al.* 1998; Golby *et al.* 1999). Beyond this, significant changes in the protein level were detected as an adaptation to fumarate compared to glycerol as carbon and energy source under aerobic conditions.

The increased level of the NADH-quinone oxidoreductase Nuo complex is contrasted by the decrease of the non-coupling respiratory enzymes NADH dehydrogenase Ndh, glucose dehydrogenase Gcd and GlpD (see section 4.2.2; Surmann *et al.* 2020). This reflects the high respiratory activity in adaption to respiratory energy conservation, when fumarate is used as substrate (Bongaerts *et al.* 1995). This is accompanied by an increase in almost all TCA cycle enzymes and the glyoxylate bypass enzyme malate synthase AceB, when glycerin is replaced with fumarate as a carbon source. Furthermore, the level of the PEP/pyruvate bypass malic enzyme MaeB and PEP-carboxykinase PckA were increased (Fig. 22). Since a strong flux to PEP and pyruvate (through PckA and MaeB) was shown for *E. coli* grown on fumarate (Holms, 1996), the increase of PckA and MaeB represents the gluconeogenic adaptation to the growth on fumarate. A similar gluconeogenetic switch and an upregulation of the TCA cycle genes is described for the transition from glucose to acetate metabolism (Oh *et al.* 2002; Kao *et al.* 2004, 2005). Furthermore, overexpression of PckA causes a glycerol-like growth rate of *E. coli* on weak carbon sources as succinate (Chao *et al.* 1993), leading to the overall conclusion that fumarate causes the need for adaptation to the gluconeogenetic pathway.

Consequently, the removal of intermediates from the TCA cycle requires an adjustment of anaplerotic reactions. This provides an explanation for the increased amount of enzymes contributing to fatty acid and AA degradation that feed directly into the TCA cycle (Surmann *et al.* 2020; Fig. 22). Acetyl-CoA C-acyltransferase FadI, and 3-hydroxyacyl-CoA dehydrogenase FadJ are known to feed the incomplete anaerobic TCA cycle by β-oxidation (Campbell *et al.* 2003), but proteomic abundances of Surmann *et al.* (2020) indicate a supportive function to the partially redundant function of 3-ketoacyl-CoA thiolase FadA and multifunctional FadB under aerobic carbon starvation.

A similar adjustment represents the increased degradation of arginine represented by the increased level of succinylornithine transaminase AstC, succinate-semialdehyde

dehydrogenase GabD, and 4-aminobutyrate aminotransferase GabT, that feed succinate to the TCA cycle. This also applies to the additional supply of pyruvate due to the increased enzyme level of tryptophanase TnaA and alanine racemase DadX from tryptophan/alanine (see section 4.2.2; Fig. 22). The decreased amino acid synthesis could be a response to the reduced growth rate observed with fumarate compared to growth on glycerol. A simultaneous increase in AA degradation and anaplerotic reactions with a decrease in several AA synthesis pathways (IlvABCDEH and LeuAB and MetACFKL) (Surmann *et al*. 2020) displays a major metabolic reorganization as a reaction on an upregulated TCA cycle in energy conserving catabolism combined with the need of gluconeogenesis in anabolism.

The slightly decreased level of the pyruvate dehydrogenase (AceE/AceF) was quite unexpected due to the simultaneous need of both TCA cycle and pyruvate bypass during aerobic growth on fumarate (Unden *et al*. 2016a). Glycerol is fed by AceE/AceF to the TCA cycle and all glycerol oxidized in the TCA cycle must pass this route, whereas during growth on fumarate only 50 % of the fumarate is channeled through the pyruvate by-pass, and the other half is directly oxidized in the TCA (Surmann *et al*. 2020).

5.2.3 The fumarate-dependent adaptation of the *E. coli* metabolism is accomplished by both DcuSR and cAMP-CRP

The specific regulation of C4DC metabolism by the DcuSR TCS (Zientz *et al*. 1998; Golby *et al*. 1998) was displayed in full extend in the proteomics analysis (see section 5.2.1). Furthermore, in the presence of oxygen a broad range of TCA cycle enzymes as well as of gluconeogenesis, bypass-, and anaplerotic-reactions were positively regulated by replacing glycrol with fumarare (Surmann *et al*. 2020; see section 5.2.2). Direct regulation by DcuSR is only described for *dctA*. Most of the TCA cycle related genes are preceded by a CRP binding site (summarized in Surmann *et al*. 2020). Therefore, the expression of *lacZ* as a reporter gene under the control of the promoter region of selected TCA cycle-related genes was tested.

The *aspA*, *pckA*, *fumA,* and *sdhC* promoter region caused a significant increase of *lacZ* expression, when replacing glycerol with fumarate, which confirms their fumarate-dependent increased protein level in transcription regulation (Surmann *et al*. 2020, Fig.23). Since both a CRP and a DcuR deficiency led to the loss of the fumarate effect (Surmann *et al*. 2020, Fig.23), it can be assumed that both regulators CRP and DcuR control the expression of the enzymes of the TCA cycle, gluconeogenesis, and the associated anaplerotic and bypass reactions depending on fumarate (Fig. 28). The DcuR binding site is poorly defined, but by motif analysis it can be assumed that *aspA* and *pckA* also have at least one DcuR binding site (Surmann *et al.* 2020; see

section 4.2.4), which is in line with the suggested regulation by DcuR and CRP. The generally very low expression in the CRP-deficient strain probably indicates an overriding function of CRP compared to DcuR.

As a poor carbon source fumarate is supposed to induce high cellular cAMP levels and to stimulate expression by cAMP-CRP (Franchini *et al*. 2015). This is supported by the strong increase during growth on fumarate of the transcriptional regulator MalT and the periplasmic binding proteins of maltose and xylose catabolism MalE and XylF (Surmann *et al*. 2020). The coding genes are known for response to cAMP mediated catabolite repression (Eppler *et al*. 1999). Furthermore, succinate as a C4DC has been shown to cause a high ratio phosphorylated EIIA to unphosphorylated EIIA (EIIA^{Glc}-P/EIIA^{Glc}) of the phosphotransferase system of glucose uptake (Hogema *et al*. 1998). Therefore, fumarate could cause a high cAMP level via a high ratio of EIIA^{Glc}-P/EIIA^{Glc} simulating 'glucose starvation' due to inactive glucose uptake. This in turn leads to a cAMP-CRP-dependent adaptation of TCA cycle, gluconeogenesis TCA cycle, gluconeogenesis, glyoxylate shunt, and the associated anaplerotic reactions as well as amino acid biosynthesis and degradation as a reaction to fumarate as a poor carbon source (Fig. 28B). A similar situation occurs in the anaerobic C4DC metabolism. The genes *dcuB, fumB,* and *frdA* (Zientz *et al*. 1998; Golby *et al*. 1999) that are induced by DcuSR under anaerobic conditions carry CRP binding consensus sequences (Surmann *et al*. 2020). Furthermore, *dcuB* and *frdA* transcription is subject to catabolite repression in *E. coli* grown on glucose (Zientz *et al*. 1998) supporting the assumption that cAMP-CRP affects DcuSR related regulation directly (Surmann *et al*. 2020; Fig. 28).
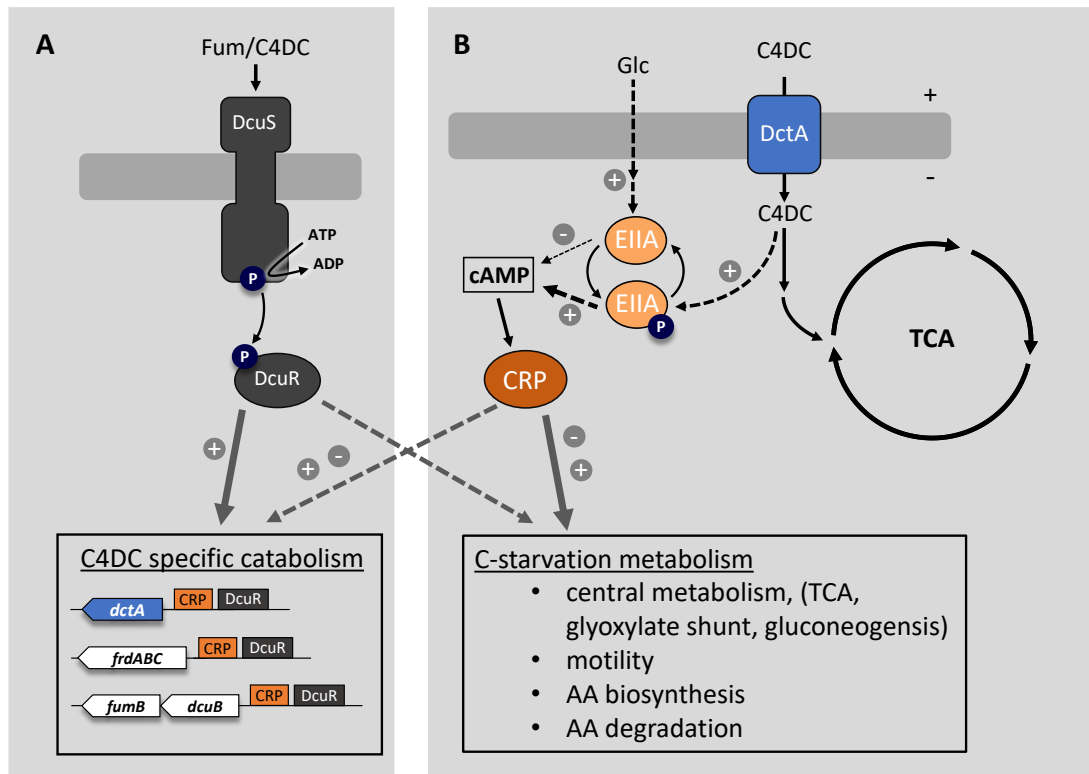
Figure 28. Scheme for regulating the expression of genes in *E. coli* in response to fumarate by the DcuSR TCS (A, direct response) and by the catabolite control (B, indirect response involving the cAMP-CRP complex). (A) The sensor kinase DcuS of the DcuSR TCS phosphorylates the response regulator DcuR in the presence of extracellular fumarate (or C4DCs), resulting in the activation of target genes carrying a DcuR site (dctA, *frdABC*, *dcuB*, *fumB* genes). DcuR regulated genes contain in addition CRP consensus sites (Surmann *et al*. 2020). The genes encode the primary transporters (DctA, DcuB) and enzymes (FrdABC, FumB) required for degradation of the C4DCs. (B) Fumarate and C4DCs are supposed to simulate 'glucose starvation' due to inactive glucose uptake and high phosphorylation of the glucose phosphotransferase system (high EIIA-P/EIIA ratio) [36], resulting in high cAMP levels, formation of the cAMP-CRP complex, and transcriptional regulation of genes with CRP sites [35,37]. The genes for the respective pathways ('C-starvation metabolism, right side) contain DcuR consensus sites and may also be affected by DcuSR. Figure from Surmann *et al*. (2020).

Overall, those data imply a link between aerobic and anaerobic C4DC metabolism and cAMP-CRP accomplished catabolite regulation. Adaption to C4DCs is mediated by cAMP and CRP. This applies to the central metabolism in particular, which agrees with the high significance of cAMP-CRP as major regulators of central metabolic genes (Kochanowski *et al*. 2017). Furthermore, DcuSR seems to regulate more than the well-established DcuSR dependent genes *dctA*, *dcuB*, *fumB* and *frdABC*. Some genes of the central metabolism could also be regulated by DcuSR and therefore a cross-regulation under aerobic and anaerobic conditions with cAMP-CRP could occur (Surmann *et al*. 2020; Fig. 28).

5.2.4 Fumarate provokes enhanced motility and chemotaxis during anaerobic growth

Under anaerobic conditions fumarate caused changes in the level of 76 proteins (see section 4.2.3), which, except for the components of fumarate respiration, are not regulated by DcuSR (see section 5.2.1). Notable among these was the significant increase in the level or trend in the

upregulation of motility proteins, including the flagellum, the flagellar motor, and basal body as well as the chemotaxis.

Fumarate is known for its strong regulatory effect on chemotaxis and swimming behavior of *E. coli*, as a high fumarate concentration switches the direction of the flagellar rotation from counterclockwise to clockwise (Barak *et al*. 1996; Prasad *et al*. 1998). A similar effect is caused by an overexpression of the chemotaxis response regulator CheY (Montrone *et al*. 1996, 1998) confirming the connection of the *E. coli* chemotaxis proteins and the fumarate effect on motility/chemotaxis protein abundance (Surmann *et al*. 2020).

Specifically, fumarate mediates an interaction between the FrdA subunit of fumarate reductase and the isolated switch complexes forming a complex with the switch protein FliG. This interaction is required for both flagellar assembly and switching the direction of flagellar rotation (Cohen-Ben-Lulu *et al*. 2008).

There seems to be a clear correlation of the upregulation of motility and chemotaxis proteins and the availability of fumarate, verifying on the protein level in the earlier observations that were obtained mainly on the behavioral, physiological and genetic level (Barak *et al*. 1996; Prasad *et al*. 1998; Montrone *et al*. 1996, 1998). However, the physiological significance of the fumarate effect on adaptive motility of *E. coli* is completely unclear.

6   Bibliography

Abo-Amer, A. E., Munn, J., Jackson, K., Aktas, M., Golby, P., Kelly, D. J. and Andrews, S. C. (2004) DNA interaction and phosphotransfer of the C_4-dicarboxylate-responsive DcuS-DcuR two-component regulatory system from Escherichia coli. *Journal of bacteriology* **186** (6), 1879-1889

Abriata, L. A., Albanesi, D., Dal Peraro, M. and Mendoza, D. de (2017) Signal Sensing and Transduction by Histidine Kinases as Unveiled through Studies on a Temperature Sensor. *Accounts of chemical research* **50** (6), 1359-1366

Alvarado, A., Behrens, W. and Josenhans, C. (2019) Protein Activity Sensing in Bacteria in Regulating Metabolism and Motility. *Frontiers in microbiology* **10**, 3055

Ashenberg, O., Keating, A. E. and Laub, M. T. (2013) Helix bundle loops determine whether histidine kinases autophosphorylate in cis or in trans. *Journal of molecular biology* **425** (7), 1198-1209

Ayers, R. A. and Moffat, K. (2008) Changes in quaternary structure in the signaling mechanisms of PAS domains. *Biochemistry* **47** (46), 12078-12086

Baba, T., Ara, T., Hasegawa, M., Takai, Y., Okumura, Y., Baba, M., Datsenko, K. A., Tomita, M., Wanner, B. L., and Mori, H. (2006) Construction of Escherichia coli K-12 in-frame, single-gene knockout mutants: the Keio collection. *Molecular systems biology* **2**, 2006.0008

Babicki, S., Arndt, D., Marcu, A., Liang, Y., Grant, J. R., Maciejewski, A. and Wishart, D. S. (2016) Heatmapper: web-enabled heat mapping for all. *Nucleic acids research* **44** (W1), W147-53

Barak, R., Giebel, I. and Eisenbach, M. (1996) The specificity of fumarate as a switching factor of the bacterial flagellar motor. *Molecular microbiology* **19** (1), 139-144

Bass, R. B., Butler, S. L., Chervitz, S. A., Gloor, S. L. and Falke, J. J. (2007) Use of Site-Directed Cysteine and Disulfide Chemistry to Probe Protein Structure and Dynamics: Applications to Soluble and Transmembrane Receptors of Bacterial Chemotaxis. *Methods in Enzymology* **423**, 25-51 In: Simon, M. I., Crane, B. R., Crane, eds. *Two-Component Signaling Systems, Part B,* Elsevier

Becker, S., Holighaus, G., Gabrielczyk, T. and Unden, G. (1996) O_2 as the regulatory signal for FNR-dependent gene regulation in Escherichia coli. *Journal of bacteriology* **178** (15), 4515-4521

Bertani, G. (1951) Studies on lysogenesis. I. The mode of phage liberation by lysogenic Escherichia coli. *Journal of bacteriology* **62** (3), 293-300

Bhate, M. P., Molnar, K. S., Goulian, M. and DeGrado, W. F. (2015) Signal transduction in histidine kinases: insights from new structures. *Structure* **23** (6), 981-994

Blattner, F. R., Plunkett, G., Bloch, C. A., Perna, N. T., Burland, V., Riley, M., Collado-Vides, J., Glasner, J. D., Rode, C. K., Mayhew, G. F., Gregor, J., Davis, N. W., Kirkpatrick, H. A., Goeden, M. A., Rose, D. J., Mau, B. and Shao, Y. (1997) The complete genome sequence of Escherichia coli K-12. *Science* **277** (5331), 1453-1462

Bongaerts, J., Zoske, S., Weidner, U. and Unden, G. (1995) Transcriptional regulation of the proton translocating NADH dehydrogenase genes (nuoA-N) of Escherichia coli by electron acceptors, electron donors and gene regulators. *Molecular microbiology* **16** (3), 521-534

Bott, M., Meyer, M. and Dimroth, P. (1995) Regulation of anaerobic citrate metabolism in Klebsiella pneumoniae. *Molecular microbiology* **18** (3), 533-546

Brown, J. H., Cohen, C. and Parry, D. A. D. (1996) Heptad breaks in α-helical coiled coils: Stutters and stammers. *Proteins* **26** (2), 134-145

Campbell, J. W., Morgan-Kiss, R. M. and Cronan, J. E. (2003) A new Escherichia coli metabolic competency: growth on fatty acids by a novel anaerobic beta-oxidation pathway. *Molecular microbiology* **47** (3), 793-805

Chao, Y. P., Patnaik, R., Roof, W. D., Young, R. F. and Liao, J. C. (1993) Control of gluconeogenic growth by pps and pck in Escherichia coli. *Journal of bacteriology* **175** (21), 6939-6944

Cheung, J. and Hendrickson, W. A. (2008) Crystal structures of C_4-dicarboxylate ligand complexes with sensor domains of histidine kinases DcuS and DctB. *The Journal of biological chemistry* **283** (44), 30256-30265

Cheung, J. and Hendrickson, W. A. (2009) Structural analysis of ligand stimulation of the histidine kinase NarX. *Structure* **17** (2), 190-201

Clark, D. P. (1989) The fermentation pathways of Escherichia coli. *FEMS Microbiology Letters* **63** (3), 223-234

Cohen-Ben-Lulu, G. N., Francis, N. R., Shimoni, E., Noy, D., Davidov, Y., Prasad, K., Sagi, Y., Cecchini, G., Johnstone, R. M. and Eisenbach, M. (2008) The bacterial flagellar switch complex is getting more complex. *The EMBO journal* **27** (7), 1134-1144

Coleman, M. D., Bass, R. B., Mehan, R. S. and Falke, J. J. (2005) Conserved glycine residues in the cytoplasmic domain of the aspartate receptor play essential roles in kinase coupling and on-off switching. *Biochemistry* **44** (21), 7687-7695

Cooley, R. B., Arp, D. J. and Karplus, P. A. (2010) Evolutionary origin of a secondary structure: π-helices as cryptic but widespread insertional variations of α-helices that enhance protein functionality. *Journal of molecular biology* **404** (2), 232-246

Davies, S. J., Golby, P., Omrani, D., Broad, S. A., Harrington, V. L., Guest, J. R., Kelly, D. J. and Andrews, S. C. (1999) Inactivation and regulation of the aerobic C_4-dicarboxylate transport (dctA) gene of Escherichia coli. *Journal of bacteriology* **181** (18), 5624-5635

Dawson, J. P., Weinger, J. S. and Engelman, D. M. (2002) Motifs of serine and threonine can drive association of transmembrane helices. *Journal of molecular biology* **316** (3), 799-805

Deutscher, J., Francke, C. and Postma, P. W. (2006) How phosphotransferase system-related protein phosphorylation regulates carbohydrate metabolism in bacteria. *Microbiol. Mol. Biol. Rev.* **70** (4), 939-1031

El Aidy, S., Derrien, M., Merrifield, C. A., Levenez, F., Doré, J., Boekschoten, M. V., Dekker, J., Holmes, E., Zoetendal, E. G., van Baarlen, P., Claus, S. P., and Kleerebezem, M. (2013) Gut bacteria-host metabolic interplay during conventionalisation of the mouse germfree colon. *The ISME journal* **7** (4), 743–755

Engel, P., Krämer, R. and Unden, G. (1992) Anaerobic fumarate transport in Escherichia coli by an fnr-dependent dicarboxylate uptake system which is different from the aerobic dicarboxylate uptake system. *Journal of bacteriology* **174** (17), 5533-5539

Engel, P., Krämer, R. and Unden, G. (1994) Transport of C_4-dicarboxylates by anaerobically grown Escherichia coli. Energetics and mechanism of exchange, uptake and efflux. *European journal of biochemistry* **222** (2), 605-614

Eppler, T. and Boos, W. (1999) Glycerol-3-phosphate-mediated repression of malT in Escherichia coli does not require metabolism, depends on enzyme IIAGlc and is mediated by cAMP levels. *Molecular microbiology* **33** (6), 1221-1231

Escherich, T. (1886) *Die Darmbakterien des Säuglings und ihre Beziehungen zur Physiologie der Verdauung*. Verlage von Ferdinand Enke, Stuttgart

Etzkorn, M., Kneuper, H., Dünnwald, P., Vijayan, V., Krämer, J., Griesinger, C., Becker, S., Unden, G. and Baldus, M. (2008) Plasticity of the PAS domain and a potential role for signal transduction in the histidine kinase DcuS. *Nature structural & molecular biology* **15** (10), 1031-1039

Farinha, M. A. and Kropinski, A. M. (1990) High efficiency electroporation of Pseudomonas aeruginosa using frozen cell suspensions. *FEMS Microbiology Letters* **58** (2), 221-225

Ferris, H. U., Dunin-Horkawicz, S., Mondéjar, L. G., Hulko, M., Hantke, K., Martin, J., Schultz, J. E., Zeth, K., Lupas, A. N., and Coles, M. (2011) The mechanisms of HAMP-mediated signaling in transmembrane receptors. *Structure* **19** (3), 378-385

Franchini, A. G., Ihssen, J. and Egli, T. (2015) Effect of Global Regulators RpoS and Cyclic-AMP/CRP on the Catabolome and Transcriptome of Escherichia coli K12 during Carbon- and Energy-Limited Growth. *PLoS one* **10** (7), e0133793

Gencheva, S. (2016*). Das ExxN-Motiv und die Phosphataseaktivität der Sensorkinase DcuS von Escherichia coli*. (*Diploma Thesis*), Institut für Mikrobiologie und Weinforschung, Johannes Gutenberg-Universität Mainz.

Golby, P., Davies, S., Kelly, D. J., Guest, J. R. and Andrews, S. C. (1999) Identification and characterization of a two-component sensor-kinase and response-regulator system (DcuS-DcuR) controlling gene expression in response to C_4-dicarboxylates in Escherichia coli. *Journal of bacteriology* **181** (4), 1238-1248

Golby, P., Kelly, D. J., Guest, J. R. and Andrews, S. C. (1998) Transcriptional regulation and organization of the dcuA and dcuB genes, encoding homologous anaerobic C_4-dicarboxylate transporters in Escherichia coli. *Journal of bacteriology* **180** (24), 6586-6596

Goldberg, S. D., Clinthorne, G. D., Goulian, M. and DeGrado, W. F. (2010) Transmembrane polar interactions are required for signaling in the Escherichia coli sensor kinase PhoQ. *Proceedings of the National Academy of Sciences of the United States of America* **107** (18), 8141-8146

Graf, S., Broll, C., Wissig, J., Strecker, A., Parowatkin, M. and Unden, G. (2016) CitA (citrate) and DcuS (C_4-dicarboxylate) sensor kinases in thermophilic Geobacillus kaustophilus and Geobacillus thermodenitrificans. *Microbiology (Reading, England)* **162** (1), 127-137

Gray, C. H. and Tatum, E. L. (1944) X-Ray Induced Growth Factor Requirements in Bacteria. *Proceedings of the National Academy of Sciences of the United States of America* **30** (12), 404-410

Griffith, K. L. and Wolf, R. E. (2002) Measuring beta-galactosidase activity in bacteria: cell growth, permeabilization, and enzyme assays in 96-well arrays. *Biochemical and biophysical research communications* **290** (1), 397-402

Gross, R., Aricò, B. and Rappuoli, R. (1989) Families of bacterial signal-transducing proteins. *Molecular microbiology* **3** (11), 1661-1667

Guest, J. R. (1979) Anaerobic growth of Escherichia coli K12 with fumarate as terminal electron acceptor. Genetic studies with menaquinone and fluoroacetate-resistant mutants. *Journal of general microbiology* **115** (2), 259-271

Guest, J. R. (1992) Oxygen-regulated gene expression in Escherichia coli. The 1992 Marjory Stephenson Prize Lecture. *Journal of general microbiology* **138** (11), 2253-2263

Gunsalus, R. P. (1992) Control of electron flow in Escherichia coli: coordinated transcription of respiratory pathway genes. *Journal of bacteriology* **174** (22), 7069-7074

Gushchin, I. and Gordeliy, V. (2018) Transmembrane Signal Transduction in Two-Component Systems: Piston, Scissoring, or Helical Rotation? *BioEssays: news and reviews in molecular, cellular and developmental biology* **40** (2), 1700197

Gushchin, I., Melnikov, I., Polovinkin, V., Ishchenko, A., Yuzhakova, A., Buslaev, P., Bourenkov, G., Grudinin, S., Round, E., Balandin, T., Borshchevskiy, V., Willbold, D., Leonard, G., Büldt, G., Popov, A. and Gordeliy, V. (2017) Mechanism of transmembrane signaling by sensor histidine kinases. *Science* **356** (6342), eaah6345

Hall, B. A., Armitage, J. P. and Sansom, M. S. P. (2011) Transmembrane helix dynamics of bacterial chemoreceptors supports a piston model of signalling. *PLoS computational biology* **7** (10), e1002204

Hanahan, D. (1983) Studies on transformation of Escherichia coli with plasmids. *Journal of molecular biology* **166** (4), 557-580

Heijne, G. von (2006) Membrane-protein topology. *Nature reviews. Molecular cell biology* **7** (12), 909-918

Heininger, A., Yusuf, R., Lawrence, R. J. and Draheim, R. R. (2016) Identification of transmembrane helix 1 (TM1) surfaces important for EnvZ dimerisation and signal output. *Biochimica et biophysica acta* **1858** (8), 1868-1875

Hendrickson, W. A. (2016) Atomic-level analysis of membrane-protein structure. *Nature structural & molecular biology* **23** (6), 464-467

Hogema, B. M., Arents, J. C., Bader, R., Eijkemans, K., Yoshida, H., Takahashi, H., Aiba, H. and Postma, P. W. (1998) Inducer exclusion in Escherichia coli by non-PTS substrates: the role of the PEP to pyruvate ratio in determining the phosphorylation state of enzyme IIAGlc. *Molecular microbiology* **30** (3), 487-498

Holms, H. (1996) Flux analysis and control of the central metabolic pathways in Escherichia coli. *FEMS microbiology reviews* **19** (2), 85-116

Hughson, A. G. and Hazelbauer, G. L. (1996) Detecting the conformational change of transmembrane signaling in a bacterial chemoreceptor by measuring effects on disulfide cross-linking in vivo. *Proceedings of the National Academy of Sciences of the United States of America* **93** (21), 11546-11551

Hulko, M., Berndt, F., Gruber, M., Linder, J. U., Truffault, V., Schultz, A., Martin, J., Schultz, J. E., Lupas, A. N. and Coles, M. (2006) The HAMP domain structure implies helix rotation in transmembrane signaling. *Cell* **126** (5), 929-940

Iuchi, S. and Lin, E. C. (1988) arcA (dye), a global regulatory gene in Escherichia coli mediating repression of enzymes in aerobic pathways. *Proceedings of the National Academy of Sciences of the United States of America* **85** (6), 1888-1892

Jacob, F., Perrin, D., Sánchez, C., Monod, J. and Edelstein, S. (2005) The operon: a group of genes with expression coordinated by an operator. C.R.Acad. Sci. Paris 250 (1960) 1727-1729. *Comptes rendus biologies* **328** (6), 514-520

Janausch, I., Zientz, E., Tran, Q., Kröger, A. and Unden, G. (2002) C_4-dicarboxylate carriers and sensors in bacteria. *Biochimica et Biophysica Acta (BBA) - Bioenergetics* **1553** (1-2), 39-56

Janausch, I. G., Garcia-Moreno, I., Lehnen, D., Zeuner, Y. and Unden, G. (2004) Phosphorylation and DNA binding of the regulator DcuR of the fumarate-responsive two-component system DcuSR of Escherichia coli. *Microbiology* **150** (Pt 4), 877-883

Janausch, I. G., Garcia-Moreno, I. and Unden, G. (2002) Function of DcuS from Escherichia coli as a fumarate-stimulated histidine protein kinase in vitro. *The Journal of biological chemistry* **277** (42), 39809-39814

Jordan, P. A., Thomson, A. J., Ralph, E. T., Guest, J. R. and Green, J. (1997) FNR is a direct oxygen sensor having a biphasic response curve. *FEBS Letters* **416** (3), 349-352

Jourlin, C., Bengrine, A., Chippaux, M. and Méjean, V. (1996) An unorthodox sensor protein (TorS) mediates the induction of the tor structural genes in response to trimethylamine N-oxide in Escherichia coli. *Molecular microbiology* **20** (6), 1297-1306

Kao, K. C., Tran, L. M. and Liao, J. C. (2005) A global regulatory role of gluconeogenic genes in Escherichia coli revealed by transcriptome network analysis. *The Journal of biological chemistry* **280** (43), 36079-36087

Kao, K. C., Yang, Y.-L., Boscolo, R., Sabatti, C., Roychowdhury, V. and Liao, J. C. (2004) Transcriptome-based determination of multiple transcription regulator activities in Escherichia coli by using network component analysis. *Proceedings of the National Academy of Sciences of the United States of America* **101** (2), 641-646

Kaper, J. B., Nataro, J. P. and Mobley, H. L. (2004) Pathogenic Escherichia coli. *Nature reviews. Microbiology* **2** (2), 123-140

Karimova, G., Pidoux, J., Ullmann, A. and Ladant, D. (1998) A bacterial two-hybrid system based on a reconstituted signal transduction pathway. *Proceedings of the National Academy of Sciences of the United States of America* **95** (10), 5752-5756

Karimova, G., Ullmann, A. and Ladant, D. (2000) Bordetella pertussis adenylate cyclase toxin as a tool to analyze molecular interactions in a bacterial two-hybrid system. *International Journal of Medical Microbiology* **290** (4-5), 441-445

Karinou, E., Compton, E. L. R., Morel, M. and Javelle, A. (2013) The Escherichia coli SLC26 homologue YchM (DauA) is a C_4-dicarboxylic acid transporter. *Molecular microbiology* **87** (3), 623–640

Karinou, E., Hoskisson, P. A., Strecker, A., Unden, G. and Javelle, A. (2017) The E. coli dicarboxylic acid transporters DauA act as a signal transducer by interacting with the DctA uptake system. *Scientific reports* **7** (1), 16331

Kay, W. W. and Kornberg, H. L. (1971) The uptake of C_4-dicarboxylic acids by Escherichia coli. *European journal of biochemistry* **18** (2), 274-281

Kim, O. B., Lux, S. and Unden, G. (2007) Anaerobic growth of Escherichia coli on D-tartrate depends on the fumarate carrier DcuB and fumarase, rather than the L-tartrate carrier TtdT and L-tartrate dehydratase. *Archives of microbiology* **188** (6), 583-589

Kim, S. and Cross, T. A. (2004) 2D solid state NMR spectral simulation of 3_{10}, α, and π-helices. *Journal of magnetic resonance* **168** (2), 187-193

Kitanovic, S., Ames, P. and Parkinson, J. S. (2011) Mutational analysis of the control cable that mediates transmembrane signaling in the Escherichia coli serine chemoreceptor. *Journal of bacteriology* **193** (19), 5062-5072

Kitanovic, S., Ames, P. and Parkinson, J. S. (2015) A Trigger Residue for Transmembrane Signaling in the Escherichia coli Serine Chemoreceptor. *Journal of bacteriology* **197** (15), 2568-2579

Kleefeld, A., Ackermann, B., Bauer, J., Krämer, J. and Unden, G. (2009) The fumarate/succinate antiporter DcuB of Escherichia coli is a bifunctional protein with sites for regulation of DcuS-dependent gene expression. *The Journal of biological chemistry* **284** (1), 265-275

Kleiger, G., Grothe, R., Mallick, P. and Eisenberg, D. (2002) GXXXG and AXXXA: common α-helical interaction motifs in proteins, particularly in extremophiles. *Biochemistry* **41** (19), 5990-5997

Kneuper, H., Janausch, I. G., Vijayan, V., Zweckstetter, M., Bock, V., Griesinger, C. and Unden, G. (2005) The nature of the stimulus and of the fumarate binding site of the fumarate sensor DcuS of Escherichia coli. *The Journal of biological chemistry* **280** (21), 20596-20603

Kochanowski, K., Gerosa, L., Brunner, S. F., Christodoulou, D., Nikolaev, Y. V. and Sauer, U. (2017) Few regulatory metabolites coordinate expression of central metabolic genes in Escherichia coli. *Molecular systems biology* **13** (1), 903

Kofoid, E. C. and Parkinson, J. S. (1988) Transmitter and receiver modules in bacterial signaling proteins. *Proceedings of the National Academy of Sciences of the United States of America* **85** (14), 4981-4985

Krämer, J., Fischer, J. D., Zientz, E., Vijayan, V., Griesinger, C., Lupas, A. and Unden, G. (2007) Citrate sensing by the C_4-dicarboxylate/citrate sensor kinase DcuS of Escherichia coli: binding site and conversion of DcuS to a C_4-dicarboxylate- or citrate-specific sensor. *Journal of bacteriology* **189** (11), 4290-4298

Langosch, D., Brosig, B., Kolmar, H. and Fritz, H. J. (1996) Dimerisation of the glycophorin A transmembrane segment in membranes probed with the ToxR transcription activator. *Journal of molecular biology* **263** (4), 525-530

Lederberg, J. and Tatum, E. L. (1946) Gene recombination in Escherichia coli. *Nature* **158** (4016), 558

Lee, G. F., Lebert, M. R., Lilly, A. A. and Hazelbauer, G. L. (1995) Transmembrane signaling characterized in bacterial chemoreceptors by using sulfhydryl cross-linking in vivo. *Proceedings of the National Academy of Sciences of the United States of America* **92** (8), 3391-3395

Lehnen, D., Blumer, C., Polen, T., Wackwitz, B., Wendisch, V. F. and Unden, G. (2002) LrhA as a new transcriptional key regulator of flagella, motility and chemotaxis genes in Escherichia coli. *Molecular microbiology* **45** (2), 521-532

Lemmin, T., Soto, C. S., Clinthorne, G., DeGrado, W. F. and Dal Peraro, M. (2013) Assembly of the transmembrane domain of E. coli PhoQ histidine kinase: implications for signal transduction from molecular simulations. *PLoS computational biology* **9** (1), e1002878

Lemmon, M. A., Flanagan, J. M., Treutlein, H. R., Zhang, J. and Engelman, D. M. (1992) Sequence specificity in the dimerization of transmembrane α-helices. *Biochemistry* **31** (51), 12719-12725

Lesne, E., Dupré, E., Locht, C., Antoine, R. and Jacob-Dubuisson, F. (2017) Conformational Changes of an Interdomain Linker Mediate Mechanical Signal Transmission in Sensor Kinase BvgS. *Journal of bacteriology* **199** (18), e00114-17

Lukas, H., Reimann, J., Kim, O. B., Grimpo, J. and Unden, G. (2010) Regulation of aerobic and anaerobic D-malate metabolism of Escherichia coli by the LysR-type regulator DmlR (YeaT). *Journal of bacteriology* **192** (10), 2503-2511

MacKenzie, K. R., Prestegard, J. H. and Engelman, D. M. (1997) A transmembrane helix dimer: structure and implications. *Science* **276** (5309), 131-133

Maloney, P. C., Kashket, E. R. and Wilson, T. H. (1974) A protonmotive force drives ATP synthesis in bacteria. *Proceedings of the National Academy of Sciences of the United States of America* **71** (10), 3896-3900

Malpica, R., Franco, B., Rodriguez, C., Kwon, O. and Georgellis, D. (2004) Identification of a quinone-sensitive redox switch in the ArcB sensor kinase. *Proceedings of the National Academy of Sciences of the United States of America* **101** (36), 13318-13323

Marina, A., Waldburger, C. D. and Hendrickson, W. A. (2005) Structure of the entire cytoplasmic portion of a sensor histidine-kinase protein. *The EMBO journal* **24** (24), 4247-4259

Mascher, T., Helmann, J. D. and Unden, G. (2006) Stimulus perception in bacterial signal-transducing histidine kinases. *Microbiology and Molecular Biology Reviews* **70** (4), 910-938

Miller, J. H. (1992) A *Short course in bacterial genetics: A handbook for Escherichia coli and related bacteria,* Cold Spring Harbor Laboratory Press, New York

Miroux, B. and Walker, J. E. (1996) Over-production of proteins in Escherichia coli: mutant hosts that allow synthesis of some membrane proteins and globular proteins at high levels. *Journal of molecular biology* **260** (3), 289-298

Möglich, A., Ayers, R. A. and Moffat, K. (2009) Structure and signaling mechanism of Per-ARNT-Sim domains. **17** (10), 1282-1294

Molnar, K. S., Bonomi, M., Pellarin, R., Clinthorne, G. D., Gonzalez, G., Goldberg, S. D., Goulian, M., Sali, A. and DeGrado, W. F. (2014) Cys-scanning disulfide crosslinking and bayesian modeling probe the transmembrane signaling mechanism of the histidine kinase, PhoQ. *Structure* **22** (9), 1239-1251

Montrone, M., Eisenbach, M., Oesterhelt, D. and Marwan, W. (1998) Regulation of switching frequency and bias of the bacterial flagellar motor by CheY and fumarate. *Journal of bacteriology* **180** (13), 3375-3380

Montrone, M., Oesterhelt, D. and Marwan, W. (1996) Phosphorylation-independent bacterial chemoresponses correlate with changes in the cytoplasmic level of fumarate. *Journal of bacteriology* **178** (23), 6882-6887

Monzel, C. (2015) *Signaltransduktion in der membranständigen Sensor-Histidinkinase DcuS von Escherichia coli,* (*Doctoral Dissertation*), Johannes Gutenberg-Universität Mainz

Müller, M. (2007). *Funktionskomplementierung des Fumaratsensors DcuS von Escherichia coli durch Hybriddimere.* (*Diploma Thesis*), Institut für Mikrobiologie und Weinforschung, Johannes Gutenberg-Universität Mainz.

Nanchen, A., Schicker, A., Revelles, O. and Sauer, U. (2008) Cyclic AMP-dependent catabolite repression is the dominant control mechanism of metabolic fluxes under glucose limitation in Escherichia coli. *Journal of bacteriology* **190** (7), 2323-2330

Neiditch, M. B., Federle, M. J., Pompeani, A. J., Kelly, R. C., Swem, D. L., Jeffrey, P. D., Bassler, B. L. and Hughson, F. M. (2006) Ligand-induced asymmetry in histidine sensor kinase complex regulates quorum sensing. *Cell* **126** (6), 1095-1108

Oh, M.-K., Rohlin, L., Kao, K. C. and Liao, J. C. (2002) Global expression profiling of acetate-grown Escherichia coli. *The Journal of biological chemistry* **277** (15), 13175-13183

Ottemann, K. M., Xiao, W., Shin, Y. K. and Koshland, D. E. (1999) A piston model for transmembrane signaling of the aspartate receptor. *Science* **285** (5434), 1751-1754

Pakula, A. A. and Simon, M. I. (1992) Determination of transmembrane protein structure by disulfide cross-linking: the Escherichia coli Tar receptor. *Proceedings of the National Academy of Sciences of the United States of America* **89** (9), 4144-4148

Parkinson, J. S. (2010) Signaling mechanisms of HAMP domains in chemoreceptors and sensor kinases. *Annual review of microbiology* **64**, 101-122

Pauling, L., and Corey, R. B. (1951) Atomic coordinates and structure factors for two helical configurations of polypeptide chains. *Proceedings of the National Academy of Sciences of the United States of America* **37** (5), 235-240

Pauling, L., Corey, R. B. and Branson, H. R. (1951) The structure of proteins; two hydrogen-bonded helical configurations of the polypeptide chain. *Proceedings of the National Academy of Sciences of the United States of America* **37** (4), 205-211

Perrenoud, A. and Sauer, U. (2005) Impact of global transcriptional regulation by ArcA, ArcB, Cra, Crp, Cya, Fnr, and Mlc on glucose catabolism in Escherichia coli. *Journal of bacteriology* **187** (9), 3171-3179

Pettersen, E. F., Goddard, T. D., Huang, C. C., Couch, G. S., Greenblatt, D. M., Meng, E. C. and Ferrin, T. E. (2004) UCSF Chimera – a visualization system for exploratory research and analysis. *Journal of computational chemistry* **25** (13), 1605-1612

Plevin, M. J., Mills, M. M. and Ikura, M. (2005) The LxxLL motif: a multifunctional binding sequence in transcriptional regulation. *Trends in biochemical sciences* **30** (2), 66-69

Polyansky, A. A., Chugunov, A. O., Volynsky, P. E., Krylov, N. A., Nolde, D. E. and Efremov, R. G. (2014) PREDDIMER: a web server for prediction of transmembrane helical dimers. *Bioinformatics* **30** (6), 889-890

Pos, K. M., Dimroth, P. and Bott, M. (1998) The Escherichia coli citrate carrier CitT: a member of a novel eubacterial transporter family related to the 2-oxoglutarate/malate translocator from spinach chloroplasts. *Journal of bacteriology* **180** (16), 4160-4165

Prasad, K., Caplan, S. R. and Eisenbach, M. (1998) Fumarate modulates bacterial flagellar rotation by lowering the free energy difference between the clockwise and counterclockwise states of the motor. *Journal of molecular biology* **280** (5), 821-828

Rabin, R. S. and Stewart, V. (1993) Dual response regulators (NarL and NarP) interact with dual sensors (NarX and NarQ) to control nitrate- and nitrite-regulated gene expression in Escherichia coli K-12. *Journal of bacteriology* **175** (11), 3259-3268

Raunser, S., Appel, M., Ganea, C., Geldmacher-Kaufer, U., Fendler, K. and Kühlbrandt, W. (2006) Structure and function of prokaryotic glutamate transporters from Escherichia coli and Pyrococcus horikoshii. *Biochemistry* **45** (42), 12796-12805

Rauschmeier, M., Schüppel, V., Tetsch, L.- and Jung, K. (2014) New insights into the interplay between the lysine transporter LysP and the pH sensor CadC in Escherichia coli. *Journal of molecular biology* **426** (1), 215-229

Riek, R. P., Rigoutsos, I., Novotny, J.- and Graham, R. M. (2001) Non-α-helical elements modulate polytopic membrane protein architecture. *Journal of molecular biology* **306** (2), 349-362

Riek, R. P., Finch, A. A., Begg, G. E. and Graham, R. M. (2008) Wide turn diversity in protein transmembrane helices implications for G-protein-coupled receptor and other polytopic membrane protein structure and function. *Molecular pharmacology* **73** (4), 1092-1104

Rigoutsos, I., Riek, P., Graham, R. M. and Novotny, J. (2003) Structural details (kinks and non-α conformations) in transmembrane helices are intrahelically determined and can be predicted by sequence pattern descriptors. *Nucleic acids research* **31** (15), 4625-4631

Russ, W. P. and Engelman, D. M. (2000) The GxxxG motif: a framework for transmembrane helix-helix association. *Journal of molecular biology* **296** (3), 911-919

Salazar, M. E., Podgornaia, A. I. and Laub, M. T. (2016) The small membrane protein MgrB regulates PhoQ bifunctionality to control PhoP target gene expression dynamics. *Molecular microbiology* **102** (3), 430-445

Sal-Man, N., Gerber, D. and Shai, Y. (2004) The composition rather than position of polar residues (QxxS) drives aspartate receptor transmembrane domain dimerization in vivo. *Biochemistry* **43** (8), 2309-2313

Salvi, M., Schomburg, B., Giller, K., Graf, S., Unden, G., Becker, S., Lange, A. and Griesinger, C. (2017) Sensory domain contraction in histidine kinase CitA triggers transmembrane signaling in the membrane-bound sensor. *Proceedings of the National Academy of Sciences of the United States of America* **114** (12), 3115-3120

Sambrook, J. and Russell, D. W. (2001) *Molecular cloning: A laboratory manual,* 3rd Ed., Cold Spring Harbor Laboratory Press, New York

Scheu, P. D., Witan, J., Rauschmeier, M., Graf, S., Liao, Y.-F., Ebert-Jung, A., Basché, T., Erker, W. and Unden, G. (2012) CitA/CitB two-component system regulating citrate fermentation in Escherichia coli and its relation to the DcuS/DcuR system in vivo. *Journal of bacteriology* **194** (3), 636-645

Scheu, P., Sdorra, S., Liao, Y.-F., Wegner, M., Basché, T., Unden, G. and Erker, W. (2008) Polar accumulation of the metabolic sensory histidine kinases DcuS and CitA in Escherichia coli. *Microbiology* **154** (Pt 8), 2463-2472

Scheu, P. D., Liao, Y.-F., Bauer, J., Kneuper, H., Basché, T., Unden, G. and Erker, W. (2010) Oligomeric sensor kinase DcuS in the membrane of Escherichia coli and in proteoliposomes: chemical cross-linking and FRET spectroscopy. *Journal of bacteriology* **192** (13), 3474-3483

Scheu, P. D., Steinmetz, P. A., Dempwolff, F., Graumann, P. L. and Unden, G. (2014) Polar localization of a tripartite complex of the two-component system DcuS/DcuR and the transporter DctA in Escherichia coli depends on the sensor kinase DcuS. *PLoS one* **9** (12), e115534

Schmidt, A., Kochanowski, K., Vedelaar, S., Ahrné, E., Volkmer, B., Callipo, L., Knoops, K., Bauer, M., Aebersold, R. and Heinemann, M. (2016) The quantitative and condition-dependent Escherichia coli proteome. *Nature Biotechnology* **34** (1), 104-110

Schneider, D. and Engelman, D. M. (2003) GALLEX, a measurement of heterologous association of transmembrane helices in a biological membrane. *The Journal of biological chemistry* **278** (5), 3105-3111

Schneider, D. and Engelman, D. M. (2004) Motifs of two small residues can assist but are not sufficient to mediate transmembrane helix interactions. *Journal of molecular biology* **343** (4), 799-804

Schubert (2018) *Kontrolle des Sensors DcuS aus Escherichia coli durch den Transporter DctA und das Glucose-PTS-System* (*Master Thesis*)), Institut für Molekulare Physiologie, Johannes Gutenberg-Universität Mainz

Schubert, C., Zedler, S., Strecker, A. and Unden, G. (2020) L-Aspartate as a high-quality nitrogen source in Escherichia coli: Regulation of L-aspartase by the nitrogen regulatory system and interaction of L-aspartase with GlnB. *Molecular microbiology*

Senes, A., Gerstein, M. and Engelman, D. M. (2000) Statistical analysis of amino acid patterns in transmembrane helices: the GxxxG motif occurs frequently and in association with beta-branched residues at neighboring positions. *Journal of molecular biology* **296** (3), 921-936

Senes, A., Ubarretxena-Belandia, I. and Engelman, D. M. (2001) The Cα—H···hydrogen bond: a determinant of stability and specificity in transmembrane helix interactions. *Proceedings of the National Academy of Sciences of the United States of America* **98** (16), 9056-9061

Senes, A., Engel, D. E. and DeGrado, W. F. (2004) Folding of helical membrane proteins: the role of polar, GxxxG-like and proline motifs. *Current opinion in structural biology* **14** (4), 465-479

Sevvana, M., Vijayan, V., Zweckstetter, M., Reinelt, S., Madden, D. R., Herbst-Irmer, R., Sheldrick, G. M., Bott, M., Griesinger, C. and Becker, S. (2008) A ligand-induced switch in the periplasmic domain of sensor histidine kinase CitA. *Journal of molecular biology* **377** (2), 512-523

Shimada, T., Fujita, N., Yamamoto, K. and Ishihama, A. (2011) Novel roles of cAMP receptor protein (CRP) in regulation of transport and metabolism of carbon sources. *PLoS one* **6** (6), e20081

Simon, G., Méjean, V., Jourlin, C., Chippaux, M. and Pascal, M. C. (1994) The torR gene of Escherichia coli encodes a response regulator protein involved in the expression of the trimethylamine N-oxide reductase genes. *Journal of bacteriology* **176** (18), 5601-5606

Six, S., Andrews, S. C., Unden, G. and Guest, J. R. (1994) Escherichia coli possesses two homologous anaerobic C4-dicarboxylate membrane transporters (DcuA and DcuB) distinct from the aerobic dicarboxylate transport system (Dct). *Journal of bacteriology* **176** (21), 6470-6478

Slavny, P., Little, R., Salinas, P., Clarke, T. A. and Dixon, R. (2010) Quaternary structure changes in a second Per-Arnt-Sim domain mediate intramolecular redox signal relay in the NifL regulatory protein. *Molecular microbiology* **75** (1), 61-75

Steinmetz, P. A. (2014) *Signalerkennung und Signaltransduktion im DctA/DcuS-Sensor-Regulatorkomplex von Escherichia coli,* (*Doctoral Dissertation*), Johannes Gutenberg-Universität Mainz

Steinmetz, P. A., Wörner, S. and Unden, G. (2014) Differentiation of DctA and DcuS function in the DctA/DcuS sensor complex of Escherichia coli: function of DctA as an activity switch and of DcuS as the C₄-dicarboxylate sensor. *Molecular microbiology* **94** (1), 218-229

Stewart, V. (2003) Biochemical Society Special Lecture. Nitrate- and nitrite-responsive sensors NarX and NarQ of proteobacteria. *Biochemical Society transactions* **31** (Pt 1), 1–10

Stock, A. M., Robinson, V. L. and Goudreau, P. N. (2000) Two-component signal transduction. *Annual review of biochemistry* **69**, 183-215

Stopp, M., Steinmetz, P. A., Schubert, C., Griesinger, C., Schneider, D. and Unden, G. (2020) Transmembrane signaling and cytoplasmic signal conversion by dimeric transmembrane helix 2 and a linker domain of the DcuS sensor kinase. *The Journal of biological chemistry* **296**, 100148

Strecker, A. (2018) Der C₄-Dicarboxylat-Metabolismus von Escherichia coli: Die Rolle von DcuA und von DcuS im Signaltransfer (*Doctoral Dissertation*), Johannes Gutenberg-Universität Mainz

Strecker, A., Schubert, C., Zedler, S., Steinmetz, P. and Unden, G. (2018) DcuA of aerobically grown Escherichia coli serves as a nitrogen shuttle (L-aspartate/fumarate) for nitrogen uptake. *Molecular microbiology* **109** (6), 801-811

Sukomon, N., Widom, J., Borbat, P. P., Freed, J. H. and Crane, B. R. (2017) Stability and Conformation of a Chemoreceptor HAMP Domain Chimera Correlates with Signaling Properties. *Biophysical journal* **112** (7), 1383-1395

Surmann, K., Stopp, M., Wörner, S., Dhople, V. M., Völker, U., Unden, G. and Hammer, E. (2020) Fumarate dependent protein composition under aerobic and anaerobic growth conditions in Escherichia coli. *Journal of proteomics* **212**, 103583

Taylor, B. L. and Zhulin, I. B. (1999) PAS Domains: Internal Sensors of Oxygen, Redox Potential, and Light. *Microbiology and Molecular Biology Reviews* **63** (2), 479-506

Tetsch, L., Koller, C., Haneburger, I. and Jung, K. (2008) The membrane-integrated transcriptional activator CadC of Escherichia coli senses lysine indirectly via the interaction with the lysine permease LysP. *Molecular microbiology* **67** (3), 570-583

Towbin, H., Staehelin, T. and Gordon, J. (1979) Electrophoretic transfer of proteins from polyacrylamide gels to nitrocellulose sheets: procedure and some applications. *Proceedings of the National Academy of Sciences of the United States of America* **76** (9), 4350-4354

Ulrich, L. E. and Zhulin, I. B. (2010) The MiST2 database: a comprehensive genomics resource on microbial signal transduction. *Nucleic acids research* **38** (suppl_1, 1 January), D401-407

Unden, G., Wörner, S. and Monzel, C. (2016) Cooperation of Secondary Transporters and Sensor Kinases in Transmembrane Signalling: The DctA/DcuS and DcuB/DcuS Sensor Complexes of Escherichia coli. *Advances in microbial physiology* **68**, 139-167

Unden, G., Steinmetz, P. A. and Degreif-Dünnwald, P. (2014) The Aerobic and Anaerobic Respiratory Chain of Escherichia coli and Salmonella enterica: Enzymes and Energetics. *EcoSal Plus* **6** (1)

Unden, G., Strecker, A., Kleefeld, A. and Kim, O. B. (2016) C₄-Dicarboxylate Utilization in Aerobic and Anaerobic Growth. *EcoSal Plus* **7** (1)

Véscovi, E. G., Ayala, Y. M., Di Cera, E. and Groisman, E. A. (1997) Characterization of the bacterial sensor protein PhoQ. Evidence for distinct binding sites for Mg^{2+} and Ca^{2+}. *The Journal of biological chemistry* **272** (3), 1440-1443

Wadolkowski, E. A., Laux, D. C. and Cohen, P. S. (1988) Colonization of the streptomycin-treated mouse large intestine by a human fecal Escherichia coli strain: role of adhesion to mucosal receptors. *Infection and immunity* **56** (5), 1036-1043

Wang, C., Sang, J., Wang, J., Su, M., Downey, J. S., Wu, Q., Wang, S., Cai, Y., Xu, X., Wu, J., Senadheera, D. B., Cvitkovitch, D. G., Chen, L., Goodman, S. D. and Han, A. (2013) Mechanistic

insights revealed by the crystal structure of a histidine kinase with signal transducer and sensor domains. *PLoS biology* **11** (2), e1001493

Weaver, T. M. (2000) The π-helix translates structure into function. *Protein science: a publication of the Protein Society* **9** (1), 201-206

Weisenburger, S., Boening, D., Schomburg, B., Giller, K., Becker, S., Griesinger, C. and Sandoghdar, V. (2017) Cryogenic optical localization provides 3D protein structure data with Angstrom resolution. *Nature methods* **14** (2), 141-144

Wissenbach, U., Kröger, A. and Unden, G. (1990) The specific functions of menaquinone and demethylmenaquinone in anaerobic respiration with fumarate, dimethylsulfoxide, trimethylamine N-oxide and nitrate by Escherichia coli. *Archives of microbiology* **154** (1), 60-66

Witan, J. (2012) *Funktion der C$_4$-Dicarboxylat-Transporter DctA und DcuB als Co-Sensoren von DcuS in Escherichia coli,* (*Doctoral Dissertation*), Johannes Gutenberg-Universität Mainz

Witan, J., Bauer, J., Wittig, I., Steinmetz, P. A., Erker, W. and Unden, G. (2012) Interaction of the Escherichia coli transporter DctA with the sensor kinase DcuS: presence of functional DctA/DcuS sensor units. *Molecular microbiology* **85** (5), 846-861

Wörner, S., Strecker, A., Monzel, C., Zeltner, M., Witan, J., Ebert-Jung, A. and Unden, G. (2016) Conversion of the sensor kinase DcuS of Escherichia coli of the DcuB/DcuS sensor complex to the C$_4$-dicarboxylate responsive form by the transporter DcuB. *Environmental microbiology* **18** (12), 4920-4930

Wörner, S., Surmann, K., Ebert-Jung, A., Völker, U., Hammer, E. and Unden, G. (2018) Cellular Concentrations of the Transporters DctA and DcuB and the Sensor DcuS of Escherichia coli and the Contributions of Free and Complexed DcuS to Transcriptional Regulation by DcuR. *Journal of bacteriology* **200** (4), e00612-17

Wuichet, K., Cantwell, B. J. and Zhulin, I. B. (2010) Evolution and phyletic distribution of two-component signal transduction systems. *Current opinion in microbiology* **13** (2), 219-225

Xiao, M., Lai, Y., Sun, J., Chen, G. and Yan, A. (2016) Transcriptional Regulation of the Outer Membrane Porin Gene ompW Reveals its Physiological Role during the Transition from the Aerobic to the Anaerobic Lifestyle of Escherichia coli. *Frontiers in microbiology* **7**, 799

Yang, J. and Zhang, Y. (2015) I-TASSER server: new development for protein structure and function predictions. *Nucleic acids research* **43** (W1), W174-81

Yuan, J., Jin, F., Glatter, T. and Sourjik, V. (2017) Osmosensing by the bacterial PhoQ/PhoP two-component system. *Proceedings of the National Academy of Sciences of the United States of America* **114** (50), E10792-E10798

Zeltner, M. (2018) *Reinigung des C$_4$-Dicarboxylat-Transporters DctA und dessen regulatorischer Einfluss auf die Aktivität der Sensorkinase DcuS,* (*Doctoral Dissertation*), Johannes Gutenberg-Universität Mainz

Zientz, E., Bongaerts, J. and Unden, G. (1998) Fumarate regulation of gene expression in Escherichia coli by the DcuSR (dcuSR genes) two-component regulatory system. *Journal of bacteriology* **180** (20), 5421-5425

Zientz, E., Janausch, I. G., Six, S. and Unden, G. (1999) Functioning of DcuC as the C$_4$-dicarboxylate carrier during glucose fermentation by Escherichia coli. *Journal of bacteriology* **181** (12), 3716-3720

Zschiedrich, C. P., Keidel, V. and Szurmant, H. (2016) Molecular Mechanisms of Two-Component Signal Transduction. *Journal of molecular biology* **428** (19), 3752-3775

7 Apendix

Table 5. *E. coli* **K12 strains with the respective genotype used in this study.**

Strain	Genotype	Reference or Source
C43(DE3)	F⁻, *ompT, gal, dcm, lon, hsdS_B(r_B⁻m_B⁻)*, λ(DE3 [*lacI lacUV5-T7p07 ind1 sam7 nin5*]), spontaneous mutation of BL21(DE3) to overproduce membrane proteins,	Miroux and Walker (1996)
IMW260	MC4100 λ[Φ(*dcuB'-'lacZ)hyb, bla⁺*] but *dcuS::cam^r*	Zientz *et al*. 1998
IMW660	C43(DE3) but *dcuS::FRT, dctA::FRT*	Schubert (2018)
XL1-blue	*recA1, endA1, gyrA96, thi-1, hsdR17, supE44, relA1, lac*, F′ [*proAB, lacIqZΔM15, Tn10* (Tet^r)]	Stratagene

Table 6. Plasmids used in this study.

Plasmid	Genotype	Reference
pMW151	His₆-DcuS expression plasmid, pET28-derivative (Kan^r)	Janausch *et al*. 2002
pMW336	pMW151 but DcuS-C199S-C471S (= DcuS_Cys0) (Kan^r)	Scheu *et al*. 2010
pMW1930	pMW336 but DcuS-K16C (Kan^r)	Scheu *et al*. 2010
pMW1931	pMW336 but DcuS-L17C (Kan^r)	Monzel and Unden (2015)
pMW1932	pMW336 but DcuS-S18C (Kan^r)	Monzel and Unden (2015)
pMW1933	pMW336 but DcuS-T19C (Kan^r)	Monzel and Unden (2015)
pMW1934	pMW336 but DcuS-T20C (Kan^r)	Monzel and Unden (2015)
pMW1935	pMW336 but DcuS-V21C (Kan^r)	Monzel and Unden (2015)
pMW1936	pMW336 but DcuS-I22C (Kan^r)	Monzel and Unden (2015)
pMW1937	pMW336 but DcuS-L23C (Kan^r)	Monzel and Unden (2015)
pMW1938	pMW336 but DcuS-M24C (Kan^r)	Monzel and Unden (2015)
pMW1939	pMW336 but DcuS-V25C (Kan^r)	Monzel and Unden (2015)
pMW2648	pMW336 but DcuS-S26C (Kan^r)	Monzel and Unden (2015)
pMW2649	pMW336 but DcuS-A27C (Kan^r)	This study
pMW2650	pMW336 but DcuS-V28C (Kan^r)	This study
pMW2651	pMW336 but DcuS-L29C (Kan^r)	This study
pMW2652	pMW336 but DcuS-F30C (Kan^r)	This study
pMW2653	pMW336 but DcuS-S31C (Kan^r)	This study
pMW2654	pMW336 but DcuS-V32C (Kan^r)	This study
pMW2655	pMW336 but DcuS-L33C (Kan^r)	This study
pMW2656	pMW336 but DcuS-L34C (Kan^r)	This study
pMW1977	pMW336 but DcuS-V35C (Kan^r)	This study
pMW1978	pMW336 but DcuS-V36C (Kan^r)	Monzel and Unden (2015)
pMW1979	pMW336 but DcuS-H37C (Kan^r)	Monzel and Unden (2015)
pMW1980	pMW336 but DcuS-L38C (Kan^r)	Monzel and Unden (2015)
pMW1981	pMW336 but DcuS-I39C (Kan^r)	Monzel and Unden (2015)
pMW1982	pMW336 but DcuS-Y40C (Kan^r)	Monzel and Unden (2015)
pMW1983	pMW336 but DcuS-F41C (Kan^r)	Monzel and Unden (2015)
pMW1984	pMW336 but DcuS-S42C (Kan^r)	Monzel and Unden (2015)
pMW1985	pMW336 but DcuS-Q43C (Kan^r)	Monzel and Unden (2015)

pMW1986	pMW336 but DcuS-I44C (Kan^r)	Monzel and Unden (2015)
pMW1987	pMW336 but DcuS-S45C (Kan^r)	Monzel and Unden (2015)
pMW1988	pMW336 but DcuS-D46C (Kan^r)	Monzel and Unden (2015)
pMW2522	pMW336 but DcuS-G190C (Kan^r)	Monzel and Unden (2015)
pMW2526	pMW336 but DcuS-G194C (Kan^r)	Stopp *et al.* 2021
pMW1842	pMW336 but DcuS-T198C (Kan^r)	Stopp *et al.* 2021
pMW1844	pMW336 but DcuS-L201C (Kan^r)	Monzel Unden (2015)
pMW1846	pMW336 but DcuS-K203C (Kan^r)	Monzel and Unden (2015)
pMW1848	pMW336 but DcuS-L205C (Kan^r)	Monzel and Unden (2015)
pMW1849	pMW336 but DcuS-K206C (Kan^r)	Monzel and Unden (2015)
pMW1851	pMW336 but DcuS-I208C (Kan^r)	Monzel and Unden (2015)
pMW1852	pMW336 but DcuS-L209C (Kan^r)	Monzel and Unden (2015)
pMW1856	pMW336 but DcuS-E213C (Kan^r)	Monzel and Unden (2015)
pMW2644	pMW336 but DcuS-P214C (Kan^r)	Monzel and Unden (2015)
pMW2645	pMW336 but DcuS-Y215C (Kan^r)	This study
pMW2568	pMW336 but DcuS-E216C (Kan^r)	This study
pMW2646	pMW336 but DcuS-I217C (Kan^r)	Schubert (2018)
pMW2566	pMW336 but DcuS-S218C (Kan^r)	This study
pMW2567	pMW336 but DcuS-T219C (Kan^r)	Schubert (2018)
pMW2683	pMW336 but DcuS-L220C (Kan^r)	Schubert (2018)
pMW2684	pMW336 but DcuS-F221C (Kan^r)	This study
pMW2599	pMW336 but DcuS-E222C (Kan^r)	This study
pMW2569	pMW336 but DcuS-Q223C (Kan^r)	Schubert (2018)
pMW2685	pMW336 but DcuS-R224C (Kan^r)	Schubert (2018)
pMW2686	pMW336 but DcuS-Q225C (Kan^r)	This study
pMW2687	pMW336 but DcuS-A226C (Kan^r)	This study
pMW2688	pMW336 but DcuS-M227C (Kan^r)	This study
pMW2689	pMW336 but DcuS-L228C (Kan^r)	This study
pMW2690	pMW336 but DcuS-Q229C (Kan^r)	This study
pMW2691	pMW336 but DcuS-S230C (Kan^r)	This study
pMW2692	pMW336 but DcuS-I231C (Kan^r)	This study
pMW2693	pMW336 but DcuS-K232C (Kan^r)	This study
pMW2694	pMW336 but DcuS-E233C (Kan^r)	This study
pMW2695	pMW336 but DcuS-G234C (Kan^r)	This study
pMW2696	pMW336 but DcuS-V235C (Kan^r)	This study
pMW2845	pMW336 but DcuS-V236C (Kan^r)	This study
pMW2846	pMW336 but DcuS-A237C (Kan^r)	This study
pMW2847	pMW336 but DcuS-V238C (Kan^r)	This study
pMW2848	pMW336 but DcuS-D239C (Kan^r)	This study
pMW2849	pMW336 but DcuS-D240C (Kan^r)	This study
pMW2850	pMW336 but DcuS-R241C (Kan^r)	This study

Table 7. Primers for site-directed mutagenesis. The Cys substitutions are highlighted by bold letters, respectively.

Primer	Sequence (5' - 3')	T_M [°C]
DcuS_P214C_for	CGGCCTGGAA**TGC**TACGAAATCTC	64.4
DcuS_P214C_rev	GAGATTTCGTA**GCA**TTCCAGGCCG	64.4
DcuS_Y215C_for	GCCTGGAACCC**TGC**GAAATCTCCAC	67.9
DcuS_Y215C_rev	GTGGAGATTTC**GCA**GGGTTCCAGGC	67.9
DcuS_I217C_for	GAACCCTACGAA**TGC**TCCACGCTGTTTG	68.0
DcuS_I217C_rev	CAAACAGCGTGGA**GCA**TTCGTAGGGTTC	68.0
DcuS_L220C_for	CGAAATCTCCACG**TGC**TTTGAGCAACGC	68.0
DcuS_L220C_rev	GCGTTGCTCAAA**GCA**CGTGGAGATTTCG	68.0
DcuS_F221C_for	CTCCACGCTG**TGT**GAGCAACGCC	67.8
DcuS_F221C_rev	GGCGTTGCTC**ACA**CAGCGTGGAG	67.8
DcuS_R224C_for	CTGTTTGAGCAA**TGC**CAGGCCATGTTG	66.5
DcuS_R224C_rev	CAACATGGCCTG**GCA**TTGCTCAAACAG	66.5
DcuS_Q225C_for	GTTTGAGCAACGC**TGC**GCCATGTTGCAG	69.5
DcuS_Q225C_rev	CTGCAACATGGC**GCA**GCGTTGCTCAAAC	69.5
DcuS_A226C_for	GAGCAACGCCAG**TGC**ATGTTGCAGTC	68.0
DcuS_A226C_rev	GACTGCAACAT**GCA**CTGGCGTTGCTC	68.0
DcuS_M227C_for	CAACGCCAGGCC**TGC**TTGCAGTCTATC	69.5
DcuS_M227C_rev	GATAGACTGCAA**GCA**GGCCTGGCGTTG	69.5
DcuS_L228C_for	CGCCAGGCCATG**TGC**CAGTCTATCAAAG	69.5
DcuS_L228C_rev	CTTTGATAGACTG**GCA**CATGGCCTGGCG	69.5
DcuS_Q229C_for	CAGGCCATGTTG**TGC**TCTATCAAAGAAGG	66.7
DcuS_Q229C_rev	CCTTCTTTGATAGA**GCA**CAACATGGCCTG	66.7
DcuS_S230C_for	GCCATGTTGCAG**TGT**ATCAAAGAAGGCG	66.6
DcuS_S230C_rev	CGCCTTCTTTGAT**ACA**CTGCAACATGGC	66.6
DcuS_I231C_for	CATGTTGCAGTCT**TGC**AAAGAAGGCGTC	66.6
DcuS_I231C_rev	GACGCCTTCTTT**GCA**AGACTGCAACATG	66.6
DcuS_K232C_for	GTTGCAGTCTATC**TGC**GAAGGCGTCGTTG	69.5
DcuS_K232C_rev	CAACGACGCCTTC**GCA**GATAGACTGCAAC	69.5
DcuS_E233C_for	CAGTCTATCAAA**TGC**GGCGTCGTTGCC	68.0
DcuS_E233C_rev	GGCAACGACGCC**GCA**TTTGATAGACTG	68.0
DcuS_G234C_for	GTCTATCAAAGAA**TGC**GTCGTTGCCG	64.8
DcuS_G234C_rev	CGGCAACGAC**GCA**TTCTTTGATAGAC	64.8
DcuS_V235C_for	CTATCAAAGAAGGC**TGC**GTTGCCGTGG	68.0
DcuS_V235C_rev	CCACGGCAAC**GCA**GCCTTCTTTGATAG	68.0
DcuS_V236C_for	CAAAGAAGGCGTC**TGT**GCCGTGGACGATC	70.9
DcuS_V236C_rev	GATCGTCCACGGC**ACA**GACGCCTTCTTTG	70.9
DcuS_A237C_for	GAAGGCGTCGTT**TGC**GTGGACGATCG	69.5
DcuS_A237C_rev	CGATCGTCCAC**GCA**AACGACGCCTTC	69.5
DcuS_V238C_for	GCGTCGTTGCC**TGC**GACGATCGCG	69.3
DcuS_V238C_rev	CGCGATCGTC**GCA**GGCAACGACGC	69.3
DcuS_D239C_for	CGTTGCCGTG**TGC**GATCGCGGCG	71.3
DcuS_D239C_rev	CGCCGCGATC**GCA**CACGGCAACG	71.3
DcuS_D240C_for	GTTGCCGTGGAC**TGT**CGCGGCGAGG	72.8
DcuS_D240C_rev	CCTCGCCGCGA**CA**GTCCACGGCAAC	72.8

| DcuS_R241C_for | CCGTGGACGAT**TGC**GGCGAGGTCAC | 71.2 |
| DcuS_R241C_rev | GTGACCTCGCC**GCA**ATCGTCCACGG | 71.2 |

Table 8. Primers for sequencing.

Primer	Sequence (5' - 3')	T_M [°C]
midcuSseq	GTTTTCTGGCGCAGGCTTTACG	62.1
pET28a_rev	GTTATGCTAGTTATTGCTCAGC	58.4
T7prom	TAATACGACTCACTATAGG	50.2

Table 9. Chemicals used in this study.

| Substance	Supplier
Acid hydrolyzed casein (AHC)	AppliChem (No. A2142.0500)
Acrylamid-mix, Rothiphorese® 30 (37.5 : 1)	Roth
Agar-Agar, Kobe I	Roth (No. 5210.3)
Agarose (SeaKem® LE Agarose)	Lonza (No. 50004)
Albumin fraction V, (Bovine serum albumin, BSA)	BioFroxx (No.9048-46-8)
Ammonium persulfate (APS)	Sigma-Aldrich
Ampicillin sodium salt	Roth
Bromophenol blue	AppliChem
Cetyltrimethylammonium bromide (CTAB)	Serva
Chloramphenicol	Fluka
Coomassie® brilliant blue G250	Serva (No. 17524.01)
Copper(II)sulfate pentahydrate	Fluka
Dimethyl sulfoxide (DMSO)	Sigma
Disodium fumarate	Merck
Disodium hydrogen phosphate (Na_2HPO_4)	Roth
Dithiothreitol (DTT)	Sigma-Aldrich
dNTP-mix	Thermo Scientific
Ethanol (denatured with 1 % methyl ethyl ketone (MEK))	VWR
Ethylenediamine tetraacetic acid disodium salt dihydrate (EDTA)	Roth
N-Ethylmaleimide (NEM)	Sigma-Aldrich
GBX developer/replenisher	Carestream Healthcare
GBX fixer/replenisher	Carestream Healthcare
α-D(+)-Glucose	Roth
Glycerol (100%)	Sigma-Aldrich

|	
Glycine	AppliChem
Isopropyl-ß-D-thiogalactopyranoside (IPTG)	Thermo Scientific
Kanamycin sulfate	Roth
LB medium (Luria/Miller)	Roth (X964)
Magnesium chloride ($MgCl_2$)	Roth
Magnesium sulfate ($MgSO_4$)	Roth
3-(N-morpholino)propane sulfonic acid (MOPS)	Roth
o-Nitrophenyl-β-D-galactopyranoside (ONPG)	Roth
1,10-phenanthroline	Sigma-Aldrich
Polyethylene glycol 6000 (PEG 6000)	Roth
Polyoxyethylene-20-sorbitan monolaurate (Tween® 20)	AppliChem
Ponceau S	Roth (No. 5938.2)
Potassium chloride	Roth
Potassium dihydrogen phosphate (KH_2PO_4)	Roth
Red-Safe™ Nucleic Acid Staining Solution	Intron
SOB medium	Roth (No. AE27.1)
Sodium carbonate (Na_2CO_3)	Sigma-Aldrich
Sodium chloride (NaCl)	Roth
Sodium dihydrogen phosphate (NaH_2PO_4)	Roth
Sodium dodecyl sulfate (SDS)	Roth
Sodium deoxycholate (SDC)	Fluka
Skimmed milk powder	Roth
Sucrose	Roth
Tetracycline hydrochloride	Merck
N,N,N',N'-Tetramethyl ethylenediamine (TEMED)	Fluka
Tris(hydroxymethyl)-aminomethane (Tris)	Roth
L-Tryptophan	Serva
WesternBright™ ECL HRP substrate	Advansta
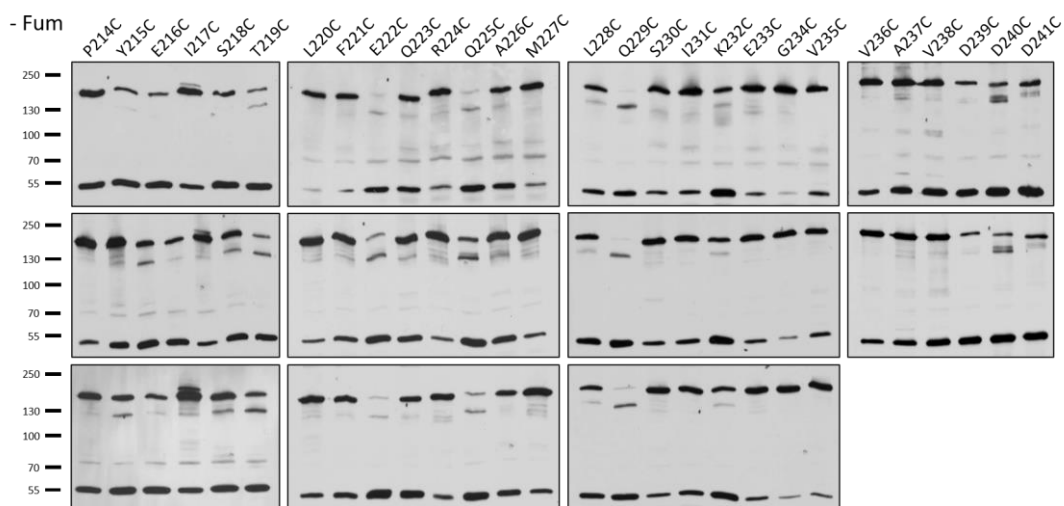
Figure 24. Detection of DcuS PAS$_C$ variants after CL with Cu^{2+} phenanthroline in the absence of fumarate. Cell protein was separated in non reducing SDS-PAGE and DcuS and CL-products were detected by chemiluminescence after Western blotting. Scans of the X-ray films are shown.
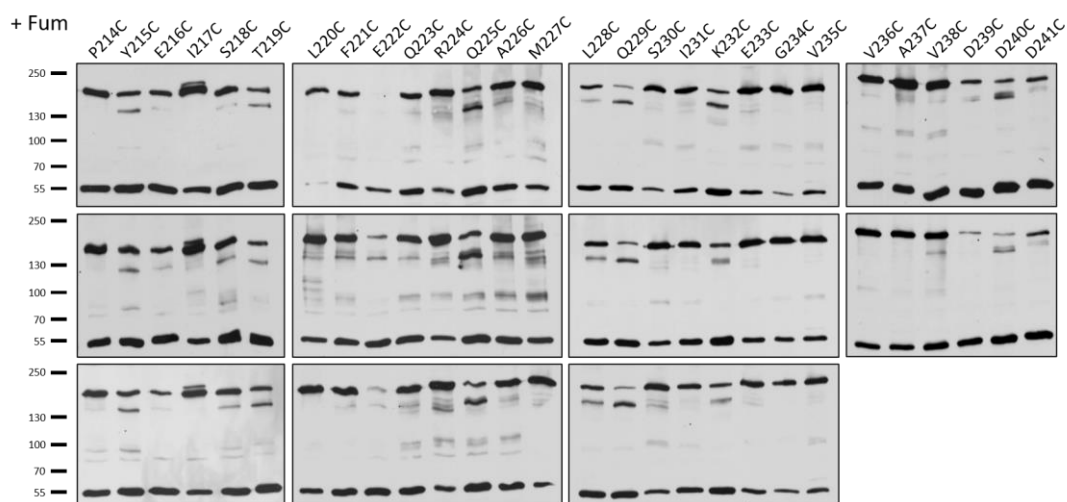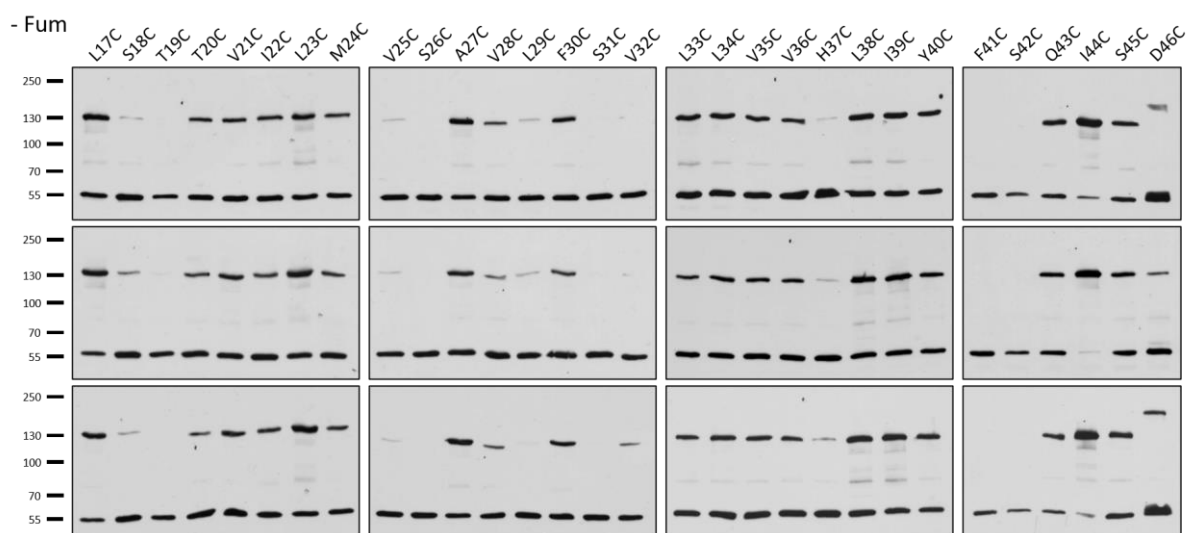

Figure 25. Detection of DcuS PAS$_C$ variants after CL with Cu^{2+} phenanthroline in the presence of fumarate. Cell protein was separated in non reducing SDS-PAGE and DcuS and CL-products were detected by chemiluminescence after Western blotting. Scans of the X-ray films are shown.
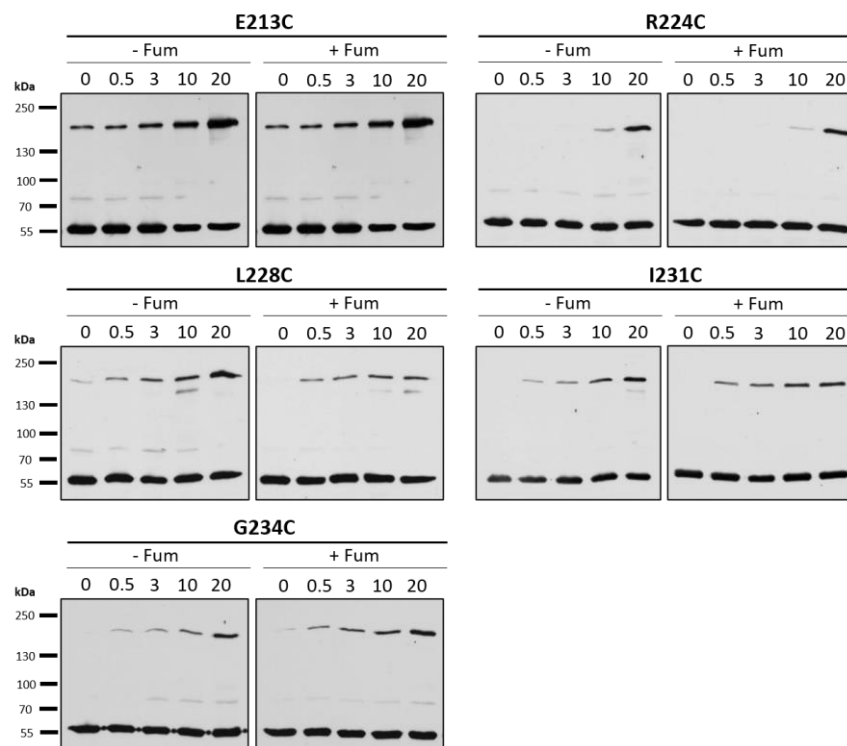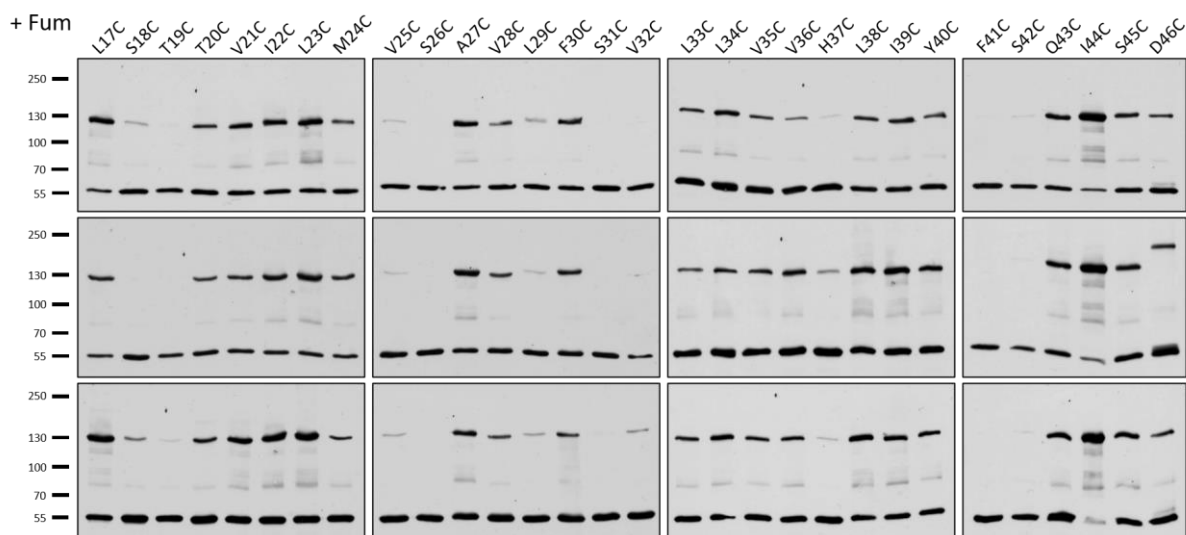
Figure 31. Detection of DcuS PASc variants after CL of bacteria with Cu²⁺ phenanthroline (kinetics of cross-linking). Cross-linking was performed in C43 (Wt), the reaction time shown above the scans (0 to 20 min) and in the absence (- Fum) or the presence (+ Fum) of fumarate. The reaction conditions are shown in Table 4. Cell protein was separated in non reducing SDS-PAGE and DcuS and CL-products were detected by chemiluminescence after Western blot. Scans of the X-ray films are shown. The scans of the Wt conditions are already published in Stopp et al. (2021) and were added for comparing purpose.
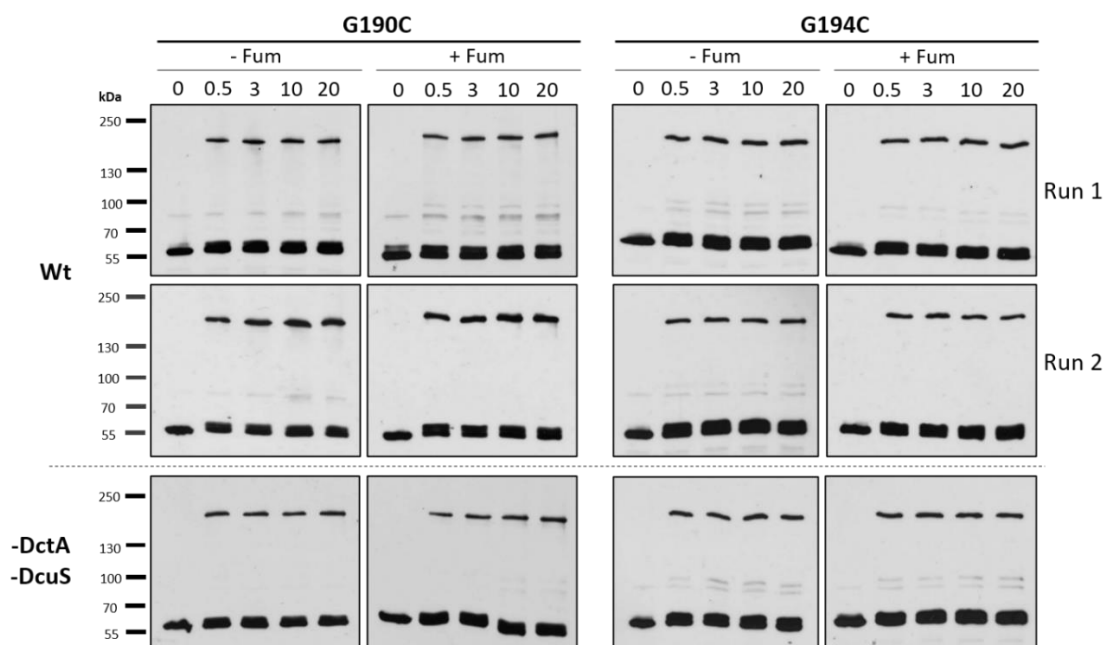

Figure 32. Detection of DcuS TM1 variants after CL with Cu²⁺ phenanthroline in the absence of fumarate. Cell protein was separated in non reducing SDS-PAGE and DcuS and CL-products were detected by chemiluminescence after Western blotting. Scans of the X-ray films are shown.

Figure 33. Detection of DcuS TM1 variants after CL with Cu²⁺ phenanthroline in the presence of fumarate. Cell protein was separated in non reducing SDS-PAGE and DcuS and CL-products were detected by chemiluminescence after Western blotting. Scans of the X-ray films are shown.

Figure 34. Detection of DcuS TM2 variants after CL of bacteria with Cu²⁺ phenanthroline (kinetics of cross-linking). Cross-linking was performed in either C43 (Wt) or IMW660 (-DctA/-DcuS), the reaction time shown above the scans (0 to 20 min) and in the absence (- Fum) or the presence (+ Fum) of fumarate. The reaction conditions are shown in Table 4. Cell protein was separated in non reducing SDS-PAGE and DcuS and CL-products were detected by chemiluminescence after Western blot. Scans of the X-ray films are shown. The dcans of the Wt conditions are already published in Stopp *et al*. (2021) and were added for comparing purpose.
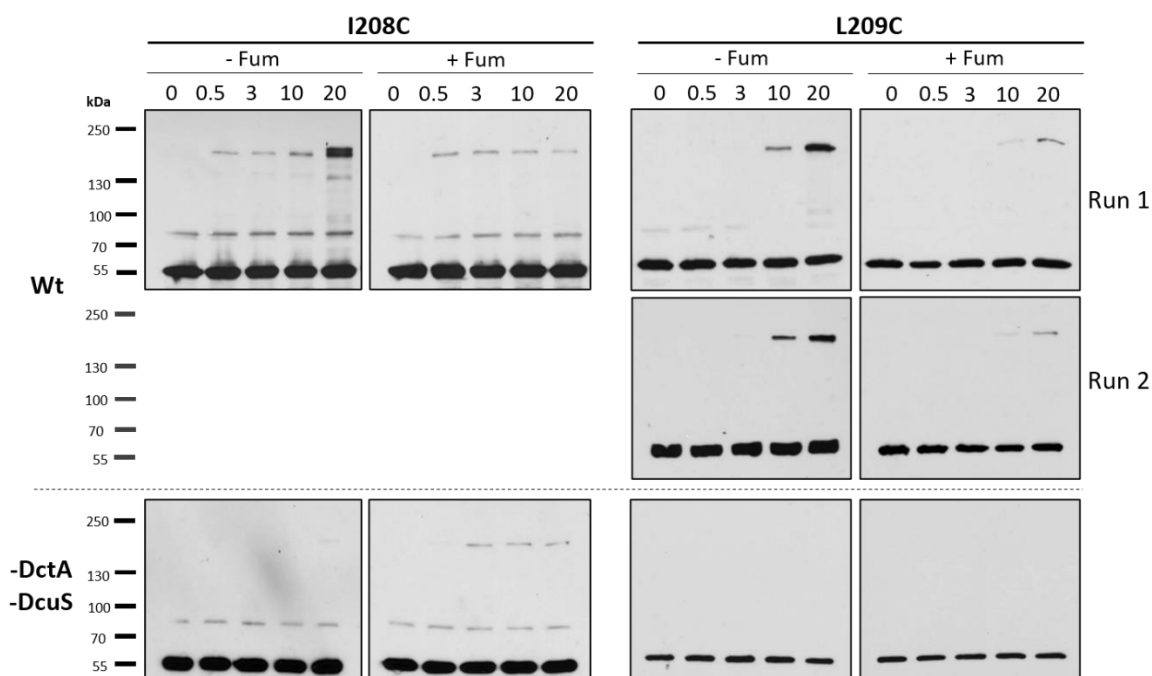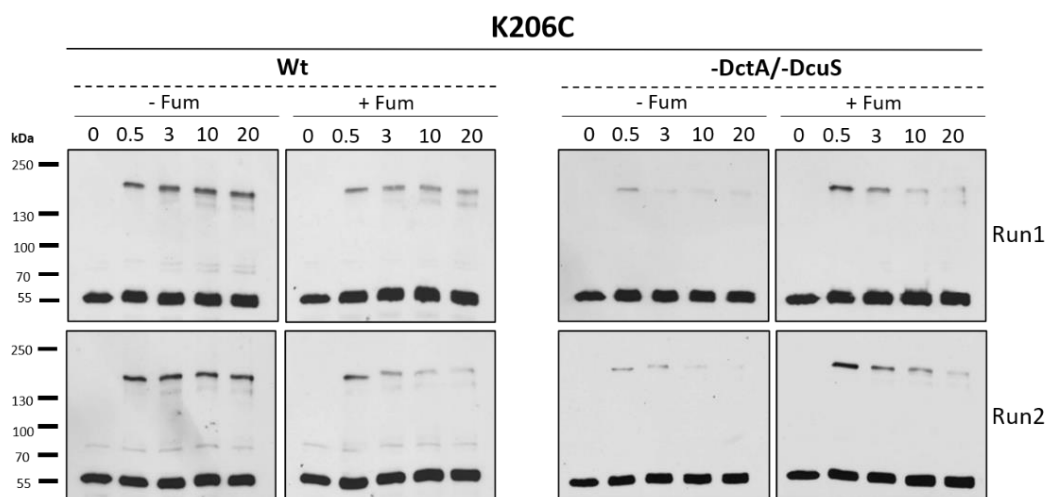
Figure 35. Detection of DcuS Linker variants I208C and L209C after CL of bacteria with Cu²⁺ phenanthroline (kinetics of cross-linking). Cross-linking was performed in either C43 (Wt) or IMW660 (-DctA/-DcuS), the reaction time shown above the scans (0 to 20 min) and in the absence (- Fum) or the presence (+ Fum) of fumarate. The reaction conditions are shown in Table 4. Cell protein was separated in non reducing SDS-PAGE and DcuS and CL-products were detected by chemiluminescence after Western blot. Scans of the X-ray films are shown. The scans of the Wt conditions are already published in Stopp *et al.* (2021) and were added for comparing purpose.
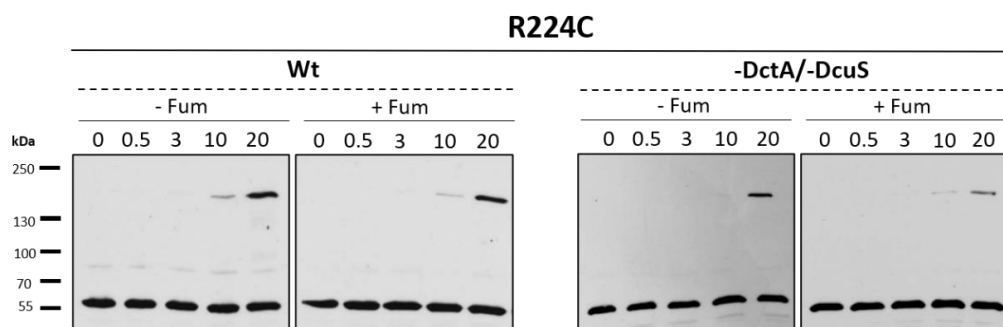

Figure 36. Detection of DcuS variant K206C in the linker after CL of bacteria with Cu²⁺ phenanthroline (kinetics of cross-linking). Cross-linking was performed in either C43 (Wt) or IMW660 (-DctA/-DcuS), the reaction time shown above the scans (0 to 20 min) and in the absence (- Fum) or the presence (+ Fum) of fumarate. The reaction conditions are shown in Table 4. Cell protein was separated in non reducing SDS-PAGE and DcuS and CL-products were detected by chemiluminescence after Western blot. Scans of the X-ray films are shown.

Figure 37. Detection of DcuS variant R224C in α1 of PAS$_C$ after CL of bacteria with Cu^{2+} phenanthroline (kinetics of cross-linking). Cross-linking was performed in either C43 (Wt) or IMW660 (-DctA/-DcuS), the reaction time shown above the scans (0 to 20 min) and in the absence (- Fum) or the presence (+ Fum) of fumarate. The reaction conditions are shown in Table 4. Cell protein was separated in non reducing SDS-PAGE and DcuS and CL-products were detected by chemiluminescence after Western blot. Scans of the X-ray films are shown.

8   Abbreviations

AHC	Acid-hydrolysed casein
APS	Ammoniumpersulfat
Arc	Aerobic respiration control
ARNT	Aryl hydrocarbon Receptor Nuclear Translocator
BACTH	Bacterial Two-Hybrid
BSA	Bovine serum albumin
CA	Catalytic and ATP-binding
Cam^r	Chloramphenicol resitence
cAMP	cyclic adenosine monophosphate
CRP	cAMP receptor protein
CTAB	Cetyltrimethylammoniumbromid
Cu^{2+}-Phenanthroline	Cu[II]-(1,10-Phenanthrolin)$_3$
DauA	Dicarboxylate uptake system protein A
DctA	Dicarboxylate transport Protein A
DcuA	Dicarboxylate uptake Protein A
DcuB	Dicarboxylate uptake Protein B
DcuC	Dicarboxylate uptake Protein C
DcuR	Dicarboxylate uptake Regulator
DcuS	Dicarboxylate uptake Sensor
DHp	Dimerization and Histidine phosphotransfer
DMSO	Dimethyl sulfoxide
dNTP	Deoxyribonucleoside triphosphate
DTT	Dithiothreitol
EDTA	Ethylenediaminetetraacetic acid
eM9	enriched M9
FNR	Fumarate nitrate reductase regulator
FumA/B/C	Fumarase A/B/C
Frd	Fumaratreductase
GpA	human Glycophorin A
HRP	Horseradish peroxidase
IPTG	Isopropyl-β-D-thiogalactopyranoside
Kan^r	Kanamycin resistence
kDa	kilo-Dalton
LB	Lysogeny broth
MQ	Menaquinone
MQH$_2$	Menachinol
MOPS	3-(N-Morpholino)-Propansulfonsäure
MTP	mikrotiter plate
MU	Millerunits
NADH	reduced Nicotinamide adenine dinucleotide
ONPG	o-Nitrophenyl--D-galactopyranosid

PAGE	Polyacrylamide gel electrophoresis
PAS	Per-ARNT-Sim
PAS_c	cytoplasmatic PAS domain
PAS_p	periplasmatic PAS domain
PBS	Phosphate buffered saline
PCR	Polymerase chain reaction
PEG	Polyethylenglycol
Per	Period Clock Protein
Q	Ubiquinone
QH_2	Ubichinol
rpm	revolutions per minute
RT	room temperature
SDS	Sodium dodecyl sulfate
Sim	Single-minded protein
SOB	Super optimal broth
SOC	Super optimal broth with catabolic repressor
TBS	Tris buffered saline
TCS	Two-component system
T_M	melting temperature
TEMED	N,N,N',N'-Tetramethylethylendiamin
Tet^r	Tetracycline resistence
TM	transmembrane
TM1	transmembranhelix 1
TM2	transmembranhelix 2
TMAO	Trimethylamin-N-oxid
Tris	Tris(hydroxymethyl)-aminomethan
Tween 20	Polyoxyethylen(20)-sorbitan-monolaurat

9   Publications

Papers

Stopp, M., Steinmetz, P. A. and Unden, G. (2021) Properties of transmembrane helix TM1 of the DcuS sensor kinase of Escherichia coli, the stator for TM2 piston signaling. *Biological chemistry.* DOI: 10.1515/hsz-2021-0254

Parts of the dissertation were published in this publication. The publication was accepted after the dissertation was already submitted. Therefore this publication is not cited in the dissertation.

Stopp, M., Schubert, C., and Unden, G. (2021) Conversion of the Sensor Kinase DcuS to the Fumarate Sensitive State by Interaction of the Bifunctional Transporter DctA at the TM2/ PAS$_C$-Linker Region. *Microorganisms* **9** (7), 1397. DOI: 10.3390/microorganisms9071397

Parts of the dissertation were published in this publication. The publication was accepted after the dissertation was already submitted. Therefore this publication is not cited in the dissertation.

Stopp, M., Steinmetz, P. A., Schubert, C., Griesinger, C., Schneider, D., and Unden, G. (2021) Transmembrane signaling and cytoplasmic signal conversion by dimeric transmembrane helix 2 and a linker domain of the DcuS sensor kinase. *The Journal of biological chemistry* **296**, 100148. DOI: https://doi.org/10.1074/jbc.RA120.015999

Surmann, K., Stopp, M., Wörner, S., Dhople, V. M., Völker, U., Unden, G., and Hammer, E. (2020) Fumarate dependent protein composition under aerobic and anaerobic growth conditions in Escherichia coli. *Journal of proteomics* **212**, 103583 DOI: 10.1016/j.jprot.2019.103583

Talks

Stopp, M., Steinmetz, P. A., Unden, G. (2018) An α-helical axis in DcuS sensor kinase connects periplasmic signal input and cytoplasmic signal conversion. Konferenz der Tagungsserie: Mechanisms of Gene Regulation, Tutzing

Posters

Stopp, M., Steinmetz, P. A., Unden, G. (2020) The role of stable and dynamic piston regions for transmembrane signaling by sensor kinase DcuS of *E. coli*. Jahrestagung der Vereinigung für Allgemeine und Angewandte Mikrobiologie (VAAM), Leipzig

Stopp, M., Strecker, A., Steinchen, W., Bange, G., Unden , G. (2019) α-helical axis dynamics in DcuS sensorkinase interdomain signal transmission. Jahrestagung der Vereinigung für Allgemeine und Angewandte Mikrobiologie (VAAM), Mainz

Stopp, M., Steinmetz, P. A., Unden, G. (2018) Structural dynamics in DcuS signal transduction in *E. coli*. Jahrestagung der Vereinigung für Allgemeine und Angewandte Mikrobiologie (VAAM), Wolfsburg *- Best Poster Presentation Award -*

10 Acknowledgement

11 Curriculum vitae

Persönliche Daten

Name: Marius Stopp

Anschrift

Telefon

E-Mail   marius.stopp@gmx.de

Geburtsdatum   05.03.1992

Geburtsort

Staatsangehörigkeit   Deutsch

Promotion

seit 05/17   Johannes Gutenberg-Universität Mainz

                    Institut für Molekulare Physiologie, Mikrobiologie und Weinforschung

                    Arbeitsgruppe Prof. Dr. G. Unden

Studium

04/15 - 03/17   Johannes Gutenberg-Universität Mainz

                    Fachbereich Biologie, Studium mit Masterabschluss (1,0)

                    Masterarbeit am Institut für molekulare Physiologie

                    Mikrobiologie und Weinforschung

                    Arbeitsgruppe Prof. Dr. Gottfried Unden

04/12 - 04/15   Johannes Gutenberg-Universität Mainz

                    Fachbereich Biologie, Studium mit Bachelorabschluss (1,7)

Freiwilliges Soziales Jahr

04/11 - 09/06   Albert Schweitzer Schule Ingelhiem

                    Förderschule mit dem Förderschwerpunkt Lernen

Schule

08/02 - 03/11   Sebastian Münster Gymnasium, Ingelheim

                    Allgemeine Hochschulreife (Note: 2,2)

12   Affidavit

Hiermit versichere ich, dass die vorliegende Dissertation von mir selbst angefertigt wurde und ich keine anderen als die angegebenen Quellen und Hilfsmittel verwendet habe.

_____   _____

Ort, Datum   Marius Stopp